January 1979

A Mathematical Hydrodynamic Circulation Model of Great Salt Lake for Resource Management

Gary Z. Watters

Charles T. Kincaid

Recommended Citation

UtahStateUniversity
MERRILL-CAZIER LIBRARY

A Mathematical Hydrodynamic Circulation Model Of Great Salt Lake for Resource Management

Gary Z. Watters and Charles T. Kincaid

Final Report

A MATHEMATICAL HYDRODYNAMIC CIRCULATION MODEL OF GREAT SALT LAKE

FOR RESOURCE MANAGEMENT

by

Gary Z. Watters
and
Charles T. Kincaid

Utah Water Research Laboratory
Utah State University
Logan, Utah 84322

June 1979

ACKNOWLEDGMENTS

DISCLAIMER

TABLE OF CONTENTS

LIST OF FIGURES

LIST OF TABLES

In the Great Basin region of this country, the resource which has always been of great importance is water. In Utah, the proper management of the resources of Great Salt Lake and the watersheds tributary to it, has become a topic of increasing concern. Recently, much emphasis has been placed on developing the recreational and industrial resources of Great Salt Lake. For optimum economic and social benefits from future development plans, the lake and its tributary watersheds need to be considered in terms of a single entity. In this regard, the Utah Water Research Laboratory (UWRL) has conducted several studies which involve hydrologic basins tributary to Great Salt Lake. Significantly lacking, however, was a comprehensive study of Great Salt Lake itself.

The research reported herein is directed towards the development of a comprehensive predictive hydrodynamic model of Great Salt Lake (see Figure 1). This model provides two general types of information. First, it provides circulation patterns within the lake for configuations and conditions imposed by the planner. This information is necessary to predict movement of pollutants, paths of freshwater inflows, and other phenomena which depend on currents. Second, the model provides information on the distribution of salinity throughout the lake. This information is vital to the industries around the lake which extract minerals from the brines of the lake. These capabilities of the model will also be valuable in providing data to be used by quality models.

It could be argued that because of a lack of field data for model verification, the development of a mathematical model was premature. Some field data on salinity are being collected regularly and the data base is steadily growing. Hopefully, the Utah Department of Natural Resources will implement a program of measuring velocities and circulation patterns to provide a data base for calibrating the hydraulic model. In any case, the initial development of a mathematical model is appropriate so that over the next few years, it can be improved and adjusted as more data become available. It seemed unwise to wait for a complete data base before launching a lengthy program of development of a mathematical model.

The objectives of the research were as follows:

1. To develop new mathematical models or incorporate existing models of the flow through the Southern Pacific causeway embankment and culverts to act as boundary conditions in mathematical circulation models of the southern and northern arms of Great Salt Lake.

2. To develop an upper-layer hydrodynamic circulation model of Great Salt Lake. As a first step toward developing a more comprehensive two-layer model, it was recognized that the main function of the lower layer within the lake may be to act as a reservoir for passing salinity from the north arm to the surface layer in the south arm. If this is indeed the case, then an upper-layer model could be constructed based on the assumption that the interface is a horizontal boundary which feeds salinity into the upper layer in some reasonable fashion to maintain continuity.

3. To attempt to develop a coupled two-layer model of Great Salt Lake. It was proposed to use the finite element technique to generate a hydrodynamic model of the circulation patterns in both the upper and lower layers. The finite element representation incorporates cubic velocity variations in the two layers to more accurately simulate the recirculation flow patterns caused by wind action on the surface and fresh water flow from the contributing streams.

4. To perform a laboratory experiment devised to evaluate the rate of salinity exchange from the lower high-density layer through the interfacial shear zone into the upper layer. It was believed that the exchange of salinity between the two layers is a direct function of the intensity of the interfacial shear and the resulting turbulent mixing at the interface.

5. To attempt to adjust the model to Great Salt Lake. All available velocity and salinity concentration data collected by the United States Geological Survey (USGS) and the Utah Geological and Mineral Survey (UGMS) during recent years was used.

6. To cooperate with researchers who are studying other aspects of the lake
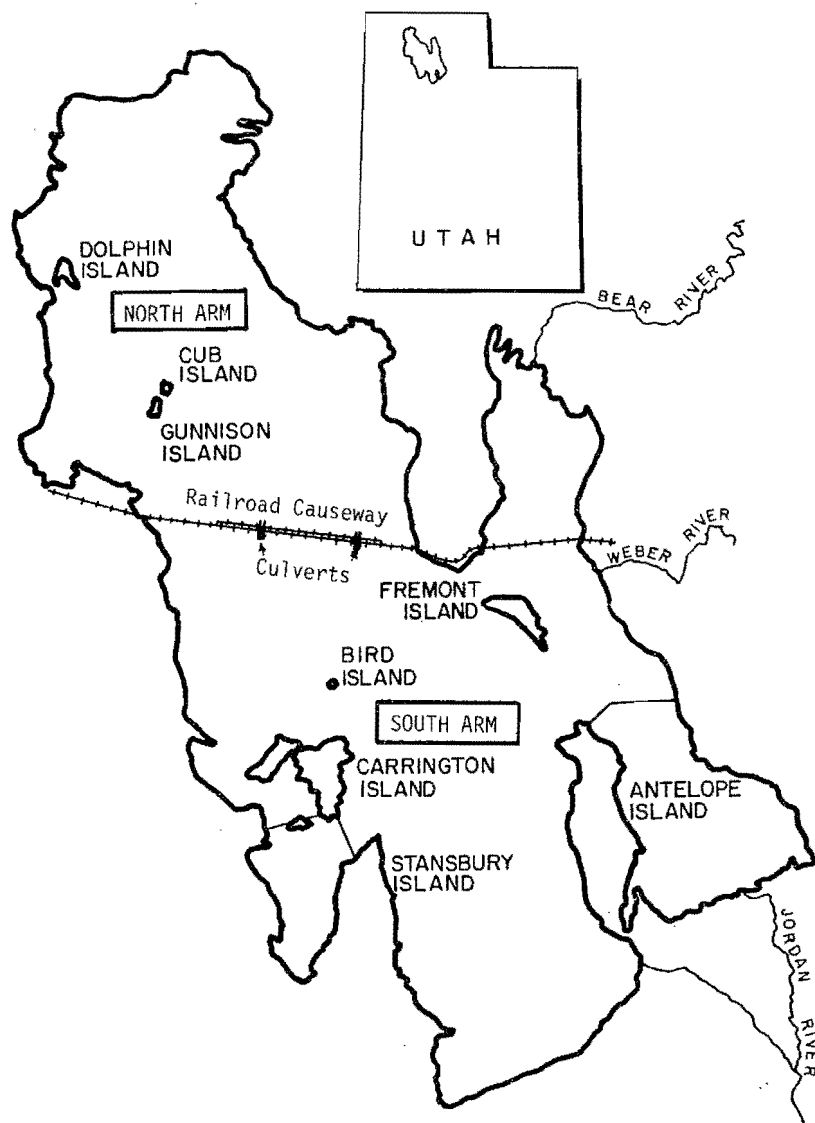
Figure 1. Map of the Great Salt Lake.

by making the mathematical model available to them.

A modeling approach utilizing equations based on the fundamental laws of physics, coupled with the application of the versatile finite element method gives the hydrodynamic and convection-dispersion models of Great Salt Lake the versatility required to examine the spectrum of management alternatives. The predictive capability is greatly enhanced in this approach by minimizing the number of empirical constants to be evaluated. It seems clear that the development of these comprehensive models of the lake is a necessary step in the subsequent development and use of both water quality and management models of this important natural resource.

2

LITERATURE REVIEW

Historical Development of
Great Salt Lake

General development

Great Salt Lake is all that remains of the largest of pluvial lakes in the Western Hemisphere (Utah Division of Water Resources 1974). The former Lake Bonneville inundated nearly 20,000 square miles in Utah, Nevada, and Idaho. The present lake is approximately 70 miles long and 40 miles wide. Its surface area, corresponding to a surface elevation of 4200 feet (msl), is nearly 1,500 square miles. The shallow depth, exhibited by an average depth of 13 feet, is characteristic of the lake. Maximum depth is approximately 35 feet. Being a terminal lake, considerable changes in the lake elevation or stage occur. Thus, while several islands are always surrounded by water, others occasionally become peninsulas defining the lake's shoreline. Of these islands, the largest are: Antelope, Carrington, Fremont, and Stansbury.

Mineral extraction from Great Salt Lake was established by the Mormon pioneers and continues today as the largest lake supported industry. Early mining of the lake's waters was limited to sodium chloride (table salt); however, current technology allows for the production of magnesium metal, liquified chlorine, gypsum, magnesium chloride, potash (potassium sulfate), sodium sulfate, lithium chloride, and bromine (Riley et al. 1975). Additional salts of magnesium, sulfur, and potassium will be mined in the future once the economy provides adequate incentives.

Both the physical appearance and natural chemistry of Great Salt Lake have been altered by the construction of rail transportation spanning the width of the lake at Promontory Point. Completion of the Lucin Cutoff's 12 miles of wooden trestle in 1904 served to separate the lake into northern and southern sections. By replacing the trestle in 1959 with a rock and gravel causeway, the Southern Pacific Railroad Company effectively divided the lake into two separate lakes. In addition to the restriction of watercraft, the causeway has disrupted the flow and hence the concentrations of brine within the two sections of the lake.

Following construction of the causeway, the brine north of the embankment has remained near saturation, while that south of the fill is clearly less concentrated. In addition, an easily defined second layer of denser brines has been created below the elevation of 4175 feet (msl) in the southern arm of the lake. While there is considerable debate over the future trends of lake stage and brine chemistry, there can be little doubt that the causeway serves to isolate the northern waters from the approximately 95 percent of all surface waters which enter the southern arm of the lake. The resulting difference in brine concentration has had a major impact upon the mineral extraction industry. Those mining the northern arm's brine have a distinct advantage over the southern arm's companies. The proper management of the lake's chemistry is of great importance when one considers the value of minerals contained in Great Salt Lake.

The idea of Great Salt Lake providing the setting for a major resort facility has endured for nearly 90 years. The late ninteenth and early twentieth centuries saw the establishment and eventual failure of several resorts. Due to the shallow slope of the lake's beaches, changes in lake surface elevation create considerable changes in shoreline location. Since the lake is a terminal lake, there is a continuous and sometimes considerable fluctuation in the lake's stage. Thus, the periodically receding shoreline left the resorts high and dry which, in turn, led to their decline in popularity. However, the concept is still alive, and commands considerable attention from those who propose the development of lakeside freshwater impoundments. Such impoundments might also be able to provide relatively fresh water for industrial development.

Prior to the mid 1960s one might characterize the overall development of and research dealing with Great Salt Lake as a succession of uncoordinated activities. Regardless, the resources of the lake have played, and will continue to play, a significant role in the economic and social development of Utah.

3

Lake literature

Due to the primary role mineral extraction has played as a lake supported industry, considerable effort has been expended to investigate the physics and chemistry of the lake. Typical of these studies are the evaporation studies published in 1965 (Peck and Dickson 1965, Dickson and McCullom Jr. 1965), and the continuing series of brine chemistry reports (Hahl and Handy 1969, Whelan 1973, Whelan and Petersen 1975 and 1977). The Utah Division of Water Resources (1974) published an excellent sourcebook of the lake's climate and hydrologic system. This report also serves to summarize the multiobjective planning variables relating to the lake's future development. Principal among the variables defined are fluctuations in the lake's elevation, and the impact of and upon water quality from the various users of the lake environment. Lin (1975) provides a survey of the circulation, currents, mixing processes, and both free surface and internal waves of the lake.

Several studies have dealt with the flows through both the causeway embankment and the two culverts which breach the embankment. Prominent among these is the USGS model (Waddell and Bolke 1973). Flows through both the fill and culverts are predicted as a function of lake stage, differences in lake stage, salinity and a myriad of other variables. Difficulties with the model lie in its rather limited base of verification data, making it applicable to a rather limited range of density and lake stage. Lin and Lee (1972) developed a Hele-Shaw model of seepage flows and Cheng and Hu (1975) reported on results of a numerical simulation; however, neither are directly applicable to the flow through the porous media of the causeway. A model of the culvert flows based upon interfacial Froude numbers and frictional effects was reported by Holley and Waddell (1976). It would appear the the greatest criticism of the causeway models is the lack of an adequate data base with which to verify any of them.

During the early 1970s legal questions concerning the altered chemistry of the lake served to simulate interest in the trends in brine chemistry within the northern and southern arms of Great Salt Lake. The first model dealing with water quality simulation within the lake was produced through the Utah Water Research Laboratory (UWRL) by Jones et al. (1976a). Long term distribution of quality constituents were modeled via a link-node technology. The dominant role of advective transport was not modeled, but rather taken from observations of long-term circulation patterns and input directly into the water quality model. The second model (Glassett and Smith 1976) employed a mass balance modeling technology for the northern arm and both the upper and lower layers of the southern arm of the lake. A third model, also employing a mass balance

technique, was published by the USGS (Waddell and Fields 1977). The primary objective of the USGS model was to examine various proposed schemes of diking the eastern shore of the lake, thus creating a series of relatively fresh water lagoons. Each of the models predicts a horizontally homogeneous brine distribution for the long term modeling of water quality; however, only the UWRL model has the ability to include advection information for the prediction of short-term events. Even this model has no capability of predicting the advection information. Expansion of the above water quality modeling to include advective or convective prediction is the primary objective of the study reported herein.

Fundamental to much ongoing research effort concerning the lake has been the development of multiobjective management studies. The overall economic and social impacts of management alternatives are developed in two reports from the UWRL (Riley et al. 1975, Jones et al. 1976b). These reports provide an overall framework for a management model of the lake system. The earlier report identified data requirements and established priorities for the development of submodels for their eventual incorporation into the overall management model. The latter paper summarizes the trade offs of management use categories and their possible impacts upon physical characteristics of the lake. Such a description of posed problems suggests avenues of studying proposed developments. A third management summary report has been produced by the Utah Department of Development Services (1977). A general management objective of retaining the lake's mineral extraction potential is proposed. This objective leads to the further study of the causeway, lake stage control measures, development of recreational enterprises on the lake's south shore, and the brine chemistry and its interaction with the causeway. Some analyses on these topics have been completed, others are underway.

Stochastic multivariate modeling of the lake's stage has been completed (James et al. 1979). The variables of fresh water discharges, evaporation, and precipitation are combined to produce a water budget-lake stage relationship. Costs of alternate stage control measures are compared with their benefits of reduced estimated damages. Investigations continue into the economic and social impacts of levee construction, upstream water consumption, and the pumping of water into the western desert.

Hydrodynamic Models

Seepage

Investigations into the seepage of unconfined and confined flows have a long history; however, none of the solutions are directly applicable to this problem. The

physical problem created by the porous causeway's construction is one of flow reversal with depth. A head gradient drives southern brines northward over the pressure (density gradient)-driven northern brines which are moving southward (see Figure 1). Thus, a bi-directional flow exists whose free surface and interface locations are unknown a priori.

Most analyses of seepage problems assume that flow is incompressible and that Darcy's law is applicable. These assumptions suggest the introduction of a potential function which greatly simplifies groundwater flow analyses. Substitution of Darcy's law into the incompressible continuity equation leads directly to Laplace's equation, $\nabla^2\Phi = 0$, where Φ is the potential function. For homogeneous, isotropic media whose interior flow is described by Laplace's equation, equipotential lines and streamlines form an orthogonal network. Since the media of the causeway is a virtual unknown, it is assumed to be both homogeneous and isotropic. This leads to a somewhat simplified interior flow structure; however, the free surface and interface boundaries lend considerable difficulty to the boundary value problem.

Lin and Lee (1972) completed a study which applied the Hele-Shaw analogy to the causeway discharges. The study succeeded in demonstrating only the relevance of the technique since limited funding did not allow for a complete range of head and density gradients to be examined. There remains some question as to the availability of liquids of appropriate density for the required tests.

The first numerical model of the porous media flow was developed by the USGS (Waddell and Bolke 1973). Although the problem is essentially steady state, the USGS chose to employ a two-layer version of a transient salt wedge model (Pinder and Cooper 1970). Rather than employ the boundary value problem solution, they also chose to recast the resulting discharge values in terms of the density and stage differences exhibited by the lake's northern and southern arms. Coefficients of the resulting equations were arrived at through multiple regression analysis. By selecting the above format of presentation one realizes a trade off. The equations for northward and southward discharges are easily employed; however, they are applicable to a rather narrow range of lake stage, and differences in lake stage and density.

A somewhat simplified approach is put forth by Glassett and Smith (1976). Their Darcian analysis includes a restriction to linear velocity profiles. Cheng and Hu (1975) provide a more complete analysis in their paper on fluid movements through causeways. Unfortunately, their published results do not correspond to observations published by the USGS (Waddell and Bolke 1973). This disagreement may be attributed to their failure to employ cross-section

dimensions representative of the Southern Pacific Causeway. The porous media model developed in this study parallels that of the Cheng and Hu (1975) model; however, it does conform to the physical dimension of the causeway.

Three noteable ideas which have not found application to the Southern Pacific Causeway are: the boundary integral equation method (BIEM); the inverse formulation; and computations of non-Darcian flows. Liggett (1977) applies the BIEM to a single density flow; however, the technique and its economy of considering only the boundary of Darcian subdomains is applicable to the bi-directional flow problem. The ease of discretization made possible by the inverse formulation (Jeppson 1969) is also applicable to the causeway embankment problem. A third alternative, that of non-Darcian flow is suggested by the Reynolds numbers computed from the Cheng and Hu (1975) and Waddell and Bolke (1973) results. Each of these ideas are topics for future research.

Culverts

The bi-directional flow characteristics exhibited within the causeway embankment also occur in the two 15-foot wide culverts which breach the causeway. In the case of the culvert flows the discharge is clearly turbulent. Three previous models have been developed for this segment of the analysis. Each employs a somewhat different approach.

A USGS model (Waddell and Bolke 1973) employs a Bernoulli equation approach wherein the head losses through the culvert are assumed to be a function of maximum relative velocity. A multiple regression analysis of discharge, stage, and density leads to an empirical model of the bi-directional discharges. Once again the resulting flows are easily computed but it must be recognized that the range of application for the analysis is limited.

Glassett and Smith (1976) produced an empirically based solution in that they assumed a typical velocity profile which reduces the analysis to a one-dimensional viewpoint. The free surface profile is also assumed, giving rise to pressure gradients as a function of gradients in layer depth. Solutions of upper and lower layers independently predict the location of the fluid interface. Adjustments are made in the posed problems until both solutions arrive at suitably close approximations of the interface location. While the concept of matching independently computed interface profiles is interesting, the previously mentioned assumptions as to velocity and free surface shapes may be misleading.

The concept of an energy balance coupled with an interfacial Froude condition is explored by Holley and Waddell (1976). Head losses are considered from the floor and

walls of the culvert, and the interface and entrance regions of the fluid flow. This analysis is a significant improvement upon the earlier Waddell and Bolke (1973) study in that restrictive assumptions have been removed. The model is shown to be more sensitive to stage and density data than head loss coefficient selection. This suggests the use of an entirely frictionless model; however, the data available at this time does not warrant further culvert modeling development along these lines.

In the initial phases of this project it was felt that an improvement upon the Glassett and Smith (1976) model was the direction which the research should take. A variable-density, hydrodynamic model of culvert flow has recently been published by Water Resources Engineers (WRE) (Norton et al. 1973). This model's verification included free surface computations and evidence of eddying in discharges over a weir. Such results led these investigators to believe that a suitable formulation could be achieved via a momentum and mass conserving model similar to that employed by WRE. Considerable time and effort were expended prior to realizing the energy basis of the problems stage-density data. Thus, the computational results of this study's culvert flow analysis, while being meaningful in some respects, may not be as economical and applicable as the Holley and Waddell study.

Lake circulation

A decision as to the type of lake model must be made. Models by Glassett and Smith (1976) and Waddell and Fields (1977) employ a mixed batch reactor or mass balance model. The advective/convective processes within the lake are completely blended with the dispersive/diffusive processes in such a model. These models provide the most economical estimates as to the long term reaction of the lake to various management alternatives; however, they fail to address the short term impact of whatever nature. In an effort to address both the short and long term problems of the lake, the UWRL developed a link-node model of the upper layer's brine (Jones et al. 1976a). One failure of this model is the necessity of developing velocity/discharge values for the various links or areas of the water body prior to model operation. This is no small task due to the scant data on lake circulation patterns, and the absolute absence of circulation information on the lake configuration as it may evolve (due to diking schemes) in years to come. Thus, a circulation model of either a two-dimensional layer-averaged, or a three-dimensional character is needed. Such a model would provide the hydraulic circulation information required by models of the convection-dispersion of constituents within the water.

Three alternatives exist for modeling the hydrodynamic circulation within Great Salt Lake's southern arm: 1) a single layer model of the upper layer fluid could be coupled with an assumed rigid body of concentrated salt brine (the southern arm's lower layer); 2) the two layers could be modeled as two constant-density layers with suitable boundary conditions specified at an interface; 3) a continuous model of both the upper and lower layers could be modeled via a variable-density model. Since the northern arm of the lake is a nearly homogeneous body of water it may be treated as a single fluid mass of virtually constant density.

The two models of circulation developed in this study are of the first type. The first model, reported by Kincaid (1979), is a fully three-dimensional simulation of free surface flows. The second, a vertically averaged two-dimensional model, is reported within this document. Kincaid (1979) provides a complete review of literature for the breadth of lake circulation models. Such a review will not be repeated herein; however, a summary of the techniques will be given.

Three generalized techniques exist for the numerical simulation of circulation phenomena. The first technique is based upon the observations of Welander (1957) that wind-induced surface stress and surface gradients determined the underlying circulation of a water body. Liggett and Hadjitheodorou (1969) produced a rigid-lid model of this theory. The assumptions of negligible Rossby number, constant density and eddy viscosity, shallow depth, and hydrostatic pressure give rise to a linear set of equations describing three-dimensional circulation. While the original paper employs a finite difference numerical approximation, a later paper (Gallagher et al. 1973) applies finite element approximations to an identical development. Noteable among similar models is the free surface model of Cheng (1977). In it he includes previously neglected nonlinear terms. Due to the recirculation character of wind-driven flows, the three-dimensional aspect of these models is most desirable. They represent the most economical fully three-dimensional analyses of lake circulation.

A second method is best described as a layer or vertically averaged model. Velocity variables are reduced to either layer-averaged values or discharges, thus creating a two-dimensional analysis in the horizontal plane. This concept has found application to the Welander (1957) theory; however, its principal application has been to the complete Navier-Stokes equations (Norton et al. 1973, Connor and Wang 1973, Leendertse 1970, Leendertse and Gritton 1971a and 1971b). This technology is applicable to flow-through situations or tidal currents which characterize reservoirs and estuaries, as well as the wind-driven circulation of shallow lakes and ponds.

Finally, there are the fully three-dimensional models which include all terms

of the Navier-Stokes equations. These models are either continuous (Spraggs and Street 1975, Kincaid 1979) or layered (Leendertse et al. 1975, Leendertse and Liu 1975, Leendetse et al. 1973, Simons 1971). Some of these models address the problems of stratification arising from thermal and salinity gradients within flows. A more general acceptance of these models will occur as the expensive solutions they offer can be justified by the problems they address.

Convection-dispersion/diffusion

The concepts and definitions as expressed by Holley (1969) in his paper on diffusion and dispersion are followed in this report. Within a Great Salt Lake model, concern lies in the horizontal dispersion and vertical diffusion of ions of various salts. Righellis (1978) and Freitas (1979) examined these respective problems and included in their literature surveys the appropriate literature. Brief summaries of both are given.

Righellis' (1978) study revealed that the bulk of research dealing with horizontal or longitudinal dispersion was restricted to fluid flows influenced by tidal action (i.e. Harleman 1974, Narayanan and Shankar 1976). Several models were discussed by George (1974); however, most are one-dimensional models which are difficult to extend to two dimensions. The paper by Huyakorn (1977), which describes the numerical model eventually employed by Righellis, also describes a dispersion coefficient as a function of the flow's point values of kinematic viscosity and its dimensionless Prandtl and Reynolds numbers. Such a description encourages one to employ dynamic, spacially-varying dispersion coefficients; however, such a complex model could not be easily monitored or controlled. Thus, for the present study a simplistic but manageable constant parameterization is employed wherein the prototype event is modeled with varying values for the diffusion coefficient until agreement between the prototype and model occurs.

Freitas (1979) indicated that the research to date on vertical diffusion between layers of stratified flows has been problem specific. Thus, while qualitative information is available from previous studies, the quantitative knowledge for general application is deficient. Parameters akin to the Richardson number are shown to be indicative of the stability of turbulent stratified flows (Harleman 1963, Ellison and Turner 1959). All findings report that as the Richardson number increases, the entrainment rate falls off rapidly. Specific application to Great Salt Lake is inhibited due to the unknown velocities within the lake, and the fact that previous models have been developed for less saline waters.

Three models (Jones et al. 1976a, Lin 1975, Glassett and Smith 1976) employ mass balance models to arrive at empirical values of diffusion coefficient (m^2/sec), rate of entrainment (m/sec), and mass flow rate (kg/sec). While being reported somewhat differently, examination reveals that all reach very similar values describing the rate at which salt is transported vertically through the halocline. None are related to the physics of the circulating flows and therefore further study, reported by Freitas (1979), was undertaken to relate vertical diffusive transport of salinity to the relative fluid velocities in the interface halocline region.

Numerical Models

Early in the research a decision was made to develop finite element modeling capabilities for the various segments of the overall circulation model. Within the reports on causeway flows (Cameron 1978), culvert flows (Martin 1979), vertically-averaged convection-dispersion (Righellis 1978), and three-dimensional free surface flows (Kincaid 1979) are substantial reviews of the numerical modeling literature as it applies to each problem respectively. To include a summary of the reviews provided in each of these reports would be too extensive. With the exception of the Righellis model, each model employs classical Galerkin finite element technology. Appropriate literature will be cited during the development of the general technology within the section dealing with numerical models. For a complete review of the application of this technology to hydraulic problems the reader is referred to any of the following texts on the topic: Chung (1978), Connor and Brebbia (1977), Huebner (1975), Pinder and Gray (1977), and Zienkiewicz (1977). Some concepts developed by Kincaid and others employed by Righellis are discussed in subsequent paragraphs.

A new concept is introduced by Kincaid (1979) with regard to the modeling of viscous, free surface flows. The use of a derivative continuous (C^1) model of a free surface is suggested by the kinematic relationship governing all interface boundaries. It is readily observed that the interior problem requires only function (C^0) continuity at element boundaries. Satisfaction of these criteria is met by a new blended element having C^1 continuous (free) surface and a C^0 continuous interior interpolation. Blending function methods for the development of two and three-dimensional elements of either C^0 or C^1 character are discussed by Watkins (1976). These same techniques are applied to the development of a hybrid or mixed interpolation C^1-C^0 element by Kincaid (1979).

As a result of employing multiple degree of freedom nodes Kincaid is forced to develop a geometry preprocessor (Barnhill 1977) for the data required of isoparametric elements. One ramification of using isoparametric

elements to fit curved boundaries is the use of the dependent variable's interpolant to model the independent variables (i.e. geometry coordinate information). As a result, unique derivative information (with respect to a natural coordinate system) is required. By preprocessing readily available C^0 coordinate information, one can produce the necessary unique derivative information.

The convective-dispersive transport model developed by Righellis (1978) is an application of "upwind" weighting discussed by Christie et al. (1976), Heinrich et al. (1977), and Huyakorn (1977). Subsequently, papers by Heinrich and Zienkiewicz (1977) and Hughes (1978) have discussed the generalization of this technology to quadratic interpolants. The fundamental idea upon which this weighting technique is based (Zienkiewicz 1977) is the recognition of parameter dependent characterizations of the convection-dispersion equation. Allowing the diffusivity term of the equation to vanish causes the appearance of a first order equation of the initial value-propagation type. This, in turn, alters the necessary boundary condition information. By attempting a classical Galerkin finite element solution of the original convection-dispersion equation, one runs the risk of overspecifying the problem by applying downstream boundary conditions to a problem which is very nearly an initial value problem. Solution to this problem is achieved through the use of an "upwind" weighting scheme which localizes the impacts of downstream information upon the overall solution.

This review of literature includes a historical review of research dealing with Great Salt Lake, and brief reviews of the hydrodynamical models to be employed and the nonclassical numerical methods to be used in obtaining solutions. The reports which derived from this research project contain detailed problem specific reviews of literature which, for the most part, have not been duplicated in this document. Specific literature will be cited in the sections detailing the development of both mathematical and numerical models.

The mathematical models employed are based on fundamental physical relationships of fluid mechanics. In the seepage flow model, steady state Darcian flow in a homogeneous porous media is assumed to occur. In the hydrodynamic models of culvert flow and circulation, the Navier-Stokes equations are applied. To simulate the mixing processes, the unsteady convection-dispersion equation in two dimensions is used. Details of the specific application of these principles follow.

Seepage Flow Model

For two-dimensional, steady flow through uniform media, Darcy demonstrated that the seepage velocity was proportional to the gradient of the total head.

$$v_s = -k \frac{\partial h}{\partial s} \quad \quad \quad (1)$$

where s is the direction of flow, k is defined as the coefficient of permeability dependent on the properties of both the fluid and the soil. The h-value in Equation 1 is referred to as the piezometric head and is given by

$$h = p/\rho g + y \quad \quad \quad (2)$$

where p is the pressure, ρ is the mass density of the fluid, g is the gravitational constant, and y is the vertical distance above some datum. Darcy's law includes any variation in fluid viscosity within the k term.

For two-dimensional flow,

$$u = -k_x \, \partial h/\partial x \quad \text{and} \quad v = -k_y \, \partial h/\partial y \quad (3)$$

for flow in the x and y coordinate directions, respectively. Coupling them with the continuity equation for two-dimensional flow,

$$\partial u/\partial x + \partial v/\partial y = 0 \quad \quad (4)$$

gives the following equation results for constant k_x and k_y.

$$k_x \, \partial^2 h/\partial x^2 + k_y \, \partial^2 h/\partial y^2 = 0 \quad . \quad . \quad (5)$$

When Equation 5 is applied throughout a specified problem domain, the analysis results in a boundary value problem.

In a two-density porous media flow problem, piezometric head is not continuous across the density interface because of the discontinuity in density. This would preclude the analysis of this problem as a single boundary value problem, thereby forcing one to perform the analysis as two boundary value problems, each with a different constant density of fluid. If the governing differential equations are formulated in terms of pressure, this limitation can be circumvented, and the boundary value problem may be posed as either a single or double domain problem. In terms of pressure, Equation 5 takes the form

$$k_x \frac{\partial^2 (p/\rho g + y)}{\partial x^2} + k_y \frac{\partial^2 (p/\rho g + y)}{\partial y^2} = 0 \quad \quad (6)$$

This is the differential equation which will be used to represent flows in this model study.

It is necessary to include boundary conditions to complete a properly posed boundary value problem. There are basically two types of boundary conditions involved with the solution of equations of the form found in Equation 5. One type deals with the values of the field variable along the domain boundaries, while the other type deals with the normal derivative values of the field variable.

A Dirichlet condition is a boundary condition where the field variable value is known on the boundary. If this value is zero, the condition is termed a homogeneous Dirichlet boundary. If it is a nonzero constant, it is called a nonhomogeneous

9

Dirichlet boundary. A Neumann boundary condition is one in which the normal derivative of the field variable at the boundary is forced to take on a given value. These, too, can be both homogeneous and nonhomogeneous. Neumann boundaries describe the normal velocity, v_n, (and flux) conditions across boundaries in seepage flow problems.

A sketch of the problem domain is shown in Figure 2. Dirichlet boundary conditions are imposed along the constant-head boundaries at each end of the flow problem. Neumann conditions are applied along the impermeable base of the fill. Along the free surface and seepage surface, the traditional boundary condition, $p = 0$, is applied.

It is clear from Figure 2 that the unknown extent of the seepage surfaces at each end and the unknown position of the interface could present problems in the solution process. In any case this problem will be solved by using the finite element method with quadratic quadrilateral elements. The details of setting up the numerical problem are related in the subsequent section.

Culvert Flow Model

The derivation of the mathematical model begins with a statement of the basic equations in three dimensions. For convenience, the use of a comma to indicate partial derivatives will be used in these complex equations, i.e., a comma followed by a subscript indicates a derivative taken with respect to the subscripted variable.

The three momentum equations, known as the Navier-Stokes equations, are

$$(\rho u)_{,t} + (\rho u^2)_{,x} + (\rho uv)_{,y} + (\rho vw)_{,z}$$

$$= \tau_{xx,x} + \tau_{yx,y} + \tau_{zx,z} - p_{,x}$$

$$\dots \quad \dots \quad (7)$$

$$(\rho v)_{,t} + (\rho uv)_{,x} + (\rho v^2)_{,y} + (\rho vw)_{,z}$$

$$= \tau_{xy,x} + \tau_{yy,y} + \tau_{zy,z} - p_{,y} - \rho g$$

$$\dots \quad \dots \quad (8)$$

$$(\rho w)_{,t} + (\rho uw)_{,x} + (\rho vw)_{,y} + (\rho w^2)_{,z}$$

$$= \tau_{xz,x} + \tau_{yz,y} + \tau_{zz,z} - p_{,z}$$

$$\dots \quad \dots \quad (9)$$

The continuity equation is

$$\rho_{,t} + (\rho u)_{,x} + (\rho v)_{,y} + (\rho w)_{,z} = 0$$

$$\dots \quad \dots \quad (10)$$

The convection-diffusion equation is

$$\sigma_{,t} + (\sigma u)_{,x} + (\sigma v)_{,y} + (\sigma w)_{,z} = 0$$

$$\dots \quad \dots \quad (11)$$

in which

u,v,w	=	velocities in the x, y, and z directions,
ρ	=	average density of the elemental fluid volume,
ρ_0	=	density of fresh water,
p	=	pressure,
τ_{ij}	=	the internal shear stresses on the viscous fluid element,
g	=	acceleration due to gravity,
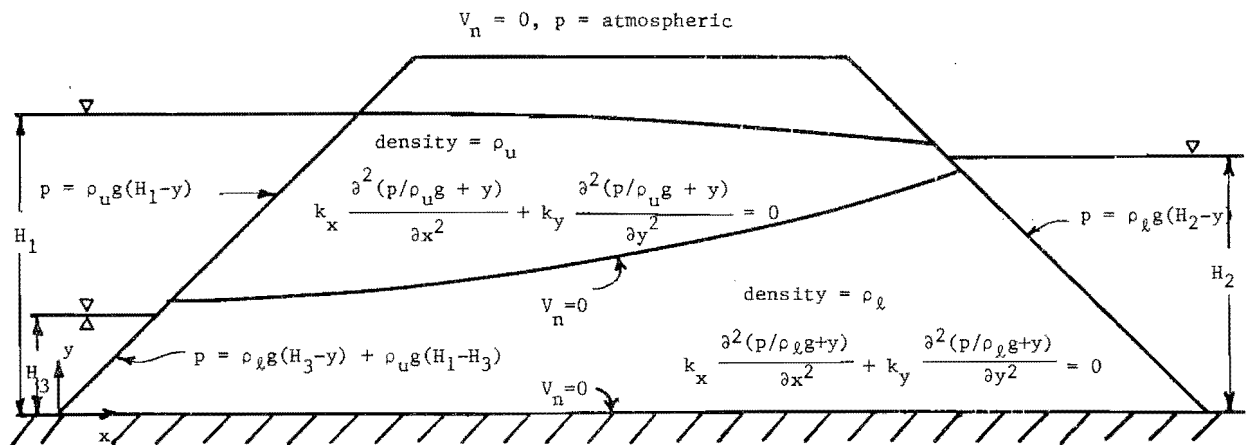
Figure 2. Boundary conditions on embankment.

σ = instantaneous density difference, $\rho - \rho_0$,
x = downstream direction,
y = vertical direction,
z = cross-stream direction, perpendicular to x and y directions,

By making proper assumptions, the complexity of the original equations will be reduced. These assumptions are as follows:

1. The flow is steady in time.

2. The transfer of momentum in the cross-stream direction is negligible, therefore the z-direction momentum equation will be eliminated.

3. The fluid density is variable in space, although the basic fluid is always treated as being incompressible.

4. The density may be written as the average value, ρ_0, plus an instantaneous deviation, σ.

$$\rho(x,y) = \rho_o + \sigma(x,y) \quad . \quad . \quad . \quad . \quad (12)$$

Moreover, the instantaneous deviation, σ, will be negligible in the momentum equations, except in the body force term, ρg, of the v-momentum equation.

5. The channel cross-section is symmetrical, though the width can vary in both the downstream and vertical direction.

6. The stresses due to wind and Coriolis forces are negligible.

Integrating the equations

The variable width will be introduced by integrating the governing equations across the width of the channel (z-direction). After integrating the equations in the cross-stream direction, it is necessary to use a combination of Leibnitz's rule, the kinematic relationship, and a force balance to incorporate the shear stresses on the sides of the channel.

Integrating the x and y momentum equations,

$$\int_{-b}^{b} [(\rho u^2)_{,x} + (\rho uv)_{,y} + (\rho uw)_{,z}] \, dz =$$

$$\int_{-b}^{b} [\tau_{xx,x} + \tau_{yx,y} + \tau_{zx,z} - P_{,x}] dz$$
$$. \quad . \quad . \quad . \quad . \quad . \quad . \quad (13)$$

$$\int_{-b}^{b} [(\rho uv)_{,x} + (\rho v^2)_{,y} + (\rho vw)_{,z}] \, dz =$$

$$\int_{-b}^{b} [\tau_{xy,x} + \tau_{yy,y} + \tau_{zy,z} - P_{,y} - \rho g] dz$$
$$. \quad . \quad . \quad . \quad . \quad . \quad (14)$$

The continuity equation is integrated to become

$$\int_{-b}^{b} [(\rho u)_{,x} + (\rho v)_{,y} + (\rho w)_{,z}] \, dz = 0$$
$$. \quad . \quad . \quad . \quad . \quad . \quad (15)$$

The integrated convection-diffusion equation is

$$\int_{-b}^{b} [(\sigma u)_{,x} + (\sigma v)_{,y} + (\sigma w)_{,z}] \, dz = 0$$
$$. \quad . \quad . \quad . \quad . \quad . \quad (16)$$

At this point, it should be noted:

1. It is necessary to obtain width average expressions for various terms in the above equation. Leibnitz's formula for changing the order of differentiation and integration is employed.

2. The internal shear stresses must be related to the boundary shear stresses. This will be done by means of a force balance on an elemental fluid particle located on the boundary of the channel. Assuming a state balance on the solid boundary, the sum of the forces for the differential free body are equated to zero.

Implementation of Leibnitz's formula introduces several additional terms. Fortunately, most of these terms can be summed to zero by using the kinematic relationship. The kinematic relationship is simply a mathematical statement that the velocity of the fluid at the boundary in a direction normal to the boundary is equal to the velocity of the boundary.

After applying Leibnitz's formula and substitution of the results of the kinematic relationship and the force balance, the governing equations can be written:

x-momentum

$$\rho(u^2 B)_{,x} + \rho(uvB)_{,y} + (pB)_{,x} - (\tau_{xx}B)_{,x}$$
$$- (\tau_{yx}B)_{,y} + (S_x^b + S_x^{-b} - 2p\ell_x)A_c$$
$$= 0 \quad . \quad . \quad . \quad . \quad . \quad . \quad (17)$$

11

y-momentum

$$\rho(uvB)_{,x} + \rho(v^2B)_{,y} + (pB)_{,y} + (\rho + \Delta\rho)\,gB$$
$$- (\tau_{xy}B)_{,x} - (\tau_{yy}B)_{,y} + (S_y^b + S_y^{-b})$$
$$- 2p\ell_y)A_c = 0 \quad . \quad . \quad . \quad . \quad . \quad (18)$$

continuity

$$(uB)_{,x} + (vB)_{,y} = 0 \quad . \quad . \quad . \quad . \quad (19)$$

convection-diffusion

$$(\sigma Bu)_{,x} + (\sigma Bv)_{,y} = 0 \quad . \quad . \quad . \quad (20)$$

where

B = the local channel width

$A_c = (1 + b_{,x}^2)^{\frac{1}{2}} (1 + b_{,y}^2)^{\frac{1}{2}}$

$\ell_x = -b_{,x} \ell_z$

$\ell_z = [1/(b_{,x}^2 + b_{,y}^2 + 1)]^{\frac{1}{2}}$

S_x, S_y = boundary shears in coordinate directions

Details of the manipulations can be found in Martin (1979).

Representation of turbulence

Since real fluids are turbulent, the system equations must be modified so the average values of interest may be separated from the random variations of turbulence. The commonly accepted method is called "ensemble averaging." The equations derived in the previous paragraphs are valid for laminar and turbulent flow; however, their dependent variables must be cast into their temporal mean value form prior to their solution. Each of the dependent variables, u, v, p, and σ, has an instantaneous component at a point composed of a temporal mean value and a turbulent fluctuation.

For the solution of our problem, it is assumed that the temporal value of the mean variable $\bar{u}$, $\bar{v}$, $\bar{p}$, $\bar{\sigma}$ does not change with time. By definition, the temporal mean value of each fluctuation u', v', p', σ' is zero.

From Schlichting (1968), it is known that the internal shear stresses, τ_{ij} are due to absolute viscosity and turbulent momentum transfer. Therefore, the τ_{ij} are made up of two components; one due to laminar stresses and the other due to "virtual" or "apparent" stresses of turbulent flow. Also from Schlichting (1968), the predominant term is the "virtual" stress.

$$\tau_{ij} = \tau_\nu - \rho\,\overline{u_i v_j}$$

or

$$\tau_{ij} = -\rho\,\overline{u_i v_j} \quad \text{since } -\rho\,\overline{u_i v_j} \gg \tau_\nu$$
$$. \quad . \quad . \quad . \quad . \quad . \quad . \quad (21)$$

To obtain a closed form of the internal stresses, an approximation analogous to the kinematic viscosity is made. The result in two dimensions is

$$\tau_{xx} = \rho[\epsilon_{xx}(2u_{,x}) + \epsilon_{yx}(u_{,y} + v_{,x})]$$
$$. \quad . \quad . \quad . \quad . \quad . \quad (22)$$

$$\tau_{yx} = \rho[\epsilon_{xx}(u_{,y} + v_{,x}) + \epsilon_{yx}(2v_{,y})]$$
$$. \quad . \quad . \quad . \quad . \quad . \quad . \quad (23)$$

$$\tau_{xy} = \rho[\epsilon_{xy}(2u_{,x}) + \epsilon_{yy}(u_{,y} + v_{,x})]$$
$$. \quad . \quad . \quad . \quad . \quad . \quad . \quad (24)$$

$$\tau_{yy} = \rho[\epsilon_{xy}(u_{,y} + v_{,x}) + \epsilon_{yy}(2v_{,y})]$$
$$. \quad . \quad . \quad . \quad . \quad . \quad . \quad (25)$$

or

$$\tau_{ij} = \rho\,\epsilon_{ik}(u_{k,j} + u_{j,k}) \quad i,j = 1,2$$
$$. \quad . \quad . \quad . \quad . \quad . \quad (26)$$

where ϵ_{ij} is an "eddy viscosity" coefficient matrix that may depend upon the mean velocities and the applied surface stresses.

$$\epsilon_{ij} = \begin{bmatrix} \epsilon_{xx} & \epsilon_{yx} \\ \epsilon_{xy} & \epsilon_{yy} \end{bmatrix} \quad . \quad . \quad . \quad (27)$$

The physical flow situation to which the mathematical model is to be applied is shown in Figure 3. The culvert shown is one of two occurring in the Southern Pacific Causeway fill. Flow of a lesser density brine occurs northward in the upper layer and a southward flow of a nearly saturated brine occurs near the bottom.

The intent is that the bi-directional flow problem be set up as a single boundary value problem with proper boundary conditions to yield the bi-directional character of the flow. Again the finite element numerical modeling technique will be used, employing quadratic triangular elements.

Two-Dimensional, Depth-Averaged
Circulation Model

Attempts to model lake circulation will be two-fold. The first approach, described in

12
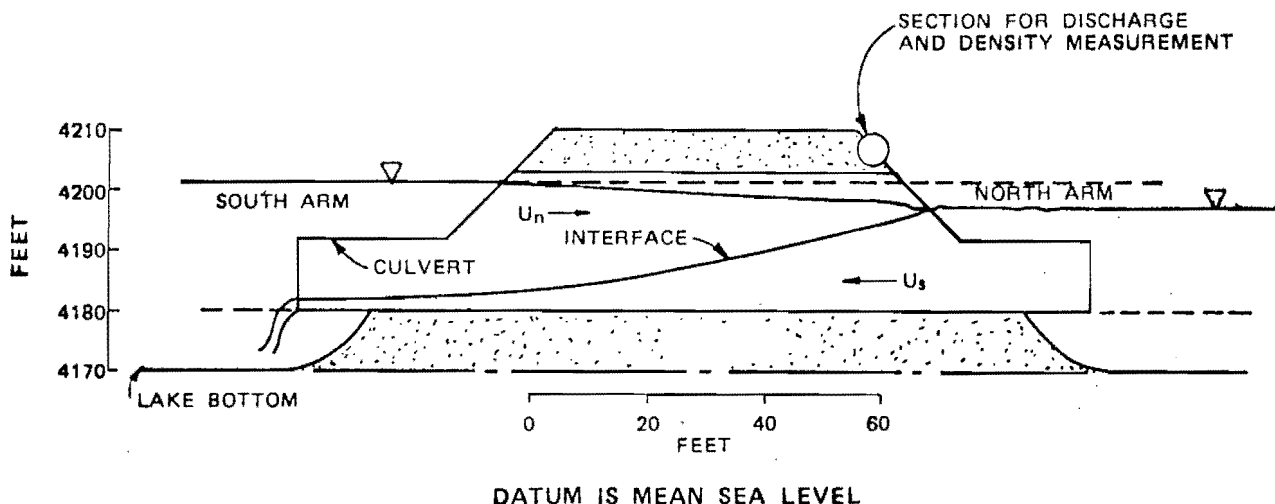
Figure 3. Schematic cross section of the east culvert.

this section, will consider two-dimensional flow in the horizontal plane with the velocities averaged over the depth. The main application will be a flow-through model where inlet and outlet velocities are specified and the wind circulation is ignored. The second approach, discussed in the next section is a three-dimension wind-driven circulation model which addresses the impact of wind shear on flow patterns.

Both approaches are intended to apply only to the upper layer of the south arm of Great Salt Lake as shown by diagonal lines on Figure 4. The three-dimensional model is capable of handling both layers in the south arm but computer size and cost limitations were encountered.

The basic equations

This two-dimensional model proceeds much as the culvert model, except circulation is in the horizontal plane. The effect of density on the circulation is assumed negligible and the rigid lid approach is used for the free surface. This technique eliminates the need to satisfy the $p = 0$ condition at the surface, and thereby introduces pressure at the surface as an unknown.

The appropriate equations are:

x-direction Navier-Stokes

$$\frac{\partial(\rho u)}{\partial t} + \frac{\partial}{\partial x}(\rho u^2) + \frac{\partial}{\partial y}(\rho u v) + \frac{\partial}{\partial z}(\rho u w) =$$

$$\rho f v - \frac{\partial p}{\partial x} + \frac{\partial \tau_{xx}}{\partial x} + \frac{\partial \tau_{yx}}{\partial y} + \frac{\partial \tau_{zx}}{\partial z}$$

$$\cdots \cdots \cdots (28)$$

y-direction Navier-Stokes

$$\frac{\partial(\rho v)}{\partial t} + \frac{\partial}{\partial x}(\rho u w) + \frac{\partial}{\partial y}(\rho v^2) + \frac{\partial}{\partial z}(\rho v w)$$

$$= \rho f u = -\frac{\partial p}{\partial y} + \frac{\partial \tau_{xy}}{\partial x} + \frac{\partial \tau_{yy}}{\partial y} + \frac{\partial \tau_{zy}}{\partial z}$$

$$\cdots \cdots \cdots (29)$$

continuity

$$\frac{\partial(\rho u)}{\partial x} + \frac{\partial(\rho v)}{\partial y} + \frac{\partial(\rho w)}{\partial z} = -\frac{\partial \rho}{\partial t}$$

$$\cdots \cdots \cdots (30)$$

where u, v, w are the x, y, z components of velocity, ρ is the fluid density, p is the pressure, f is the coriolis term and τ is the shear stress. Because this analysis only applies to steady, constant density flow with hydrostatic pressure variation vertically, the above equations can be simplified somewhat.

Integration over the depth introduces the average x (east) and y (north) velocities $\bar{u}$ and $\bar{v}$ respectively. The approach used follows Wang and Connor (1975) and also introduces pressure and bottom and surface shear. Internal shear is represented using a scalar eddy viscosity. The resulting equations are:

x-direction

$$h\left(\bar{u}\frac{\partial \bar{u}}{\partial x} + \bar{v}\frac{\partial \bar{u}}{\partial y}\right) = hf\bar{v} + \frac{\tau_x^s}{\rho}$$

$$- \frac{1}{2}C_f \bar{u}\sqrt{\bar{u}^2 + \bar{v}^2} - \frac{h}{\rho}\frac{\partial p^s}{\partial x}$$

$$+ 2\varepsilon^*\frac{\partial}{\partial x}\left(\frac{\partial h\bar{u}}{\partial x}\right) + \varepsilon^*\frac{\partial}{\partial y}\left(\frac{\partial h\bar{u}}{\partial y} + \frac{\partial h\bar{v}}{\partial x}\right)$$

$$\cdots \cdots \cdots (31)$$

13

DOLPHIN
ISLAND

UTAH

NORTH ARM

CUB
ISLAND

GUNNISON
ISLAND

BEAR RIVER

Railroad Causeway

Culverts

WEBER RIVER

FREMONT
ISLAND

BIRD
ISLAND

SOUTH ARM

CARRINGTON
ISLAND

ANTELOPE
ISLAND

STANSBURY
ISLAND

JORDAN RIVER
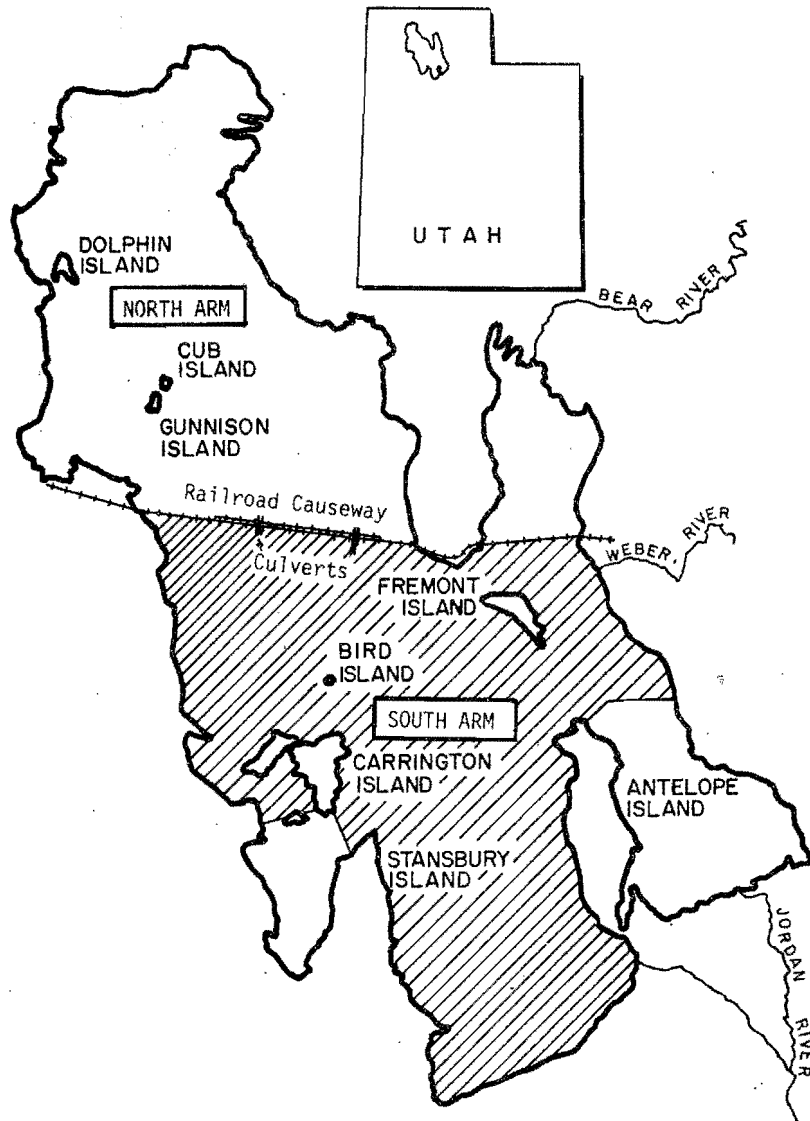
Figure 4. Map of the Great Salt Lake illustrating portion to which circulation model applies.

y-direction

$$h \left(\bar{u} \frac{\partial \bar{v}}{\partial x} + \bar{v} \frac{\partial \bar{v}}{\partial y} \right) = - h f \bar{u} + \frac{\tau_y^s}{\rho}$$

$$- \frac{1}{2} C_f \bar{v} \sqrt{\bar{u}^2 + \bar{v}^2} - \frac{h}{\rho} \frac{\partial p^s}{\partial y}$$

$$+ 2\varepsilon^* \frac{\partial}{\partial y} \left(\frac{\partial h \bar{v}}{\partial y} \right) + \varepsilon^* \frac{\partial}{\partial x} \left(\frac{\partial h \bar{u}}{\partial y} + \frac{\partial h \bar{v}}{\partial x} \right)$$

$$\cdots \cdots \cdots \cdots (32)$$

continuity

$$\frac{\partial h \bar{u}}{\partial x} + \frac{\partial h \bar{v}}{\partial y} = w_s \cdots \cdots \cdots (33)$$

where h is the depth of flow, ε^* is the depth-averaged eddy viscosity, τ^s is the surface shear (wind), p^s is the surface pressure, C_f is the bottom friction coefficient, and w_s is the lateral outflow, e.g. evaporation.

Boundary conditions imposed will be discussed in more detail later; however, they basically concern setting the normal velocity to zero at the solid lateral boundaries of the lake. The exceptions are those locations where flow enters or leaves the lake (rivers, causeway culverts, and causeway seepage).

Numerical simulation will again employ the finite element method utilizing quadratic

14

quadrilateral elements. The element geometry and shape will be passed into the convection-dispersion model, along with the velocity field, to predict lake mixing.

Three-Dimensional Hydrodynamic Circulation Model

Prior to development of the three-dimensional mathematical model, the overall strategy is described. An unsteady development will be made with simplification to the steady state model undertaken in the following section detailing the numerical model. The completely formed implicit nature of the finite element technique makes minimization of computer core requirements one criteria in model development. Employing the hydrostatic assumption, the pressure problem will be reduced to one of free surface. The resulting two-dimensional free surface problem will be uncoupled from the solution of the Navier-Stokes equations. Both the non-linear aspects of the Navier-Stokes equations and the uncoupled solution technique imply the necessity of an iterative solution. However, nonlinearity cannot be avoided, and uncoupling not only saves on core requirement, but also allows for the use of an efficient linear symmetric solver for the free-surface portion of the problem.

The right-handed Cartesian coordinate system is used. The x-coordinate direction corresponds to east, y corresponds to north, making the z-coordinate point vertically upward. These coordinates are also denoted as 1, 2, and 3 respectively in the indicial notation which is used periodically. With regard to indicial notation it would be best to note the following: use of a single subscript implies an element of a vector; use of multiple subscripts implies a matrix or tensor; and repeating an index in a single term implies summation unless otherwise noted. For clarity in the mathematical expressions to follow, partial differentiation is denoted by a subscript preceded by a comma.

Navier-Stokes equations

The following equations are an Eulerian description of the movement of a constant density fluid. In the literature these equations are often referred to as describing the conservation of momentum and are commonly known as the Navier-Stokes equations. The equation shown below includes the turbulent Reynolds stress terms. In indicial notation the equations are

$$\frac{du_i}{dt} = F_i - g\delta_{i3} - \frac{1}{\rho} p_{,i} + \left(\frac{\tau'_{ji}}{\rho} - \overline{u'_i u'_j} \right)_{,j}$$

. . . . (34)

in which

u_i = $u_i(x,y,z,t)$ = components of the velocity vector (fps)

p = scalar pressure = $-1/3 \, \tau_{kk}$ (lb/ft^2)

ρ, = density (slug/ft^3)

τ_{ji} = elements of a stress tensor from which the average normal stress (pressure) has been removed (lb/ft^2)

$\overline{u'_i u'_j}$ = elements of the turbulent Reynolds stress tensor (u'_i being the turbulent fluctuation of the u_i component of velocity, ft^2/sec^2)

$\frac{du_i}{dt}$ = total derivative of u_i = $u_{i,t} + u_j u_{i,j}$

t = time (sec)

F_i = force terms (ft/sec^2)

The force terms, F_i, in the above expression are restricted to the coriolis forces, i.e.

$$F_1 = F_x = 2\Omega(v \sin \phi - w \cos \phi)$$

$$F_2 = F_y = -2\Omega u \sin \phi$$

$$F_3 = F_z = 2\Omega u \cos \phi \qquad . \quad . \ (35)$$

in which

u, v, and w = $u_1, u_2,$ and u_3

Ω = angular velocity of the earth (7.2722 x 10^{-5} radians/sec)

ϕ = latitude (radians)

Shear stress and velocity relationships

Within Equation 34 there are two stress terms which require further definition. The first is the shear stress term, τ'_{ji}, which derives from the laminar description of flow. It is assumed that a Newtonian description is adequate to describe the laminar regime. Thus,

$$\tau'_{ji} = \mu D_{ji} = \mu(u_{j,i} + u_{i,j}) \quad . \quad . \quad . \ (36)$$

in which

μ = absolute viscosity (lb-sec/ft)

D_{ji} = deformation tensor (sec^{-1})

When in the laminar regime, the Reynolds stresses ($u'_i u'_j$), are absent. However, application of the present model is, for the most part, in the turbulent regime.

Modeling of the turbulent regime is achieved through the use of the Reynolds stress tensor. Several possible models appear in Hinze (1975). All of these models relate the stress tensor to the deformation tensor. Hinze makes the observation that one may relate two second order tensors through the use of a zero, second, or fourth order

15

tensor. The use of a first order tensor (vector) is not a tractable alternative.

If carefully examined, the zero-order tensor is nothing more than the Newtonian model of Equation 36. The expression is

$$\overline{-u_i'u_j'} = -1/3 \, \overline{u_k'u_k'} \, \delta_{ij} + \varepsilon_s D_{ij}$$

$$. \quad . \quad . \quad . \quad . \quad . \quad . \quad (37)$$

where ε_s is a scalar eddy viscosity, and $1/3 \, \overline{u_k'u_k'}$ develops from a consideration of the contraction of

$$\overline{-u_i'u_j'} = \varepsilon_s D_{ij}. \quad . \quad . \quad . \quad . \quad . \quad . \quad (38)$$

for diagonal terms. This new term is defined as the turbulence pressure, p_t, and is commonly collected with the scalar pressure term, p, to form a single pressure variable.

The second alternative, that of a second-order tensor for eddy viscosity, is more difficult to employ. Hinze (1975) develops the barest details of the second-order tensor. Modelers of hydraulic phenomena have assumed a great deal of freedom on the selection of appropriate eddy viscosity values. This can be readily seen in various reports (Wang and Connor 1975, Spraggs and Street 1975).

Since an alternative of the second-order tensor is to have all off-diagonal values equal to zero, one must retain the turbulence pressure in the model. Consequently, this model is

$$\overline{-u_i'u_j'} + 1/3 \, \overline{u_k'u_k'} \, \delta_{ij} = (\varepsilon_t)_{ik} D_{kj}$$

$$. \quad . \quad . \quad . \quad . \quad . \quad . \quad (39)$$

where $(\varepsilon_t)_{ik}$ is the eddy viscosity tensor. Now, since the Reynolds stress tensor is symmetric, the product of the eddy viscosity and deformation tensor must be symmetric as well. A pseudo vector representation is achieved via a symmetry assumption for the eddy viscosity tensor. The eddy viscosity tensor may be written as

$$(\varepsilon_t)_{ij} = \begin{bmatrix} \varepsilon_1 & \varepsilon_{12} & \varepsilon_{13} \\ \varepsilon_{21} & \varepsilon_2 & \varepsilon_{23} \\ \varepsilon_{31} & \varepsilon_{32} & \varepsilon_3 \end{bmatrix} ; \; i,j = 1,2,3$$

where $(\varepsilon_t)_{ij} = (\varepsilon_t)_{ji}$ and ε_{ij} for $i = j$ is taken to be ε_i. Substitution of these expressions into Equation 34 yields the following three equations

$$\frac{du}{dt} = F_x - \frac{1}{\rho}(p)_{,x} + (\nu + \varepsilon_1)\nabla^2 u + \varepsilon_{12}\nabla^2 v + \varepsilon_{13}\nabla^2 w$$

$$\frac{dv}{dt} = F_y - \frac{1}{\rho}(p)_{,y} + \varepsilon_{12}\nabla^2 u + (\nu + \varepsilon_2)\nabla^2 v + \varepsilon_{23}\nabla^2 w$$

$$\frac{dw}{dt} = F_z - \frac{1}{\rho}(p)_{,z} - g + \varepsilon_{13}\nabla^2 u + \varepsilon_{23}\nabla^2 v + (\nu + \varepsilon_3)\nabla^2 w$$

$$. \quad . \quad . \quad . \quad . \quad . \quad . \quad . \quad (40)$$

in which

$\nabla^2 \phi$ = Laplacian operator = $\phi_{,xx} + \phi_{,yy} + \phi_{,zz}$
ν = kinematic viscosity of the laminar regime = μ/ρ

Variation of eddy viscosity has been assumed small enough to neglect terms including their derivatives.

Application of the numerical model to these equations will result in the expression of boundary conditions in terms of velocities and their gradients. Often one wishes to employ shear stress boundary conditions, and although it is not immediately apparent, the above equations do not allow their use.

Stress boundary conditions derive from the application of the numerical technique to the stress terms. Therefore, consider the following form of the Navier-Stokes equations

$$\frac{du}{dt} = F_x - \frac{1}{\rho}(p)_{,x} + \frac{1}{\rho}\tau_{jx,j}^T$$

$$\frac{dv}{dt} = F_y - \frac{1}{\rho}(p)_{,y} + \frac{1}{\rho}\tau_{jy,j}^T$$

$$\frac{dw}{dt} = F_z - \frac{1}{\rho}(p)_{,z} - g + \frac{1}{\rho}\tau_{jz,j}^T \quad . \quad . \quad (41)$$

in which

$$\tau_{ji}^T = \tau_{ji}' - \overline{\rho u_j'u_i'} + 1/3 \, \overline{\rho u_k'u_k'} \, \delta_{ji}$$

and $j = 1$, 2, and 3. This form of the free surface Navier-Stokes equations, while producing a somewhat more complicated viscous term, does give one the required stress boundary conditions for the problems considered herein.

Hydrostatic pressure assumption

In order to simplify the model, one assumes the pressure to be adequately approximated by its hydrostatic component. The horizontal pressure distribution is therefore a function of the free surface elevation. Thus we have for the pressure the following expression

$$p = (h - z)\rho g + \text{constant} \quad . \quad . \quad . \quad (42)$$

where h is the free surface elevation as a function of time and spatial variables x and y only. Substitution of this approximation will follow application of the numerical technique. This order of events is brought about due to the sequence of differentiation and integration by parts. Failure to employ the pressure term throughout the initial development would bring about a loss of terms in the derivation.

Wind and current-induced boundary stress

Forces which drive the flow are of considerable importance. Aside from the

minor effect of coriolis forces, one must be concerned with the parameterization of free surface wind stresses which drive the fluid, and bottom stresses which inhibit the flow. Both stresses are best modeled as functions of the overlying fluid's velocity.

In the case of wind induced stress the total stress is a sum of surface friction and form drag. However, this hypothesis leads to a coefficient which is a function of wind speed. Such a parameterization is not necessary in a first generation model of this type. Constant wind speed over the entire water body is not an unattractive assumption for testing a model of this complexity. Thus, wind-induced stress is assumed to be a function of the square of the wind speed, i.e.

$$\tau = C \rho |V_w|^2$$

where τ is the total wind induced stress, C is a leading coefficient, V_w is the wind speed, and ρ is the density of the driven fluid. This form, which includes the fluid density, is convenient since the real variable is stress divided by density. Several papers (Cheng et al. 1976, Liggett and Hadjitheodorou 1969, Norton et al. 1973) employ the assumption that a 30 kilometer per hour wind induces a surface stress of one dyne per square centimeter. From such an assumption it may be deduced that the leading coefficient, C, must equal 1.439×10^{-6}.

Application of this expression to the x, y, and z component Navier-Stokes equations requires one to decretize components of the shear. It is assumed in the present model that the wind acts tangential to the free surface. Thus, as the surface slope is altered, so is the wind stress vector. The projected direction of the wind vector is assumed a known constant in the xy plane. Knowing the magnitude and the xy projection, evaluation of the vector's components can be made. Finally, the components of wind induced stress are

$$\tau_x = C \rho u_w |V_w|$$
$$\tau_y = C \rho v_w |V_w|$$
$$\tau_z = C \rho w_w |V_w| \quad . \quad . \quad . \quad . \quad . \quad (43)$$

in which τ_i are the components of the stress vector, and u_w, v_w, and w_w are the wind velocity vector's components in the x, y, and z directions respectively.

A quadratic relationship in velocity is also employed in the parameterization of the bottom stress. The components of the stress vector are

$$\tau_x = C_{fx} \rho u |V|$$
$$\tau_y = C_{fy} \rho v |V|$$
$$\tau_z = C_{fz} \rho w |V| \quad . \quad . \quad . \quad . \quad . \quad (44)$$

where the τ_i are the components of the stress vector, C_{fi} are the bottom friction coefficients, and u, v, and w are the components of the fluid velocity vector, V. The bottom friction coefficients, C_{fi}, are defined as (Wang and Connor 1975)

$$C_{fi} = \begin{cases} 1/8 \ f & : \text{Darcy-Weisbach} \\ g/C^2 & : \text{Chezy} \\ (n/1.49)^2 g/H^{1/3} & : \text{Manning} \end{cases}$$

$$. \quad . \quad . \quad . \quad . \quad (45)$$

where different Darcy-Weisbach friction factors, Chezy C-values or Manning's n may be chosen for the different component directions. For a bottom surface with a Manning's n of 0.025, one finds for a depth of 30 feet a C_f of approximately 0.003.

Mass Conservation

It is already known that only constant-density, incompressible flows will be considered, so the general mass conservation expression is

$$\nabla \cdot \vec{V} = 0 \quad . \quad . \quad . \quad . \quad . \quad . \quad . \quad (46)$$

where

$$\vec{V} = \text{the velocity vector} = u\vec{i} + v\vec{j} + w\vec{k}$$

and

$$\nabla \cdot \vec{V} = \text{divergence of the velocity vector}$$
$$= u_{i,i} = u_{,x} + v_{,y} + w_{,z}$$

Equation 46 is usually referred to as the continuity equation, and is often said to be the incompressibility condition. One should be cautious in this regard since a fluid may be incompressible while not being of constant density.

Kinematic relationship

If one does not allow interaction or transport between the fluids at an interface (i.e. free surface), then one has created a membrane. There will exist a unique relationship between the fluid velocity and the free surface configuration. Consider the following description of the free surface

$$h(x,y,t) - z = 0 \quad . \quad . \quad . \quad . \quad (47)$$

This will be a true expression only at the free surface. Taking this equation's total derivative,

$$w|_{z=h} = h_{,t} + u|_{z=h} h_{,x} + v|_{z=h} h_{,y}$$

$$. \quad . \quad . \quad . \quad . \quad . \quad (48)$$

where $|_{z=h}$ implies evaluation of the preceding expression at z equals h (i.e. at

17

the interface or free surface). Equation 48 is known as the kinematic relationship. Note that as one moves about the free surface, a continuous vertical velocity is dependent upon a continuous representation of not only the horizontal velocities, but also the free surface gradients.

Pressure equation

Several approaches are possible in the development of an uncoupled formulation. An examination of the various approaches leads one to conclude that the basic technique employed in all is the summation of the three Navier-Stokes equations. Prior to their summation each equation is operated on by the partial derivative of its component direction. For example, the x-component equation is operated on by an x partial derivative operator. Using Equations 41 and assuming constant eddy viscosity values, the indicated partials yield

$$\left(\frac{du}{dt}\right)_{,x} = F_{x,x} - \frac{1}{\rho}(p)_{,xx} + \varepsilon_1 A_{,x} + \varepsilon_{12} B_{,x} + \varepsilon_{13} C_{,x}$$

$$\left(\frac{dv}{dt}\right)_{,y} = F_{y,y} - \frac{1}{\rho}(p)_{,yy} + \varepsilon_{12} A_{,y} + \varepsilon_2 B_{,y} + \varepsilon_{23} C_{,y}$$

$$\left(\frac{dw}{dt}\right)_{,z} = F_{z,z} - \frac{1}{\rho}[(p)_{,z} + \rho g]_{,z} + \varepsilon_{13} A_{,z} + \varepsilon_{23} B_{,z}$$

$$+ \varepsilon_3 C_{,z} . \quad . \quad . \quad . \quad . \quad . \quad . \quad . \quad (49)$$

where

$$A = 2u_{,xx} + u_{,yy} + u_{,zz} + v_{,xy} + w_{,xz}$$

$$B = v_{,xx} + 2v_{,yy} + v_{,zz} + u_{,xy} + w_{,yz}$$

$$C = w_{,xx} + w_{,yy} + 2w_{,zz} + u_{,xz} + v_{,yz}$$

While it would be attractive to include all terms in the computations, there is a great motivation to eliminate the third derivative terms. Their evaluation within the proposed numerical technique would require the inversion of a ten by ten matrix at each of the integration points within the model. Such a computation is prohibitive in a nonlinear, iterative model, and Olson (1976) has shown it to be unnecessary. Thus, our equation is

$$\frac{1}{\rho}[(p)_{,xx} + (p)_{,yy} + ((p)_{,z} + \rho g)_{,z}]$$

$$= 2\Omega(v_{,x} - u_{,y})\sin\phi + (u_{,z} - w_{,x})\cos\phi]$$

$$- \left[\frac{dD}{dt} + u_{,x}^2 + v_{,y}^2 + w_{,z}^2 + 2u_{,y}v_{,x}\right.$$

$$\left. + 2v_{,z}w_{,y} + 2u_{,z}w_{,x}\right] . \quad . \quad . \quad . \quad (50)$$

where d/dt is the total derivative and D is the divergence of the velocity vector. Note that the total derivative of the divergence

of velocity is more meaningful in a steady-state analysis than the partial derivative which is employed in unsteady analysis. The above formulation of the pressure problem is employed in the current model.

Convection-Dispersion Model

A substance will diffuse proportionally to its concentration gradient. This process is known as Fick's law of diffusion. This first law states,

$$\frac{dm}{dt} = - D_m \frac{\partial c}{\partial s}$$

in which

$\frac{dm}{dt}$ = the rate of transport of substance

c = concentration of diffusive substance

D_m = molecular diffusion coefficient

s = coordinate normal to the unit area through which it passes

This phenomenon is caused by molecular diffusion. If there is no turbulence this basic law applied to a mass balance within a differential control volume would be the governing equation for the process of diffusion.

Turbulent diffusion

When a flow field is turbulent, the substance mixes at a much greater rate than under Fickian diffusion. This is because of the fluid's variance from its average motion. Applying a mass balance to a differential control volume and then time-averaging the terms and utilizing an analogy to Fick's law yields the following convection-diffusion equation,

$$\frac{\partial \bar{c}}{\partial t} + \bar{u}\frac{\partial \bar{c}}{\partial x} + \bar{v}\frac{\partial \bar{c}}{\partial y} + \bar{w}\frac{\partial \bar{c}}{\partial z} = (D_m + e_x)\frac{\partial^2 \bar{c}}{\partial x^2}$$

$$+ (D_m + e_y)\frac{\partial^2 \bar{c}}{\partial y^2} + (D_m + e_z)\frac{\partial^2 \bar{c}}{\partial z^2} . \quad . \quad (51)$$

in which

$\bar{c}$ = time averaged concentration of diffusive substance

x, y, z = orthogonal coordinates (Cartesian)

$\bar{u}, \bar{v}, \bar{w}$ = time averaged velocities in x, y, and z directions, respectively

D_m = molecular diffusion coefficient

e_x, e_y, e_z = turbulent diffusion coefficients in x, y, and z directions, respectively

The turbulent diffusion coefficients are the result of turbulent mixing and designate how the turbulent flow affects the diffusive process.

18

It is clear that the combined diffusion coefficients ($D_m + e_x$, $D_m + e_y$, $D_m + e_z$) for a turbulent flow field must be substantially greater than the diffusion coefficient in Fickian diffusion (D_m) because the turbulence greatly increases the rate at which a substance will diffuse. Consequently, the Fickian coefficient is neglected in turbulent flow.

Dispersion

In integrating Equation 51 in the z-direction to form a two-dimensional equation, the effect of the vertically varying velocity on convection must be accounted for. This vertical variation in velocity causes an additional lateral spreading when viewed in the horizontal x-y plane and the phenomenon is referred to as dispersion. To compensate for this event, the diffusion coefficients must be increased to accurately represent what occurs. Rewriting Equation 51 in two-dimensions, dropping the bar notation, and adding a source-sink term and a decay term while changing the diffusion coefficient to a dispersion coefficient gives the following convection-dispersion equation,

$$\frac{\partial c}{\partial t} + u\frac{\partial c}{\partial x} + v\frac{\partial c}{\partial y} - \frac{\partial}{\partial x}\left(D_x\frac{\partial c}{\partial x}\right) - \frac{\partial}{\partial y}\left(D_y\frac{\partial c}{\partial y}\right)$$

$$+ \alpha + \beta = 0 \quad . \quad . \quad . \quad . \quad . \quad . \quad (52)$$

in which

c = concentration of dispersive substance

x,y = orthogonal coordinates (Cartesian)

D_x, D_y = dispersion coefficients in x and y directions, respectively

u,v = vertically averaged component velocities in x and y directions, respectively

α = source-sink term

β = decay term (function of c)

t = time

The dispersion coefficient is a combination of the molecular, turbulent, and dispersive effects.

Use of convection-dispersion equation

Equation 52 is used to model the dispersion of a concentrated substance in a fluid flow. The dependent variable is the concentration. All of the other parameters are considered known throughout the entire domain. The physical geometry supplies all of the spatial information. The substance has its own decay rate. The source-sink term simulates physical injections of substance. The velocities are supplied by either field or laboratory measurements or the numerical steady-state hydrodynamic model referred to earlier.

Assumptions used in model application

Because this model is being developed to apply to the upper layer of Great Salt Lake's south arm, simplifying assumptions made should not detract from the model's ability to simulate the prototype. In accordance with these objectives, three basic assumptions made about the south arm's layer are incorporated in the model. They are as follows:

1. The south arm's upper layer has no variation in depth and a two-dimensional process is assumed. Since the layer's depth is very small compared to its areal extent, the use of a two-dimensional model seems justified.

2. The layer is of constant density and the dispersive substance does not change the layer's density.

3. The dispersive substance is well-mixed in the vertical direction. The wind and wave action on the shallow lake layer should make this a valid assumption.

These assumptions allow the use of Equation 52 in developing a solution to mixing problems in the upper layer of Great Salt Lake's south arm.

Transfer of salinity into upper layer of south arm

The assumed mechanism for introduction of salinity into the upper layer of the south arm of the lake is the entrainment of salinity from the saturated lower layer. Because molecular diffusion is not adequate to account for measured salinity transfer, it is believed that interfacial shear and the subsequent turbulence generated at the interface (pycnocline) is the most logical cause of relatively high entrainment rates.

Accordingly, a laboratory study was made to determine the dependency of entrainment on interfacial shear. The interfacial shear was presumed dependent on the velocity differences in the two layers. Because of the experimental nature of the problem, the characteristic parameters of the system were verified and formed into dimensionless groups for purposes of data analysis and presentation. The set of characteristic parameters were determined to be:

D = depth of the bottom layer $\doteq L$ ($\doteq$ defined as 'dimensionally')

ΔV = velocity difference between the upper and lower layers $\doteq LT^{-1}$

κ = rate of salinity transport (entrainment) per unit area = $FL^{-2}T^{-1}$

$\Delta\rho$ = density difference between the upper and lower layers = FT^2L^{-4}

ρ_u = density of upper layer = FT^2L^{-4}

19

g = acceleration due to gravity = LT^{-2}

ν_u' = kinematic viscosity of upper layer = L^2T^{-1}

Deciding to represent, within the model, the lower layer of the southern basin as essentially stagnant allowed the kinematic parameter, ΔV, to be further reduced to V_u, the upper layer velocity.

Having a set of seven parameters with three independent dimensions requires four dimensionless groups to accurately define the system. These parameters were arranged as follows

$$\frac{\kappa D}{V_u^3 \Delta \rho} = f\left(\frac{V_u D}{\nu_u} , \frac{\Delta \rho}{\rho_u} , \frac{\Delta \rho g D}{\rho_u V_u^2}\right) \quad . \quad . \quad (53)$$

in which

$\dfrac{V_u D}{\nu_u}$ = Reynolds number (Re)

$\dfrac{\Delta \rho g D}{\rho_u V_u^2}$ = Richardson number (Ri)

These four dimensionless numbers are presumed to represent the stratified flow condition of the southern basin, thus permitting a model to be designed.

For fluid-flow conditions with large Reynolds numbers (turbulent flow), the effects of viscosity are small. This situation causes the viscosity to no longer be a characteristic parameter of the phenomenon, thereby making it possible to remove the Reynolds number from the list of dimensionless parameters. Based upon the kinematic and geometric conditions within the Salt Lake, a Reynolds number range of approximately 300,000 to 1,000,000 is estimated, thereby satisfying the necessary condition of turbulent flow. Thus, the initial seven defining quantities have been reduced to six which is a manageable number of quantities to permit modeling the interfacial shear zone of the Great Salt Lake in the laboratory.

Chosen now are the following three scale factors: $g_r = 1$, $\Delta \rho_r / \rho_{u_r} = 1$, and $D_r = 10$, where D_r is the ratio of prototype to model depth.

Specifying that the Richardson numbers are equal in model and prototype gives the following equation expressing relationships between model-prototype parameter ratios.

$$\frac{\Delta \rho_r \; g_r \; D_r}{\rho_{u_r} \; V_{u_r}} = 1 \quad . \quad . \quad . \quad . \quad . \quad (54)$$

Further specifying that the fluid densities in model and prototype are equal ($\rho_{u_r} = 1$ and $\Delta \rho_{u_r} = 1$) results in the following relations for velocity and time ratios.

$$V_r = \sqrt{D_r} \quad . \quad . \quad . \quad . \quad . \quad . \quad (55)$$

$$T_r = \sqrt{D_r} \quad . \quad . \quad . \quad . \quad . \quad . \quad (56)$$

Combining the dimensionless expression containing κ

$$\kappa_r = \frac{V_{u_r}^3 \; \Delta \rho_{u_r}}{D_r} \quad . \quad . \quad . \quad . \quad . \quad (57)$$

With Equations 54, 55, and 56 reveals that

$$\kappa_r = \sqrt{D_r} \quad . \quad . \quad . \quad . \quad . \quad . \quad (58)$$

The known velocity range within Great Salt Lake does not exceed 1.0 fps, hence the maximum model velocity becomes 0.316 fps. The model Reynolds number based upon these velocities is still large enough to represent turbulent flow in the model.

To summarize, a laboratory model one-tenth the depth of Great Salt Lake's bottom layer has been designed. The fluids used are similar in density to those found within Great Salt Lake. Flow velocities in the model range up to a maximum of 0.32 fps.

The mathematical models of the previous section must now be transformed into numerical models. Two differing approaches may be taken in developing steady state finite element models. There is the method of weighted residuals, which is the classical straight-forward theory applying to differential equations, and the more physically meaningful development resulting from the energy approach of Oden (1971). For clarity, the method of weighted residuals is presented. The discussion below is intended only as an outline of the finite element method (FEM). For a more detailed development of the concepts involved, the reader is referred to Zienkiewicz (1977). Following the general development, application of this technique will be made to each of the previously developed mathematical models.

Galerkin Method of Weighted Residuals

A brief description of the method of weighted residuals will be given. One begins with the partial differential equation (PDE) representing the physical system

$$L[r(x,y,z,t)] = f(x,y,z,t)$$

where L represents the partial differential operator, $r(x,y,z,t)$ represents the dependent variables, and $f(x,y,z,t)$ is the collection of terms which do not involve a differential process. An approximation to the unknown exact solution is sought. The approximation will take the form

$$L[r(x,y,z,t)] = f(x,y,z,t)$$

$$r_n^*(x,y,z,t) = c_k B_k(x,y,z,t);$$

$$k = 1,2, ..., n \quad . \quad . \quad . \quad . \quad (59)$$

where c_k are constants (to be determined) and the B_k a set of n functions. One might be fortunate enough to select a set of functions in which the exact solution lies. However, in general, the approximation will differ in some hopefully small way from the exact solution. Substituting the approximation, one finds that the PDE no longer yields an exact equality. It is written as

$$L[r_n^*(x,y,z,t)] - f(x,y,z,t) = R_n(x,y,z,t)$$

$$. \quad . \quad . \quad . \quad . \quad . \quad (60)$$

where $R_n(x,y,z,t)$ is denoted the residual.

The method of weighted residuals arises from setting to zero the inner product of this residual and an arbitrary set of weight functions. Thus

$$(W_i, R_n) = 0 \quad . \quad . \quad . \quad . \quad . \quad (61)$$

where the inner product (u,v) is defined by

$$(u,v) = \int_\Omega uv \, dxdydz$$

and the domain, Ω, is assumed to be three-dimensional. Setting the inner product to zero forces the residual to be orthogonal to the weight functions. Substituting Equation 60 into Equation 61, one finds

$$\int_\Omega W_i (L[r_n^*(x,y,z,t)] - f(x,y,z,t)) \, dxdydz = 0 \quad . \quad . \quad (62)$$

where $i = 1,2, ..., n$ so that n equations result for the solution of the n different constants, c_k. The result is that the constants c_k are selected such that the residual is forced to zero in an average sense.

An appropriate selection of weight functions must now be made. Different selections lead to different forms of the method of weighted residuals. Common forms are the collocation method, the least squares method, and the Galerkin method. The best known and most appropriate form for the present model is that of Galerkin. This technique requires that one select the weighting functions, W_i, to be identical to the approximating functions. Equation 62 becomes

$$\int_\Omega B_i (L[c_k B_k(c,y,z,t)] - f(x,y,z,t)) \, dxdydz = 0 \quad . \quad . \quad (63)$$

where i, k = 1,2,3, ..., n. With the residual forced to be orthogonal to each of the approximating functions, one is able to find the best approximation to the exact solution.

Historically the Galerkin method of weighted residuals was developed as a Rayleigh-Ritz technique. As such, the approximating and weight functions are defined upon the entire domain. Each point used in the approximating functions is related in some way to every other point. Thus, setting the problem's equations into a matrix framework one would readily see a full stiffness matrix. The finite element method remedies this situation by discretizing the domain and thereby localizing the approximation's interconnectedness. The development of these ideas follows.

Finite Element Method

Several key points delineate the finite element model, but fundamental to all is the discretization of the total or global domain into subdomains. Equations or expressions unique to the subdomains are often described as local, and the subdomains themselves are often called elements. A second key point, and one that makes discretization work is the definition of local approximating functions. Fundamental to local approximating functions is their reformation as interpolation or shape functions which product elemental (or local) degrees of freedom. The third criteria is the replacement of the global integration with a summation of local integrations. Finally, recognizing that the degrees of freedom are the unknowns (e.g. velocity, pressure, potential, concentration), and that they are constant for a given iteration, one removes them from the integrand and achieves a matrix formation of the finite element method. Each of these ideas will be discussed in the following paragraphs.

Discretization of the global problem domain is conceptually easy to visualize. One is simply dividing the global domain, Ω, into a family of interconnected local domains, Ω_e. Prior to making the discretization, one must consider the shape of elements to be employed in the analysis. Obviously, acutely angular domains in two dimensions are well suited for the use of triangular elements. Domains of a rectangular character may be better solved by employing elements of a rectangular shape. Of course, any rectangular domain can be discretized for triangular shaped elements; however, the increased degrees of freedom of a triangular mesh may well make such a decision economically unattractive. The present discussion is general in scope, so as not to require a specific element selection at this time.

As a result of discretization, one can treat each element individually. Then, by moving through the entire sequence of ele-

ments, one arrives at a complete or global formulation for the given problem. Regardless of the discretization's local shape, a sparse global matrix formulation is achieved. This gives rise to economies of solution and core storage in the numerical scheme. This point distinguishes the finite element technique from that of the Rayleigh-Ritz.

Use of elements to describe the global domain forces one to redefine the global approximating functions, $c_k B_k$, on a local domain. Each element being characteristically identical, one may couple the element or local approximating functions and thus achieve a global approximation. Mention should be made of the form which the approximating function takes in this analysis. First, one should note that sets of monomials (polynomials) are employed almost exclusively due to their integration and differentiation properties. In the research reported herein they are employed to the exclusion of trigonometric or exponential functions. Secondly, it has been found convenient to not only redefine the approximating functions locally, but to reform them into what are called interpolating polynomials or shape functions. This new form of the approximating functions gives rise to what are known as nodal degrees of freedom. For the sake of clarity a one-dimensional example is developed in the following discussion.

To illustrate the concepts of shape functions and nodal degrees of freedom, consider the quadratic approximation on the unit interval [0,1]. Note that the approximating functions of Equation 59 may simply be redefined on the unit interval, i.e.

$$r_3^*(x) = c_1 B_1 + c_2 B_2 + c_3 B_3$$
$$= c_1(1) + c_2(x) + c_3(x^2) \qquad . \quad . \quad (64)$$

where the independent variable, x, is defined on the interval [0,1]. If we assume to know the values of $r_3^*(x)$ at three selected points, we may write three equations and solve for the coefficients, c_i. For example, select the points 0, 1/2, and 1, and we have the following set of equations.

$$r_3^*(0) = c_1$$
$$r_3^*(\tfrac{1}{2}) = c_1 + \tfrac{1}{2}c_2 + \tfrac{1}{4}c_3 \qquad . \quad . \quad . \quad . \quad (65)$$
$$r_3^*(1) = c_1 + c_2 + c_3$$

Solution of these equations yields

$$c_1 = r_3^*(0)$$
$$c_2 = -3r_3^*(0) + 4r_3^*(\tfrac{1}{2}) - r_3^*(1) \qquad . \quad . \quad (66)$$
$$c_3 = 2[r_3^*(0) - 2r_3^*(\tfrac{1}{2}) + r_3^*(1)]$$

Substituting these expressions into our local approximating function and collecting

monomials which multiply the point values of $r_3^*(x)$, one finds the following expressions (where point values of $r_3^*(x)$ are denoted r_k; $k = 1, 2$, and 3 for $x = 0, 1/2$, and 1 respectively)

$$r_3^*(x) = (2x-1)(x-1)\ r_1 + 4x(1-x)\ r_2$$
$$+ x(2x-1)\ r_3 . \quad . \quad . \quad . \quad . \quad (67)$$

Figure 5 depicts the approximating functions represented in Equations 64 and 67. One can see that each set of functions serves to approximate any variable, $r_3^*(x)$ on the unit interval. However, the latter form's polynomials have the character of being zero valued at two of the three points (0, 1/2, 1). At their single non-zero point the functions have a unit value. Associated with each polynomial is a point value of the variable, $r_3^*(x)$. In finite element terminology one denotes a preselected point as a node, the interval as an element, and values of the variable, $r_3^*(x)$, at the prescribed points as nodal degrees of freedom. The characteristic values of the interpolating polynomials give rise to characteristic shapes, thus the name shape functions. Finally, we rewrite Equation 67 as a summation of shape functions produced with nodal degrees of freedom. Thus we have

$$r_3^*(x) = N_1(x)r_1 + N_2(x)r_2 + N_3(x)r_3$$
$$= N_k(x)r_k;\ k = 1,2,3 \quad . \quad . \quad . \quad (68)$$

where

$$N_1(x) = (2x-1)(x-1)$$
$$N_2(x) = 4x(1-x)$$
$$N_3(x) = x(2x-1)$$

The terminology of interpolating polynomial, interpolating function, and shape function will be used interchangeably in the sections to follow. In the section which discuss the hybrid element, the concept of nodal degrees of freedom will be expanded to include derivative information of the variable. Such nodes are denoted multiple degree of freedom nodes.

The final concept in the finite element method is the replacement of the global integration of Equation 63 with a summation of elemental or local integrations. This is achieved through the proper definition of the interpolating polynomials. Proper definition is a function of the completeness and compatibility of the polynomials as discussed in Zienkiewicz (1977). Both criteria deal with the selection of monomials which yield correct integrations. Equations 63 may be rewritten as

$$\sum_{e=1}^{m} \int_{\Omega_e} N_i(L[N_k r_k])\ dxdydz = \sum_{e=1}^{m} \int_{\Omega_e} N_i\ f\ dxdydz$$
$$\quad . \quad . \quad . \quad . \quad . \quad . \quad . \quad . \quad (69)$$

Approximating functions, B_i

1). $\quad$ 1

2). $\quad$ x

3). $\quad$ x^2
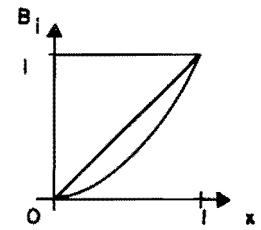
Interpolating polynomials or shape functions, N_i

1). $\quad$ $(2x-1)(x-1)$

2). $\quad$ $4x(1-x)$

3). $\quad$ $x(2x-1)$
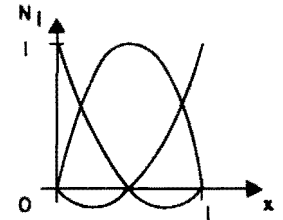
Figure 5. One-dimensional quadratic interpolation functions.

where i, $k = 1, 2, ..., n$; n equals the number of elemental degrees of freedom; and m equals the number of elements in the discretized domain. Before this integral expression is complete, it must be cast into a matrix form. This is achieved by recognizing that the solution of the problem is an evaluation of the nodal degrees of freedom. For a given time step, or iteration, the nodal degrees of freedom are constant, and for this reason, they may be extracted from the integrand. As an example, for a linear problem

$$\sum_{e=1}^{m} \int_{\Omega_e} \{N_i\}(L[\{N_k\}^T])dxdydz\ \{r_k\}$$
$$= \sum_{e=1}^{m} \int_{\Omega_e} \{N_i\}\ f\ dxdydz \quad . \quad . \quad . \quad . \quad (70)$$

where $\{\ \}$ implies a column vector and $\{\ \}^T$ implies a row vector. Of course, for a non-linear operator, L, the operator equation is dependent upon the dependent variable and not only its shape function. The summation of elemental integrations implies the formation of a global set of equations. This is achieved through the interconnectedness of the elemental nodal degrees of freedom.

This is essentially the Galerkin finite element method. There are a great many details which have been omitted. However, a complete development of the finite element method is not within the scope of this investigation. For details on the completeness and compatibility of interpolating polynomials, the selection of appropriate shape functions, and a multitude of other details, the reader is referred to any of several books on the finite element method (Finlayson 1972, Oden 1972, Zienkiewicz 1977).

Isoparametric elements

Due to the irregular shape of natural occurring geometries, it is assumed that some accommodation must be made for their curvilinear boundaries. This accommodation takes the form of an isoparametric finite element formulation. In the case of a three-dimensional domain, the isoparametric formulation handles arbitrary Cartesian geometry by establishing a unique map between the unit cube, $[0,1]^3$, and each element. All computations are carried out on the unit cube. Thus, the shape functions are defined on the cube, and all integrations are on either the cube itself or its boundaries. In two-dimensional problems one maps between the Cartesian geometry and a unit square $[0,1]^2$. Two difficulties arise in the use of isoparametric elements. First, they require numerical integration, which is discussed in the next subsection. Secondly, their use requires that a relationship be developed between derivatives in the natural coordinates (of the unit cube) and derivatives in the Cartesian coordinates.

For the development of derivative information, we must first define the mapping between the unit domain and the Cartesian geometry. For three-dimensional problems the isoparametric transformations are

$$x = \{N_k(\xi,\eta,\zeta)\}^T \{x_k\}$$

$$y = \{N_k(\xi,\eta,\zeta)\}^T \{y_k\} \qquad . \quad . \quad . \quad . \quad (71)$$

$$z = \{N_k(\xi,\eta,\zeta)\}^T \{z_k\}$$

where $k = 1, 2, \ldots, n$; n being the number of elemental degrees of freedom; the N_k are functions of the unit cube's natural coordinates, (ξ, η, ζ); and the x_k, y_k, and z_k are vectors of element nodal coordinates. In isoparametric transformations the interpolating polynomials employed to interpolate the geometry are identical to those used to interpolate the dependent variables.

Having a parameterization of the Cartesian geometry in terms of the natural coordinates enables one to relate the derivatives of the two coordinate systems to one another. Toward this end consider the chain rule expansions of the natural coordinate derivatives. They are

$$N_{,\xi} = N_{,x}\, x_{,\xi} + N_{,y}\, y_{,\xi} + N_{,z}\, z_{,\xi}$$

$$N_{,\eta} = N_{,x}\, x_{,\eta} + N_{,y}\, y_{,\eta} + N_{,z}\, z_{,\eta}$$

$$N_{,\zeta} = N_{,x}\, x_{,\zeta} + N_{,y}\, y_{,\zeta} + N_{,z}\, z_{,\zeta}. \quad . \quad (72)$$

Written in matrix form one has

$$\begin{Bmatrix} N_{,\xi} \\ N_{,\eta} \\ N_{,\zeta} \end{Bmatrix} = \begin{bmatrix} x_{,\xi} & y_{,\xi} & z_{,\xi} \\ x_{,\eta} & y_{,\eta} & z_{,\eta} \\ x_{,\zeta} & y_{,\zeta} & z_{,\zeta} \end{bmatrix} \begin{Bmatrix} N_{,x} \\ N_{,y} \\ N_{,z} \end{Bmatrix} = [J] \begin{Bmatrix} N_{,x} \\ N_{,y} \\ N_{,z} \end{Bmatrix}$$

$$. \quad . \quad . \quad . \quad . \quad . \quad . \quad (73)$$

where $[J]$ is known as the Jacobian. Producting both sides of this expression with the coefficient matrix's inverse, one finds

$$\begin{Bmatrix} N_{,x} \\ N_{,y} \\ N_{,z} \end{Bmatrix} = [J]^{-1} \begin{Bmatrix} N_{,\xi} \\ N_{,\eta} \\ N_{,\zeta} \end{Bmatrix}$$

$$= \frac{1}{|J|} \begin{bmatrix} (y_{,\eta}z_{,\xi}-y_{,\xi}z_{,\eta}) & -(y_{,\zeta}z_{,\xi}-y_{,\xi}z_{,\zeta}) & (y_{,\zeta}z_{,\eta}-y_{,\eta}z_{,\zeta}) \\ -(x_{,\eta}z_{,\xi}-x_{,\xi}z_{,\eta}) & (x_{,\zeta}z_{,\xi}-x_{,\xi}z_{,\zeta}) & -(x_{,\zeta}z_{,\eta}-x_{,\eta}z_{,\zeta}) \\ (x_{,\eta}y_{,\xi}-x_{,\xi}y_{,\eta}) & -(x_{,\zeta}y_{,\xi}-x_{,\xi}y_{,\zeta}) & (x_{,\zeta}y_{,\eta}-x_{,\eta}y_{,\zeta}) \end{bmatrix}$$

$$\bullet \begin{Bmatrix} N_{,\xi} \\ N_{,\eta} \\ N_{,\zeta} \end{Bmatrix} \qquad . \quad . \quad . \quad . \quad . \quad . \quad . \quad . \quad (74)$$

where the determinant of the Jacobian is

$$|J| = x_{,\zeta}(y_{,\eta}z_{,\xi}-y_{,\xi}z_{,\eta}) - y_{,\zeta}(x_{,\eta}z_{,\xi}-x_{,\xi}z_{,\eta})$$

$$+ z_{,\zeta}(x_{,\eta}y_{,\xi}-x_{,\xi}y_{,\eta}) \quad . \quad . \quad . \quad . \quad (75)$$

The geometry derivatives (i.e. $x_{,\xi}$, $x_{,\eta}$ etc.) may readily be evaluated from Equation 71. Thus one has achieved a tractable form of evaluating the first derivative Cartesian expressions in three-dimensional analyses.

Consider for a moment the possibility of evaluating second or third-order derivatives. In the case of the pressure formulation in the three-dimensional analysis, one might contemplate the latter. For the first derivative situation three derivatives exist, and consequently a three by three matrix is inverted to develop the necessary derivative expressions. The parallel to be drawn is that the number of derivatives determines the size of the matrix to be inverted. In the case of second derivatives, there are six derivative expressions, and a six by six matrix must be inverted. Finally, in the case of third derivatives, there are ten derivative expressions indicating the inversion of a ten by ten matrix. One can now appreciate the economy of neglecting expressions with third derivatives in the three-dimensional pressure formulation.

Numerical integration

In the previous subsection on isoparametric elements it was mentioned that their use required the simultaneous use of numerical integration. Exact integration

would be possible, although cumbersome, only if the integrands were comprised of simple polynomials. An examination of Equation 74 reveals that a polynomial denominator has been introduced into our integrands containing first derivatives. One no longer has a simple polynomial, and exact integration may be impossible. At this point, numerical integration is the obvious choice.

Two points should be noted prior to the development of numerical integration techniques. First, one must be aware that both domain, Ω, and domain boundary, $\partial\Omega$, integrations are carried out on the unit cube or unit square. In paragraphs to follow, the domain integration will be considered. The somewhat cumbersome boundary integrations for three-dimensional domains are developed in the work of Kincaid (1979). Secondly, since integration is always on the unit cube, one may wish to store integration information on peripheral devices for repeated use.

Due to the polynomial character of our integrals, Gaussian quadrature is employed in their numerical evaluation. From Stroud (1971) it is known that in one dimension, employing m integration points yields the exact integration of a 2m-1 degree polynomial. For example, for a linear polynomial one uses a one-point rule, and for a quadratic or cubic polynomial, one uses a two-point rule. Since the posed problems are in two and three dimensions, one simply applies this integration technique to each dimension. In two dimensions the linear rule would exactly integrate a bi-linear polynomial. Similarly, the cubic rule would exactly integrate a bi-cubic polynomial. The extension to three dimensions is analogous.

Boundary conditions

In discussing both the problem formulation and the numerical results some terminology regarding the boundary conditions is required. From the finite difference literature one has Dirichlet and Neumann boundary conditions. Boundary conditions are differentiated according to the type of information specified. Defining a nodal velocity value is a Dirichlet boundary condition. A Neumann specification defines a nodal velocity gradient. The finite element literature spawns the phrases geometric and natural boundary conditions. These terms define how a boundary condition is preset. Geometric conditions refer to specifying nodal quantities of either Dirichlet or Neumann character. Natural boundary conditions arise through the boundary integrals. Often, the boundary integrand is recognized as a physically meaningful quantity. Setting it to zero defines a homogeneous natural boundary condition. Evaluation of the boundary integral results in a nonhomogeneous natural boundary condition. The homogeneous or nonhomogeneous description is used with the Dirichlet, Neumann, and geometric boundary condition descriptions as well.

Seepage Model

Both a single domain and two domain problem formulation were examined during the period of model development. The governing PDE (Equation 6) is identical for both approaches to a numerical solution. Essentially identical models result from both formulations. Only the handling of interface boundary conditions and the movement thereof delineates the two models. Quadratic, quadrilateral elements are employed.

Application of the Galerkin method of weighted residuals to Equation 6 yields

$$\int_{\Omega} N_i \left[k_x (p/\rho g + y)_{,xx} + k_y (p/\rho g + y)_{,yy} \right] dxdy = 0 \qquad . \qquad (76)$$

where the N_i are shape functions for $i = 1, 2, ..., n$, n being the number of degrees of freedom. Unnecessarily high polynomial degrees can be avoided by reducing the order of differentiation within the integrand. Green's second identity applied to Equation 76 gives

$$-\int_{\Omega} N_{i,x}\, k_x (p/\rho g + y)_{,x}$$
$$+ N_{i,y}\, k_y\, (p/\rho g + y)_{,y}\, dxdy$$

$$+\int_{\partial\Omega} N_i \left[k_x (p/\rho g + y)_{,x}\, \ell_y \right.$$
$$\left. + k_y\, (p/\rho g + y)_{,y}\, \ell_y \right] ds = 0 \qquad . \qquad (77)$$

where ℓ_x and ℓ_y are the direction cosines of the outward directed normal. Employing local interpolant for pressure and local or element integration, one finds the finite element analogue of Equation 77 to be

$$-\sum_{e=1}^{m} \int_{\Omega_e} k_x \{N_{i,x}\}\{N_{j,x}\}^T$$
$$+ k_y \{N_{i,y}\}\{N_{j,y}\}^T\, dxdy\, \{p_j\}$$

$$=\sum_{e=1}^{m} \int_{\partial\Omega_e} N_i \left[k_x\, P_{,x}\, \ell_x + k_y\, (P_{,y} + \rho g)\, \ell_y \right] ds$$
$$+\sum_{e=1}^{m} \int_{\Omega_e} N_{i,y}\, k_y\, \rho g\, dxdy \qquad . \qquad . \qquad . \qquad (78)$$

where i and j are the local degrees of freedom, and m is the number of elements.

Boundary conditions

The boundary integral on the right hand side of Equation 78 is a natural boundary condition. It describes the flux through an external boundary of the domain. In the case of a single domain formulation, both the free surface and the impervious boundary of the domain require that this term be zero. This is a homogeneous natural boundary condition. For the two-domain case, the interface boundary is also a homogeneous natural boundary condition. Of course, in the interior of the problem the boundary integral is never evaluated. The resulting final form of the equation is

$$\sum_{e=1}^{m} \int_{\Omega_e} k_x \{N_{i,x}\}\{N_{j,x}\}^T + k_y \{N_{i,y}\}\{N_{j,y}\} \, dxdy \, \{P_j\}$$

$$= \sum_{e=1}^{m} \int_{\Omega_e} k_y \, N_{i,y} \, \rho g \, dxdy \quad . \quad . \quad . \quad . \quad . \quad (79)$$

where the density is that of the element being modeled. Figure 6 and Table 1 combine to give a summary of the boundary conditions applicable to the external boundaries of the domain. The resulting formulations are both symmetric and banded. A Cholesky solver was employed to solve the global equation systems.

Solution schemes

As mentioned previously, the problem of stratified bi-directional potential flow cannot be formulated explicitly because the locations of the free surface and density interface are not known a priori. However, it is known that both of these surfaces must satisfy the homogeneous natural boundary condition. It is also known that pressure must be continuous across the interface and that pressure on the free surface is atmospheric. The final solution can then be found by 1) assuming locations of these two surfaces, 2) enforcing either the Neumann or the Dirichlet boundary condition at each surface, and 3) adjusting the free surface and density interface based on how well the other boundary condition is met. This procedure is repeated until a desired tolerance is met.

There are two schemes possible for solving this problem with a pressure schemes possible for solving this problem with a pressure formulation. The first scheme employed was to model the problem as a single domain with the interface delineated as a string of interior element edges. In this formulation the pressure continuity on the interface is automatically met, so the solution technique must be keyed to whether or not the Neumann condition is met along this interior surface. Because velocities are derivative properties and only C^o continuous elements are used, it was questionable whether this method would converge.

The second scheme was similar to that used by Cheng and Hu (1975) except that the modeling parameter was pressure rather than piezometric head. The problem domain was divided into two constant-density regions. The homogeneous Neumann boundary condition was employed along the upper and lower boundaries for both regions. This natural boundary condition is automatically met along these surfaces for both regions when Equation 79 is used to formulate the element equations. The testing criteria for the density interface is whether or not the pressures in the upper and lower regions are equal along the interface. The Dirichlet boundary conditions along the sides for both schemes are simply the hydrostatic pressures of the overlying fluid.

Since little is known of the permeability properties of the causeway fill to which this model is applied, isotropic permeabilities have been assumed. Anisotropy has been introduced in the model development with the only restriction being that the local coordinate axes must coincide with the major and minor permeability axes of the soil matrix.

Culvert Model

The Galerkin method of weighted residuals was applied to Equations 17 through 20 following substitution of the constitutive relationship and a velocity squared parameterization of edge shear stress. Applying Green's second identity (integration by parts) and the boundary shear stress relationships, one obtains the equations shown in Table 2. Solution techniques presented by Kawahara et al. (1976), Norton et al. (1973), and Gartling (1974) were examined before programming the Newton-Raphson and Picard iteration techniques. Due largely to its initial successes, the Newton-Raphson procedure was selected for the culvert flow analysis.

In general the application of the Newton-Raphson scheme to a system of n equations in n unknowns is represented by

$$[J] \, \{\Delta x\} = \{F(x^{(m)})\} \quad . \quad . \quad . \quad . \quad (80)$$

where

$\{\Delta x\} = \{x(m) - x(m+1)\}$ = vector of incremental unknowns

$\{F(x^{(m)})\}$ = the equations f_1 evaluated using the previous iterate of the dependent variable, $x(m)$

Table 1. Boundary conditions on the seepage domain.

| Boundary	Label	Type	Relationship
Entrance, exit	A	Essential, Geometric Dirichlet	$p = \rho_u \, g \, (H_1 - y)$
Exit	B	Essential, Geometric Dirichlet	$p = \rho_\ell \, g \, (H_3 - y) + \rho_u \, g \, (H_1 - H_3)$
Entrance, exit	C	Essential, Geometric Dirichlet	$p = \rho_\ell \, g \, (H_2 - y)$
Free surface	D	Essential, Geometric Dirichlet Natural Boundary Condition Neumann	$p = $ atmospheric pressure $v_n = $ normal velocity $= 0$
Interface	E	Essential, Geometric Dirichlet	P (upper domain) $= P$ (lower domain)
Impervious layer	F	Natural Boundary Condition Neumann	$v_n = $ normal velocity $= 0$
Seepage face	G	Essential, Geometric Dirichlet	$P = $ atmospheric pressure
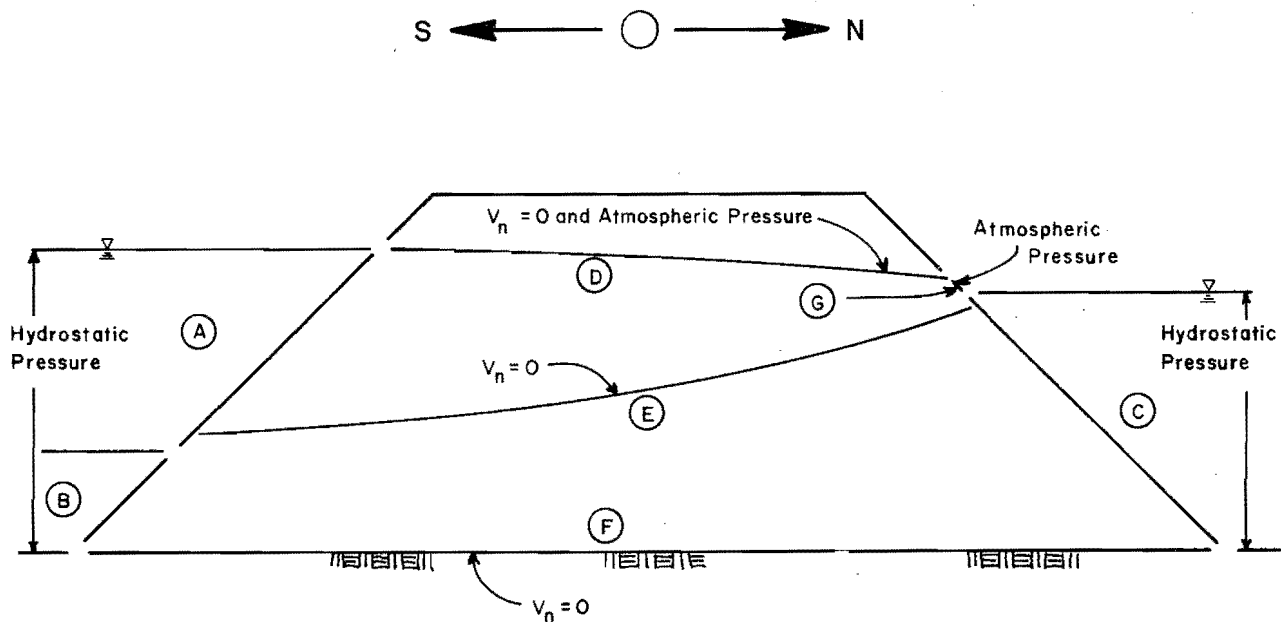
Figure 6. Boundary condition specifications for the bi-directional porous media problem.

27

[J] = the Jacobian matrix of derivatives

Application of these concepts to the equations of Table 2 gives rise to an elemental stiffness matrix of the form

$$
\begin{array}{cccc}
\text{Six} & \text{Six} & \text{Three} & \text{Three} \\
\text{Columns} & \text{Columns} & \text{Columns} & \text{Columns}
\end{array}
$$

$$
\begin{array}{l}
\text{Six}\\\text{Rows}\\[2em]
\text{Six}\\\text{Rows}\\[2em]
\text{Three}\\\text{Rows}\\[2em]
\text{Three}\\\text{Rows}
\end{array}
\begin{bmatrix}
\dfrac{\partial f_1}{\partial u_j} & \dfrac{\partial f_1}{\partial v_j} & \dfrac{\partial f_1}{\partial p_j} & \dfrac{\partial f_1}{\partial \sigma_j} \\[1em]
\dfrac{\partial f_2}{\partial u_j} & \dfrac{\partial f_2}{\partial v_j} & \dfrac{\partial f_2}{\partial p_j} & \dfrac{\partial f_2}{\partial \sigma_j} \\[1em]
\dfrac{\partial f_3}{\partial u_j} & \dfrac{\partial f_3}{\partial v_j} & \dfrac{\partial f_3}{\partial p_j} & \dfrac{\partial f_3}{\partial \sigma_j} \\[1em]
\dfrac{\partial f_4}{\partial u_j} & \dfrac{\partial f_4}{\partial v_j} & \dfrac{\partial f_4}{\partial p_j} & \dfrac{\partial f_4}{\partial \sigma_j}
\end{bmatrix}
\begin{bmatrix}
\Delta u_1 \\ \vdots \\ \Delta u_6 \\ \Delta v_1 \\ \vdots \\ \Delta v_6 \\ \Delta p_1 \\ \Delta p_2 \\ \Delta p_3 \\ \Delta \sigma_1 \\ \Delta \sigma_2 \\ \Delta \sigma_3
\end{bmatrix}
=
\begin{bmatrix}
\{f_1\} \\[1em] \{f_2\} \\[1em] \{f_3\} \\[1em] \{f_4\}
\end{bmatrix}
$$

$$
\begin{array}{ccc}
18\text{x}18 & 18\text{x}1 & 18\text{x}1
\end{array}
$$

. . . . (81)

Triangular shapes are employed to discretize the domain. The dependent variables of velocity are interpolated with a six node, quadratic element, while the pressure and density are modeled linearly with a three node element. These interpolants combine to yield an 18 degree of freedom element stiffness matrix. Best results were obtained when only the unknown dependent variables were included in the differentiation process of developing the Jacobian's terms. That is to say, those terms (boundary integrals) which would not be considered unknowns, and were therefore omitted from the stiffness matrix. For a complete definition of all elements of the Jacobian the reader is referred to Martin (1979).

Boundary conditions

Due to the form of the equations employed (i.e. momentum and mass balance), boundary conditions of lake elevation and density were not sufficient to drive the boundary value problem. Testing of the numerical model revealed that velocities along the influent boundary of the domain were required for a stable, iterative solution. The bi-directional character of the culvert discharge, coupled with a required influent velocity profile, imply that the interface location be specified prior to solving the problem.

It is apparent at this point that a momentum and mass balance model does not have the necessary freedom to independently predict the discharge and interface location within the culverts. A better solution might be achieved through the implementation of

interfacial Froude techniques (Stommel and Farmer 1953, Assaf and Hecht 1974). Holley and Waddell (1976) developed such a model which included the possible impact of various minor losses; however, the data available are not of sufficient quality to either prove or disprove the applicability of any technique. Their results do suggest that an improved data base might well show that a frictionless analysis employing the interfacial Froude criteria would be adequate to solve the culvert discharge problem. Since the technology of such a solution is readily available (i.e. Holley and Waddell 1976), and the lack of data cannot be remedied via the present study, the model of momentum and mass balance has been employed to study the convection-diffusion process.

Model application

A restricted (10-foot long) section of the culvert's overall length was modeled. This was done in order to eliminate difficulties with the size of the global stiffness matrix, and distortion of the triangular elements. Figure 7 depicts the domain's boundaries.

Dirichlet velocity boundary conditions were applied to the influent boundaries (BC, EF), the free surface (DE), and the culvert bottom (AB). The momentum equations describe the total change in velocity; therefore, once an influent profile is known the effluent profile is predicted. Both the free surface and culvert bottom represent impervious boundaries where the
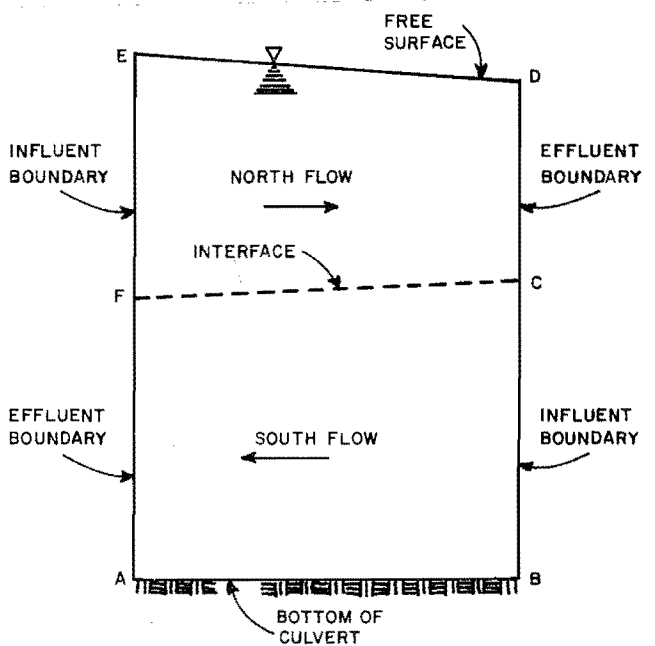

Figure 7. Definitive sketch of the restricted culvert domain.

Table 2. Finite element model of the culvert flows governing equations.

Navier-Stokes   x-direction

$$\{f_1\} = \int_\Omega [\{N\}\, B(uu_{,x} + vu_{,y}) + \{N_{,x}\}\, B\,(\varepsilon_{xx} 2u_{,x} + \varepsilon_{yx}\, u_{,y}) + \{N_{,y}\}\, B\,(\varepsilon_{xx}\, u_{,y}) + \{N_{,x}\}\, B\, \varepsilon_{yx}\, v_{,x}$$

$$+ \{N_{,y}\}\, B\,(\varepsilon_{xx}\, v_{,x} + \varepsilon_{yx}\, 2v_{,y}) - \{N_{,x}\}\, B\, p/\rho]\; dxdy$$

$$+ \int_\Omega \{N\}\, [C_f (u^2 + v^2)^{\frac{1}{2}} u - 2p\, \ell_x]\, A_c\; dxdy$$

$$+ \int_{\partial\Omega} \{N\}\, B\, [\ell_x\, p/\rho + \frac{C_f}{2}\,(u^2 + v^2)^{\frac{1}{2}}\, u]\, ds\; = \; 0$$

y-direction

$$\{f_2\} = \int_\Omega [\{N_{,x}\}\, B\,(\varepsilon_{yy}\, u_{,y} + \varepsilon_{xy}\, 2u_{,x}) + \{N_{,y}\}\, B\, \varepsilon_{xy}\, u_{,y} + \{N\}\, \left(1 + \frac{\sigma}{\rho}\right)\, gB + \{N\}\, B\,(uv_{,x} + vv_{,y})$$

$$+ \{N_{,x}\}\, B\, \varepsilon_{yy}\, v_{,x} + \{N_{,y}\}\, B\,(\varepsilon_{yy}\, 2v_{,y} + \varepsilon_{xy}\, v_{,x}) - B\, \{N_{,y}\}\, p/\rho]\; dxdy$$

$$+ \int_\Omega \{N\}\, [C_f\,(u^2 + v^2)^{\frac{1}{2}}\, v - 2p\, \ell_y]\, A_c\; dxdy$$

$$+ \int_{\partial\Omega} \{N\}\, B\, \left[\ell_y\, p/\rho + \frac{C_f}{2}\,(u^2 + v^2)^{\frac{1}{2}}\, v\right]\, ds\; = \; 0$$

continuity

$$\{f_3\} = \int_\Omega \{M\}\, [u_{,x} B + v_{,y} B + u B_{,x} + v B_{,y}]\; dxdy\; = \; 0$$

convection-diffusion

$$\{f_4\} = \int_\Omega [\{M\}\, \frac{B}{\rho}\,(u\, \sigma_{,x} + v\sigma_{,y}) + \frac{B}{\rho}\,(e_x\, \{M_{,x}\}\, \sigma_{,x} + e_y\, \{M_{,y}\}\, \sigma_{,y})]\; dxdy$$

$$- \int_{\partial\Omega} \{M\}\, \frac{B}{\rho}\, [e_x\, \ell_x\, \sigma_{,x} + e_y\, \ell_y\, \sigma_{,y}]\; ds = 0$$

normal flux is known to be identically zero. Of course, tangential components of velocity are computed on these boundaries. Influent profiles were assumed to have a quadratic shape. The input of characteristic values of both magnitude and slope give rise to an automatic initialization of the required profiles.

Shear stress boundary conditions may be characterized as either Dirichlet stress or Neumann velocity boundary constraints. Regardless of the characterization adopted, these stresses are modeled as quadratic functions of the velocity (Wang and Connor 1975). The boundary stress opposes the velocity and may be easily broken into x and y components.

Early in the study of model behavior it was determined that a minimum number of Dirichlet pressure boundary constraints should be employed. The reasoning here is that specification of a nodal value of pressure implied the elimination of its associated equation. Within the model, the mass conservation or continuity equation was associated with pressure. Thus, specification of pressure brought about a less mass-conserving model. Tests made without Dirichlet pressure constraints yielded the best results. Initially, it was feared that failure to specify any fixed pressure would lead to a floating solution; however, it appears that employing a Newton-Raphson solution technique gives the solution enough of a fix via its initially imposed hydrostatic guess.

Finally, the fourth variable, density, must be constrained. The proposed models of the lake will determine density values on both sides of the culvert; therefore, they may be employed to completely define the influent and effluent densities of the culvert flows. Both the free surface and culvert bottom boundaries may be modeled as either Dirichlet or Neumann boundaries. Waddell and Bolke (1973) reported that both the northward and southward discharges were homogeneous. Thus, the region of interest is the interface. The problem of interest is the minimization of density transport through this internal boundary. Consequently, one can justify the use of Dirichlet constraints upon the free surface and culvert bottom by noting that these constraints insure a tangential gradient of zero. Neumann constraints could be employed; however, in an effort to define a single problem area (i.e. the interface) they were not.

Constraints upon the velocities, pressure, and density have now been described as they were applied to the modified culvert domain. Admittedly, the problem examined does not address the question of discharge as a function of lake stage (elevation) and density; however, modeling the mechanism of turbulent diffusion is relevant to the project in that future two-layer models of the southern arm of Great Salt Lake will require such a mechanism to control the mass transport between the saturated and unsaturated brines.

Two-Dimensional, Depth-Averaged Circulation Model

Equations 31, 32, and 33 were set up in finite element form using the Galerkin method of weighted residuals. Quadratic quadrilateral elements were used with the velocity represented quadratically and the pressure represented linearly over each element. The weight functions used in the two Navier-Stokes equations were the quadratic shape functions, whereas in the continuity equation the linear shape functions were used (Hood and Taylor 1974).

The dissipation terms in the Navier-Stokes equations were integrated by parts to reduce the order of the derivatives in the equations and to introduce boundary conditions. The boundary integrals resulting from the integration and how they are evaluated are discussed later.

The resulting element stiffness matrix has 18 degrees of freedom and the constituent equations are shown in Table 3. Integrals were evaluated numerically using Gauss-Legendre quadrature. The equations were solved using the Picard technique (Gartling 1974) where the nonlinear terms $[C_x]$, $[C_y]$, and $[F]$ were assumed to be zero initially. The nonlinear terms were introduced on the

second iteration and the numerical solution was permitted to cycle until an acceptable change in velocities and pressures was reached.

Boundary conditions

Boundary conditions imposed were those judged minimally required to result in a stable, accurate solution. At all boundary points, velocity components were resolved into normal and tangential values using the average intersection angle at the boundary node. In some cases where desirable, velocities at boundary nodes were given zero values; however, in general the normal velocity was set to zero and the tangential velocity was solved for. The exception is at sections of the boundary where flow enters or leaves the domain. At these points flow velocities are fixed to guarantee continuity of flow into and out of the domain.

Provision is also made for evaporation loss in the model. Because of the high rate of evaporation in Great Salt Lake, a substantial portion of the water budget is allocated to evaporation. Consequently, continuity of flow into and out of the domain must be adjusted to reflect evaporation losses.

Boundary integrals which resulted when the dissipation terms were integrated by parts relate to the shear at the lateral boundaries of the lake. Because the lake is extremely broad and shallow, the effect of bottom shear dominates lateral boundary shear. Hence the lateral surface integrals are neglected. Bottom shear is evaluated via a velocity-squared formula which relates shear stress to the Manning n-value. The shear stress opposes the direction of the resultant depth-averaged velocity.

Surface shear is caused by wind and is assumed constant in magnitude and direction over the entire lake surface. The values of surface shear stress are obtained from Equations 43.

The eddy viscosity term is selected arbitrarily. Because solution stability is quite dependent on this parameter, it will be made as small as possible and yet yield a stable solution.

Three-Dimensional, Steady-State Circulation Model

Finite element model of the velocity formation

Application of the finite element method to the shear form of the Navier-Stokes equations will be shown. Use of integration by parts is employed to create the boundary integrals from the viscous terms of the equations and implications of the various boundary integrals will be discussed.

Table 3. Finite element method applied to the two-dimensional depth-averaged Navier-Stokes equations and continuity.

Navier-Stokes x-direction

$$\sum_{e=1}^{m} \int_{\Omega_e} [\varepsilon^*[K_x]\{U\} + (\varepsilon^*[L_x] + [B_x])\{V\} + [D_x]\{P^S\} + [C_x]\{U\}]dxdy = \sum_{e=1}^{m} \int_{\Omega_e} \left[\frac{\tau_x^S}{\rho}\{N\} - [F_x]\{U\}\right]dxdy$$

$$[K_x] = 2\{M\}^T\{H\}\{N_x\}\{N_x\}^T + 2\{M_x\}^T\{H\}\{N_x\}\{N\}^T + \{M\}^T\{H\}\{N_y\}\{N_y\}^T + \{M_y\}^T\{H\}\{N_y\}\{N\}^T$$

$$[L_x] = \{M_x\}^T\{H\}\{N_y\}\{N\}^T + \{M\}^T\{H\}\{N_y\}\{N_x\}^T$$

$$[B_x] = -f\{M\}^T\{H\}\{N\}\{N\}^T$$

$$[D_x] = \frac{1}{\rho}\{M\}^T\{H\}\{N\}\{M_x\}^T$$

$$[C_x] = \{M\}^T\{H\}\{N\}\{N\}^T\{U\}\{N_x\}^T + \{M\}^T\{H\}\{N\}\{N\}^T\{V\}\{N_y\}^T$$

$$[F_x] = \frac{1}{2}C_f \sqrt{(\{N\}^T\{U\})^2 + (\{N\}^T\{V\})^2} \{N\}\{N\}^T$$

Navier-Stokes y-direction

$$\sum_{e=1}^{m} \int_{\Omega_e} [\varepsilon^*[K_y]\{V\} + (\varepsilon^*[L_y] + [B_y])\{U\} + [D_y]\{P^S\} + [C_y]\{V\}]dxdy = \sum_{e=1}^{m} \int_{\Omega_e} \left[\frac{\tau_y^S}{\rho}\{N\} - [F_y]\{V\}\right]dxdy$$

$$[K_y] = 2\{M\}^T\{H\}\{N_y\}\{N_y\}^T + 2\{M_y\}^T\{H\}\{N_y\}\{N\}^T + \{M\}^T\{H\}\{N_x\}\{N_x\}^T + \{M_x\}^T\{H\}\{N_x\}\{N\}^T$$

$$[L_y] = \{M_y\}^T\{H\}\{N_x\}\{N\}^T + \{M\}^T\{H\}\{N_x\}\{N_y\}^T$$

$$[B_y] = f\{M\}\{H\}\{N\}\{N\}^T$$

$$[D_y] = \frac{1}{\rho}\{M\}\{H\}\{N\}\{M_y\}^T$$

$$[C_y] = \{M\}^T\{H\}\{N\}\{N\}^T\{U\}\{N_x\}^T + \{M\}^T\{H\}\{N\}\{N\}^T\{V\}\{N_y\}^T$$

$$[F_y] = \frac{1}{2}C_f \sqrt{(\{N\}^T\{U\})^2 + (\{N\}^T\{V\})^2} \{N\}\{N\}^T$$

Continuity

$$\sum_{e=1}^{m} \int_{\Omega_e} [[A_x]\{U\} + [A_y]\{V\} - \{M\} w_s] dA = 0$$

$$[A_x] = \{M\}^T\{H\}\{M\}\{N_x\}^T + \{M_x\}^T\{H\}\{M\}\{N\}^T$$

$$[A_y] = \{M\}^T\{H\}\{M\}\{N_y\}^T + \{M_y\}^T\{H\}\{M\}\{N\}^T$$

The three Navier-Stokes equations contain four dependent variables. They include the pressure (eventually the free surface elevation) and each of the three components of the velocity vector. An arbitrary interpolation of each of the velocity variables could be written as

$$u_i = N_k(x,y,z,t)(u_i)_k \quad \ldots \quad (82)$$

where $i = 1$, 2, and 3; $k = 1$, 2, $\ldots$, n; and N_k is a set of three-dimensional shape functions common to all three velocities. The weighting functions for each of the Navier-Stokes equations will be the N_k. Substituting these expressions into the steady state form of Equation 41, and using the resultant as the differential operator in Equation 69, one finds the initial form of the finite element equations for the shear formulation of the Navier-Stokes equations (see Table 4).

Table 4. Finite element method applied to the shear formulation of the x-component Navier-Stokes equation.

$$\sum_{e=1}^{m} \int_{\Omega_e} \{N_i\} \left[(Q_j u_j) - 2\Omega(\sin \phi \ (N_j v_j) - \cos \phi \ (N_j w_j)) + \frac{1}{\rho} (p + p_t)_{,x} - \frac{1}{\rho} \tau_{jx,j}^T \right] dxdydz \ = \ 0$$

After integration by parts one has

$$\sum_{e=1}^{m} \int_{\Omega_e} \{N_i\} \left[(Q_j u_j) - 2\Omega(\sin \phi \ (N_j v_j) - \cos \phi \ (N_j w_j)) + \frac{1}{\rho} p_{t,w} \right] dxdydz$$

$$+ \frac{1}{\rho} \sum_{e=1}^{m} \int_{\Omega_e} \{N_{i,x}\} (\tau_{xx}^T - p) + \{N_{i,y}\} \tau_{yx}^T + \{N_{i,z}\} \tau_{zx}^T \ dxdydz$$

$$= \sum_{e=1}^{m} \int_{\partial \Omega_e} \{N_i\} [(\tau_{xx}^T - p) \ell_x + \tau_{yx}^T \ \ell_y + \tau_{zx}^T \ \ell_z] \ ds$$

Substituting constitutive relations and boundary shears we have

$$\sum_{e=1}^{m} \int_{\Omega_e} \{N_i\} \left[(Q_j u_j) - 2\Omega(\sin \phi \ (N_j v_j) - \cos \phi \ (N_j w_j)) + \frac{1}{\rho} p_{t,x} \right] - \frac{1}{\rho} \{N_{i,x}\} p + [\varepsilon_1 [R_{ij}]$$

$$+ \{N_{i,x}\} \{S_{1j}\}^T] \ \{u_j\} + [\varepsilon_{12} [R_{ij}] + \{N_{i,y}\} \{S_{1j}\}^T] \{v_j\} + [\varepsilon_{13} [R_{ij}]$$

$$+ \{N_{i,z}\} \{S_{1j}\}^T] \{w_j\} \ dxdydz = \sum_{e=1}^{m} \int_{\partial \Omega_e} \{N_i\} (\tau_{zx}^a - p^a \ \ell_x) \ell_z \ ds$$

$[R_{ij}] = \{N_{i,k}\} \{N_{j,k}\}^T; \ \{S_{ij}\}^T = \varepsilon_{ik} \{N_{j,k}\}^T;$

$Q_j = (N_k u_k) \{N_{j,x}\}^T + (N_k v_k) \{N_{j,y}\}^T + (N_k w_k) \{N_{j,z}\}^T$

$[\ ] = $ matrix $= [\{u\} \{v\}^T] = [uv]$

$(\ ) = $ scalar $= (\{u\}^T \{v\}) = (uv)$

$\{ \ \} = $ column vector

$\{ \ \}^T = $ row vector, transpose of the column vector

Boundary shear terms

Applying integration by parts to both the visous and normal pressure terms, one finds

$$\sum_{e=1}^{m} \int_{\Omega_e} \{N_i\}(p_{,x} - \tau^T_{jx,j})\,dxdydz$$

$$= \sum_{e=1}^{m} \int_{\Omega_e} \{N_{i,x}\}(-p + \tau^T_{xx})$$

$$+ \{N_{i,y}\}\tau^T_{yx} + \{N_{i,z}\}\tau^T_{zx}\ dxdydz$$

$$- \sum_{e=1}^{m} \int_{\partial\Omega_e} \{N_i\}((\tau^T_{xx}-p)\ell_x + \tau^T_{yx}\ell_y + \tau^T_{zx}\ell_z)\ ds \qquad (83)$$

While it may not initially appear to be, the above expression is tractable.

In order to show the tractable nature of this boundary integral, consider the positive z elemental face shown in Figure 8. Assume a static equilibrium exists (i.e. $F_x = 0$), where positive shears lie on positive faces. The summation of x-directed forces yields

$$-(\tau_{xx} - p)\frac{dy^2}{2}\,h_{,y} + (\tau_{xx} - p)\left(\frac{dy^2}{2}\,h_{,y}\right.$$

$$\left. + dxdy\,h_{,x}\right) - \tau_{yx}\frac{dx^2}{2}\,h_{,x}$$

$$+ \tau_{yx}\left(\frac{dx^2}{2}\,h_{,x} + dxdy\,h_{,y}\right)$$

$$+ (\tau^a_{zx} - p^a\ell_x)\ dxdy - \tau_{zx}\ dxdy = 0$$

$$\qquad\qquad\qquad\qquad (84)$$
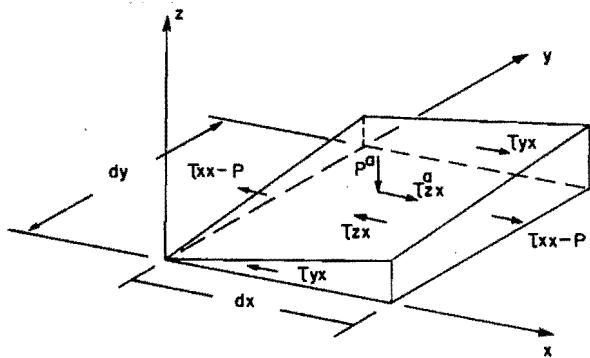
Figure 8. Static evaluation of the x-component shears on the positive z elemental face.

where h is a parameterization of the positive z face of the elemental area under consideration. Rearranging and dividing through by the elemental area, dxdy, one finds

$$\tau^a_{zx} - p^a\ell_x = -(\tau_{xx} - p)h_{,x} - \tau_{yx}h_{,y} + \tau_{zx}$$

$$\qquad\qquad\qquad\qquad (85)$$

where τ^a_{zx} is the applied, x-direction shear stress, and p^a is the applied normal pressure.

Relationships between surface gradients and components of the normal vector may be developed from vector analysis. Note that the normal vector is perpendicular to any vector tangent to the surface. Therefore, the dot product of any tangent vector with the normal vector will be identically zero. Neglecting any second-order contributions, tangent vectors along the x and y coordinate axes of Figure 8 are respectively

$$\vec{T}_x = dx\ \vec{i} + 0\ \vec{j} + h_{,x}\ dx\ \vec{k}$$

$$\vec{T}_y = 0\ \vec{i} + dy\ \vec{j} + h_{,y}\ dy\ \vec{k} \qquad (86)$$

The normal vector is

$$\vec{n} = \ell_x\ \vec{i} + \ell_y\ \vec{j} + \ell_z\ \vec{k} \qquad\qquad (87)$$

where ℓ_x, ℓ_y, and ℓ_z are the direction cosines of the outward directed normal vector, $\vec{n}$. Taking the dot products one finds

$$h_{,x} = -\ell_x/\ell_z$$

$$h_{,y} = -\ell_y/\ell_z \qquad\qquad\qquad (88)$$

Substitution of Equations 88 into Equation 85 yields

$$(\tau^a_{zx} - p^a\ell_x)\ell_z = (\tau_{xx} - p)\ell_x + \tau_{yx}\ell_y + \tau_{zx}\ell_z$$

$$\qquad\qquad\qquad\qquad (89)$$

Substituting this expression into Equation 83 one finds

$$\sum_{e=1}^{m} \int_{\Omega_e} \{N_i\}(p_{,x} - \tau^T_{jx,j})\ dxdydz$$

$$= \sum_{e=1}^{m} \int_{\Omega_e} \{N_{i,x}\}(\tau^T_{xx} - p) + \{N_{i,y}\}\tau^T_{yx}$$

$$+ \{N_{i,z}\}\tau^T_{zx}\ dxdydz$$

$$- \sum_{e=1}^{m} \int_{\partial\Omega_e} \{N_i\}(\tau^a_{zx} - p^a\ell_x)\ell_z\ ds \quad\cdot\quad (90)$$

Since τ_{zx}^a and p^a may be parameterized as functions of overlying velocities and depth respectively, the boundary integral is tractable. The boundary integrand approximations for other components and boundaries are summarized in Equations 91 where repeated indices do not imply summation. Determination of positive or negative signs of stresses on the elemental face is automatically achieved from the signs of the direction cosines which multiply the boundary terms.

$$(\tau_{ix}^a - p^a \ell_x)\ell_i = (-p + \tau_{xx})\ell_x + \tau_{yx}\ell_y + \tau_{zx}\ell_z$$

$$(\tau_{iy}^a - p^a \ell_y)\ell_i = \tau_{xy}\ell_x + (-p + \tau_{yy})\ell_y + \tau_{zy}\ell_z$$

$$(\tau_{iz}^a - p^a \ell_z)\ell_i = \tau_{xz}\ell_x + \tau_{yz}\ell_y + (-p + \tau_{zz})\ell_z$$

$$\cdots \cdots \cdots \quad (91)$$

If one were to consider problems whose boundaries were planes of constant geometry (i.e. rectangular solids), a further simplification would be possible. Such an assumption allows one to rewrite the boundary integral for the positive z face as

$$-\sum_{e=1}^{m} \int_{\Omega_e} (\tau_{zx}^T \ell_z - p^a \, \ell_x) \, ds \quad \cdots \quad (92)$$

where the product of the direction cosines ℓ_x and ℓ_z is approximated by ℓ_x. This, in turn, allows the original pressure term to be reformed through integration by parts. Thus, Equation 90 becomes

$$\sum_{e=1}^{m} \int_{\Omega_e} \{N_i\}(p_{,x} - \tau_{jx,j}^T) \, dxdydz$$

$$= \sum_{e=1}^{m} \int_{\Omega_e} \{N_i\}(p_{,x}) + \{N_{i,x}\}\tau_{xx}^T + \{N_{i,y}\}\tau_{yx}^T$$

$$+ \{N_{i,z}\}\tau_{zx}^T \, dxdydz - \sum_{e=1}^{m} \int_{\partial\Omega_e} \{N_i\}(\tau_{zx}^a)\ell_z \, ds$$

$$\cdots \cdots \cdots \quad (93)$$

The importance of this observation is that the velocity solution, for rectangular problem domains, requires pressure gradient information only. Evaluation of pressure values at integration points is no longer necessary. Finally, the shear model is seen to be tractable due to its physically meaningful boundary integrand.

Since the dependent variables of the numerical model are velocities and not shears, an appropriate constitutive relationship relating stress to rate of deformation is required. Now, in addition to the non-homogeneous natural boundary condition for surface shear, one must employ velocity boundary conditions. Both Dirichlet and Neumann geometric specifications are used. The Neumann boundary conditions arise from the use of multiple degree of freedom nodes. Table 5 presents a matrix summary of the finite element model for the velocity formulation with substitutions having been made for internal stresses and hydrostatic pressure.

Finite element model of the pressure formulation

For the finite element model of the pressure (free surface) formulation, one selects the pressure shape functions as weight functions. One may approximate pressure as

$$p = M_k p_k; \quad k = 1, 2, \ldots, n \quad \cdots \quad (94)$$

where M_k is a set of shape functions appropriate for the interpolation of pressure, the p_k are the nodal values of pressure, and n is the number of elemental degrees of freedom for the pressure variable. The finite element equivalent of Equation 50 is

$$\frac{1}{\rho}\sum_{e=1}^{m} \int_{\Omega_e} \Big(\{M_{i,x}\}p_{,x} + \{M_{i,y}\}p_{,y}$$

$$+ \{M_{i,z}\}(p_{,z} + \rho g)\Big) \, dxdydz$$

$$- \frac{1}{\rho}\sum_{e=1}^{m} \int_{\partial\Omega_e} \{M_i\}(p_{,x}\ell_x + p_{,y}\ell_y$$

$$+ (p_{,z} - \rho g)\ell_z) \, ds \quad \cdots \cdots \quad (95)$$

$$= \frac{1}{\rho}\sum_{e=1}^{m} \int_{\Omega_e} \{M_i\}(2\Omega((u_{,y} - v_{,x})\sin\phi$$

$$+ (w_{,x} - u_{,z})\cos\phi) + \frac{dD}{dt} + u_{,x}^2 + v_{,y}^2 + w_{,z}^2$$

$$+ 2u_{,z}w_{,x} + 2v_{,z}w_{,y} + 2u_{,y}v_{,x}) \, dxdydz$$

where integration by parts has been applied to the pressure terms. Substitution may now be made for hydrostatic pressure. Equations 42 substituted into Equation 95 yields

$$g\sum_{e=1}^{m} \int_{\Omega_e} \Big(\{M_{i,x}\}\{M_{j,x}\}^T\{h_j\} + \{M_{i,y}\}\{M_{j,y}\}^T\{h_j\}\Big) \, dxdydz$$

$$- g\sum_{e=1}^{m} \int_{\partial\Omega_e} \{M_i\}(h_{,x}\ell_x + h_{,y}\ell_y + 0 \, \ell_z) \, ds$$

$$= g\sum_{e=1}^{m} \int_{\Omega_e} \{M_i\} \, \theta \, dxdydz \quad \cdots \cdots \quad (96)$$

Table 5. Final form of the finite element model of the velocity formulation.

$$[A]\{x\} = \{b\}$$

$$[A] = \begin{bmatrix}
\sum\limits_{e=1}^{m} \int\limits_{\Omega_e} \{N_i\}\{Q_j\}^T + \varepsilon_1[R_{ij}] & \sum\limits_{e=1}^{m} \int\limits_{\Omega_e} \{N_i\}(-2\Omega\sin\phi\{N_j\}^T) + \varepsilon_{12}[R_{ij}] & \sum\limits_{e=1}^{m} \int\limits_{\Omega_e} \{N_i\}(2\Omega\cos\phi\{N_j\}^T) + \varepsilon_{13}[R_{ij}] \\
\quad + \{N_{i,x}\}\{S_{1j}\}^T \, dxdydz & \quad + \{N_{i,y}\}\{S_{1j}\}^T \, dxdydz & \quad + \{N_{i,z}\}\{S_{1j}\}^T \, dxdydz \\[2ex]
\sum\limits_{e=1}^{m} \int\limits_{\Omega_e} \{N_i\}(2\Omega\sin\phi\{N_j\}^T) + \varepsilon_{12}[R_{ij}] & \sum\limits_{e=1}^{m} \int\limits_{\Omega_e} \{N_i\}\{Q_j\}^T + \varepsilon_2[R_{ij}] & \sum\limits_{e=1}^{m} \int\limits_{\Omega_e} \varepsilon_{23}[R_{ij}] + \{N_{i,z}\}\{S_{2j}\}^T \, dxdydz \\
\quad + \{N_{i,x}\}\{S_{2j}\}^T \, dxdydz & \quad + \{N_{i,y}\}\{S_{2j}\}^T \, dxdydz & \\[2ex]
\sum\limits_{e=1}^{m} \int\limits_{\Omega_e} \{N_i\}(-2\Omega\cos\phi\{N_j\}^T) + \varepsilon_{13}[R_{ij}] & \sum\limits_{e=1}^{m} \int\limits_{\Omega_e} \varepsilon_{13}[R_{ij}] + \{N_{i,y}\}\{S_{3j}\}^T \, dxdydz & \sum\limits_{e=1}^{m} \int\limits_{\Omega_e} \{N_i\}\{Q_j\}^T + \varepsilon_3[R_{ij}] \\
\quad + \{N_{i,x}\}\{S_{3j}\}^T \, dxdydz & & \quad + \{N_{i,z}\}\{S_{3j}\}^T \, dxdydz
\end{bmatrix}$$

$$\{x\} = \left\{ \begin{array}{c} u \\ \\ v \\ \\ w \end{array} \right\}$$

$$\{b\} = \left\{ \begin{array}{c}
\sum\limits_{e=1}^{m} \int\limits_{\Omega_e} \{N_{i,x}\}(P) \, dxdydz + \sum\limits_{e=1}^{m} \int\limits_{\partial\Omega_e} \{N_i\}\left(\dfrac{\tau^a_{\ell x}}{\rho} - (P)\ell_x\right)\ell_\ell \, ds \\[3ex]
\sum\limits_{e=1}^{m} \int\limits_{\Omega_e} \{N_{i,y}\}(P) \, dxdydz + \sum\limits_{e=1}^{m} \int\limits_{\partial\Omega_e} \{N_i\}\left(\dfrac{\tau^a_{\ell y}}{\rho} - (P)\ell_y\right)\ell_\ell \, ds \\[3ex]
\sum\limits_{e=1}^{m} \int\limits_{\Omega_e} \{N_{i,z}\}(P) \, dxdydz + \sum\limits_{e=1}^{m} \int\limits_{\partial\Omega_e} \{N_i\}\left(\dfrac{\tau^a_{\ell z}}{\rho} - (P)\ell_z\right)\ell_\ell \, ds - \sum\limits_{e=1}^{m} \int\limits_{\Omega_e} \{N_i\} g \, dxdydz
\end{array} \right\}$$

where: $\{Q_j\} = (N_k u_k)\{N_{j,x}\} + (N_k v_k)\{N_{j,y}\} + (N_k w_k)\{N_{j,z}\}$ $\quad \{S_{ij}\}^T = \varepsilon_{i1}\{N_{j,x}\}^T + \varepsilon_{i2}\{N_{j,y}\}^T + \varepsilon_{i3}\{N_{j,z}\}^T$

$[R_{ij}] = \{N_{i,x}\}\{N_{j,x}\}^T + \{N_{i,y}\}\{N_{j,y}\}^T + \{N_{i,z}\}\{N_{j,z}\}^T$ $(P) = \{(M_j)^T(h_j) - z\} g$

where Θ represents the right hand side of the pressure equation. Note that three-dimensional integration is called for while the pressure has been approximated by a two-dimensional free surface elevation variable. Also note that the boundary integral is a nonhomogeneous natural boundary condition. Since specifying the Neumann or natural boundary condition everywhere on the problem's boundary would lead to a floating solution (a singular coefficient matrix), one must select at least one free surface node to have a Dirichlet boundary condition.

An expression in the Θ term which deserves mention is the total derivative of the divergence of the velocity vector. Recall from the mathematical model section that the divergence of the velocity vector is denoted D. Other formulations have only a partial derivative in time of D, and the term could be neglected entirely in this steady state analysis. However, by combining some previously neglected terms with the time partial, a total derivative of D is obtained. It is conceivable that the total derivative may change, and therefore the term is retained. Both approaches are examined in the results which follow in the subsequent section.

The question arises as to how one approximates dD/dt in this analysis. One observes that D should be identically zero. But in the approximations made for velocity there is no guarantee of continuity being satisfied pointwise or in an average sense in the problem domain. Therefore, the desired total change in D is simply the negative of D which can be evaluated from information at a previous iteration, i.e.

$$\frac{dD}{dt} = -(u_{,x} + v_{,y} + w_{,z}) \quad . \quad . \quad . \quad . \quad (97)$$

At this point the finite element model of the pressure problem is complete, and may be written as

$$g \sum_{e=1}^{m} \int_{\Omega_e} [M_{i,x}M_{j,x} + M_{i,y}M_{j,y}] \, dxdydz \, \{h_j\}$$

$$= g \sum_{e=1}^{m} \int_{\partial\Omega_e} \{M_i\}(h_{,x}\ell_x + h_{,y}\ell_y) \, ds$$

$$+ \sum_{e=1}^{m} \int_{\Omega_e} \{M_i\}[2\Omega\,((u_{,y} - v_{,x})\,\sin\,\phi$$

$$+ (w_{,x} - u_{,z})\,\cos\,\phi) - (u_{,x} + v_{,y} + w_{,z})$$

$$+ u_{,x}^2 + v_{,y}^2 + w_{,z}^2 + 2u_{,z}w_{,x} + 2v_{,z}w_{,y}$$

$$+ 2u_{,y}v_{,x}] \, dxdydz \quad . \quad . \quad . \quad . \quad (98)$$

Previous mention has been made of the three-dimensional integration of a two-dimensional shape function. In this regard, it is found to be extremely advantageous to employ elements with vertical edges. Failure to use such elements would result in vertically aligned integration points being associated with a family of free surface points. The coordinates of each of these free surface points would have to be found, probably by a Newton-Raphson technique. This expensive possibility may be avoided by employing vertical-edged elements. Each integration point's vertical projection retains the same horizontal coordinates as the integration point. Thus the velocity information at a given horizontal location is associated with unique free surface coordinates.

Alternative velocity formulation

An alternative finite element model for the velocity is examined. The continuity equation has not been employed explicitly in either of the velocity or pressure formulations. This may lead to a model exhibiting poor mass conservation characteristics. In an effort to produce a more mass conserving model, the third Navier-Stokes equation is replaced by the continuity equation. Since one must solve for the same number of unknowns, one must retain the velocity shape functions as weight functions. The finite element equation is

$$\sum_{e=1}^{m} \int_{\Omega_e} \{N_i\}(\{N_{j,x}\}^T\{u_j\} + \{N_{j,y}\}^T\{v_j\}$$

$$+ \{N_{j,z}\}^T\{w_j\}) \, dxdydz = 0 \quad . \quad . \quad (99)$$

Integration by parts is not required. The hope is that by including the continuity equation one may expect improved pointwise mass conservation within the problem domain.

Element shape and interpolant selections

Quadrilateral shapes were selected for the development of the three-dimensional circulation model. Perhaps the most innovative concept in the development of this model has been the creation of mixed interpolation elements which have the ability to better seal the boundaries of a domain against indiscriminant gains and/or losses in mass. Blended interpolants were employed to develop a new and unique blend of the Bogner and Adini elements. A complete development of this and other elements required in the analysis can be found in Kincaid (1979).

Development of the mixed interpolant element requires the use of multiple degree of freedom nodes. In turn, the use of this element in an isoparametric form required the

development of derivative geometry information at the node. The difficulty here lies in the derivative being with respect to an arbitrary natural coordinate system. Creation of a preprocessing technique which produces the uniquely determined information is also discussed in Kincaid (1979).

While somewhat simplified domains will be examined in the results section, the general isoparametric formulation is programmed for the solution of more general problems. Commonly employed numerical integration schemes are used in the evaluation of the volume and surface integrals of the formulation.

Solution techniques and iterative scheme

At this point the numerical models of both the velocity and pressure problems have been described in some detail. The uncoupled nature of these problems requires an iterative solution. Successive solutions to first the velocity and then the free surface (pressure) will be sought until an arbitrarily defined convergence or iteration count is achieved. Due to the nonlinear nature of the velocity problem, considerable emphasis is placed upon its solution. The free surface problem is linear and symmetric, and therefore its solution is rather straightforward. Both segments (velocity and pressure) of the overall problem are cast in their fully implicit form. This is a result of the finite element method.

Solution of the velocity problem.
By integrating the elemental equations and coupling their contributions through the common nodal degrees of freedom of adjacent elements, a global matrix formulation is achieved. The resulting velocity formulation is both nonlinear and nonsymmetric. Several attempts have been made by investigators (Gartling 1974, Kawahara et al. 1974) to economize on the solution of the viscous problem. Most of these techniques move the nonlinear and/or nonsymmetric contributions from the global stiffness matrix to the global load vector. The remaining linear system of equations (which may be symmetric) is solved using standard methods. Some of these techniques allow one to reform the load vector instead of the stiffness matrix in the interative loop. All of these economized solutions require that the problem not be heavily nonlinear in character.

Gartling (1974) studied the solution of the viscous fluid flow problem in two dimensions and concluded that a Picard iteration technique was appropriate. The Picard technique is substantially different from the economized solutions in that the nonlinearity and nonsymmetry are retained in the stiffness matrix. Nonlinear terms are defined as functions of the previous iterate's solution. Thus our global system is

$$[\tilde{\approx}{C}(\tilde{u}^{n-1}) + \tilde{\approx}{K}] \; \tilde{u}^{n} = \tilde{F} \quad . \quad . \quad . \quad .(100)$$

where $\approx$ implies matrix, $\sim$ implies vector, $\tilde{\approx}{C}(u^{n-1})$ is the nonlinear portion and $\tilde{\approx}{K}$ the linear contribution to the global stiffness matrix, and the superscripts, n, and $n-1$ imply the current and previous iterate respectively. In the above expression $\tilde{u}$ is the solution vector of all velocity components, and $\tilde{F}$ is the global load vector. Complete definitions of the matrix and vector elements may be found in Kincaid (1979). While the proposed solution technique is at best marginally economical for large matrices, it appears to offer the best stability and convergence for flows considered herein.

Having decided upon the velocity solution's global representation, one must select a numerical method by which the solution is achieved. Gaussian elimination was employed. However, standard Gaussian elimination calls for the complete formulation of the global problem prior to implementation of the solver. For the problem which motivated this research, it was anticipated that very large matrices would be required. Thus their complete formulation could conceivably require huge amounts of core storage. An alternative is to form the global matrix in a way that allows the solution to sweep through the problem as it is formed. The trade off for such a technique is the considerable amount of information which must be stored on disks or other peripheral devices. Such a method for linear symmetric systems of equations was first developed by Irons (1970). The method is known as the frontal technique. A nonsymmetric form of this frontal technique has been developed by Hood (1976).

While the basic technology of Hood's frontal solver remains unchanged, the author found it economical to introduce an addressing system within the solver which employed single rather than double dimensioned arrays. A second economy upon the original code is the development of a diagonal pivot search. The Hood solver sought the maximum pivot over the entire set of completely summed matrix elements. While such a search guarantees the best pivot selection, it was determined that maximal pivots were always located on the diagonal for the proposed problems. Thus, the development of the restrictive diagonal pivot search leads to identical solutions at a reduced cost. Finally, during the testing stage of the model development it was observed that a considerable number of geometric boundary conditions were being employed. A version of the solver was developed which takes advantage of this characteristic. In the original code geometric boundary conditions were substituted into the global matrix and the variable was solved for as though it were an unknown. The authors chose to eliminate the known variables at the element level and therefore reduce the

core requirements of the global model. For details on the available options within the solver, the reader is referred again to Kincaid (1979).

Solution of the pressure problem. Due to the linear, symmetric nature of the pressure problem, one has many available solvers for this portion of the problem. The Bathe and Wilson (1976) solver for symmetric linear systems has been chosen for this segment of the overall solution. Use of a minimum of Dirichlet boundary conditions may make for a marginally stable set of equations. The routine, COLSOL, was selected over the more common Choleski solver due to this stability consideration.

Iterative scheme. The sequence of events in finding a solution to a given problem is the following. First, initial conditions of a horizontal free surface, homogeneous velocity field, and a prescribed wind velocity are assumed. Second, the iterative loop for velocity and pressure is entered. The velocity problem, driven by the wind and pressure gradients, is solved for updated velocity information. The pressure problem, driven by its velocity dependent right hand side, is solved for the free surface elevation. The new free surface alters the problem geometry slightly and the updated velocity solution of the previous iteration is incorporated as the velocity problem is formed and solved again. Similarly the velocities are now altered along with the geometry, so the pressure problem is reformed and solved. The iterative cycle continues until either of two situations occur. If the change in the velocity and free surface variables drops below a prescribed level, the iteration is terminated. Failing to reach a prescribed convergence criteria, the problem will continue to iterate until reaching a prescribed maximum number of iterations. Upon reaching this maximum, the current solution is dumped to peripheral and print devices giving the operator a chance to study the problem's solution before committing additional time and funds. For greater detail on the solvers and the iterative scheme the reader is referred to the appendices of Kincaid (1979) where a program listing is included.

Finite Element Representation of the Convection-Dispersion Equation

Galerkin and "upwinding" methods

In the Galerkin method of weighted residuals, the weighting functions are identical to the interpolation (or shape) functions. This is not the case in the "upwinding" method. The "upwinding" technique, as shown by Christie et al. (1976), Heinrich et al. (1977), and Huyakorn (1977), for convection-dispersion equations, uses a skewed weighting scheme. The interpolation functions are of the standard form as used in the Galerkin method. The difference is in the equation's weighting functions which are skewed with more emphasis (weighting) on the portion of the element that is upwind (upstream). For a convection-dominated problem this technique finds its justification in removing the severe longitudinal oscillations which can occur with the Galerkin method. The result is a solution with a better degree of accuracy, fewer numerical oscillations, without too many additional computations.

Representation of terms in the convection-dispersion equation

Not all of the terms of the governing Equation 52 are developed in quite the same manner. There are five different groups of terms. They are as follows:

1. $u \frac{\partial c}{\partial x}$, $v \frac{\partial c}{\partial y}$ (convective terms)

2. $-\frac{\partial}{\partial x} \left(D_x \frac{\partial c}{\partial x} \right)$, $-\frac{\partial}{\partial y} \left(D_y \frac{\partial c}{\partial y} \right)$ (dispersive terms)

3. α (source-sink term)

4. β (decay term)

5. $\frac{\partial c}{\partial t}$ (time rate of change term)

The basic development of each group will be shown as it is used in the model. The column vector $\{W\}$ represents the weighting functions. The column vectors $\{N\}$ and $\{M\}$ are the element's velocity and concentration shape functions respectively.

Convective terms. All of the variables in the convective terms vary from node to node, thus,

$$u^{(e)}(x,y) = \{N\}^T \{u\}^{(e)} = \{N_1, N_2, \ldots N_n\} \begin{Bmatrix} u_1 \\ u_2 \\ \cdot \\ \cdot \\ \cdot \\ u_n \end{Bmatrix}$$

$$\frac{\partial c}{\partial x}^{(e)} = \{M_{,x}^{(e)}\}^T \{c\}$$

The superscript (e) indicates the values of the variable for a particular element but will be dropped in future equations as a convenience in writing them. The subscripts on the expanded notation indicate the local node numbers of the element. Combining the variables and applying the weighting functions to create the inner product yields,

$$\left(W, u \frac{\partial c}{\partial y} \right) = \int_{\Omega_e} \{W\} \{N\}^T \{u\} \{M_{,y}\}^T \, dxdy \, \{c\} \quad \ldots \ldots \ldots (101)$$

Dispersive terms. The dispersion coefficients are assumed constant over

an element and require no interpolation functions. The dispersion terms are integrated using Green's second identity (integration by parts) to create boundary terms within the governing equation and reduce the order of the differential equation. Prior to this process, the inner product was taken of the weighting functions and the weighted residual. The resulting expressions are:

$$\left(W, \ \frac{\partial}{\partial x} \left(D_x \ \frac{\partial c}{\partial x}\right)\right) = \int_{\Omega_e} \{W_{,x}\} \ D_x \ \{M_{,x}\}^T \ dxdy \ \{c\}$$

$$- \int_{\partial\Omega_e} \{W\} \ D_x \ \{M_{,x}\}^T \{c\} \ \ell_x \ ds \quad . \quad . \quad . \ (102)$$

Further mention of the boundary integral in the above equation will be made later when the boundary conditions are discussed.

Source-sink term. The source-sink term is handled in the same manner as the dispersion coefficients as it is constant over an element. This term's formulation results in the following equality.

$$(W, \alpha) = \int_{\Omega_e} \{W\} \ \alpha \ dxdy \quad . \quad . \quad . \quad . \ (103)$$

Decay term. The decay term is a first order reaction of the form $\beta = \kappa C$ where κ is the coefficient of decay. The coefficient will be constant over an element and the term's formulation results in the following equality.

$$(W, \beta) = \int_{\Omega_e} \{W\} \ \kappa \ \{M\}^T \ dxdy \ \{c\} \quad . \quad . \ (104)$$

Time rate of change term. The time rate of change term cannot be represented by the Galerkin or "upwinding" methods. Since the interpolation functions are dependent only on spatial information, the derivative of concentration with respect to time cannot be expressed with the interpolation functions. This dilemma is solved by using a finite difference representation of the rate of concentration change.

$$\frac{\partial c}{\partial t} \ = \ \frac{c^{t + \Delta t} - c^t}{\Delta t}$$

Now, applying the interpolation functions, weighting functions, and taking the inner product gives

$$\frac{\partial c}{\partial t} = \frac{1}{\Delta t} \int_{\Omega_e} \{W\}\{M\}^T \ dxdy \{c^{t + \Delta t}\}$$

$$- \frac{1}{\Delta t} \int_{\Omega_e} \{W\}\{M\}^T \ dxdy \ \{c^t\} \quad . \quad . \quad . \ (105)$$

This model does not simply add the rate of change term to be convection-dispersion equation as shown in Equation 52 for its unsteady state solution. Rather, it also incorporates spacial averages at the advanced time step. This implicit method of time stepping is inherently stable but not exceptionally accurate. A more accurate and inherently stable method is the Crank-Nicolson method. This technique adds the time rate of change term of the convection-dispersion equation and also averages the concentration and load vector, i.e.

$$[M] \left\{\frac{\partial c}{\partial t}\right\} + [K]\{c\} = \{f\} \quad . \quad . \quad . \quad . \ (106)$$

where

$$\frac{\partial c}{\partial t} \ \simeq \ \frac{c^{t + \Delta t} - c^t}{\Delta t}$$

$$c \ \simeq \ \frac{c^{t + \Delta t} + c^t}{2}$$

$$f \ \simeq \ \frac{f^{t + \Delta t} + f^t}{2}$$

The matrices [M] and [K] are the so-called "mass" and "stiffness" matrices, respectively. This approach is better than the implicit method because it reduces the numerical influence of the size of the time increment (Carnahan et al. 1969).

Types of elements used

The computer model developed has the capability to use three types of quadrilateral elements in its solution process. They are described in Table 6. The first type is an isoparametric element with quadratically varying interpolation functions. This allows the element to have curvilinear sides. The second type of element has linearly varying interpolation functions with linear sides. Zienkiewicz (1977) gives a complete explanation of the first two types of elements that are used in the model. Element No. 3 is a combination of the first two types of elements.

Boundary conditions

There are two types of boundary conditions incorporated in the model. Geometric-Dirichlet boundary conditions are employed to specify concentration at specific nodes. Neumann-natural boundary conditions are identified as the boundary integrands of the convection-dispersion equation (see Equation 102). These natural boundary conditions are set to zero and omitted from the governing equations incorporated in the computer program. They are homogeneous natural boundary conditions.

Table 6. Description of elements.

Element No.	Type of Concentration Interpolation Function {M}	Type of Velocity Interpolation Function {N}	No. of Nodes on Element	Remarks
1	Quadratic	Quadratic	corner 4 mid-side 4 TOTAL 8	All information processed at all 8 nodes.
2	Linear	Linear	corner 4 mid-side 0 TOTAL 4	All information processed at all 4 nodes.
3	Linear	Quadratic	corner 4 mid-side 4 TOTAL 8	Velocity information processed at all 8 nodes. Concentration information processed at corner nodes only.

Finite element convection-dispersion equation

To put all this information into perspective, the following two equations show the finite element formulation of the steady and unsteady state versions of the governing equation.

Steady-state

$$\sum_{e=1}^{m} \int_{\Omega_e} [\{W\}\{(Nu)\{M_{,x}\}^T + (Nv)\{M_{,y}\}^T\}$$

$$+ D_x\{W_{,x}\}\{M_{,x}\}^T + D_y\{W_{,y}\}\{M_{,y}\}^T]dxdy\{c\}$$

$$+ \{W\}\alpha = 0 \quad . \quad . \quad . \quad . \quad . \quad (107)$$

Unsteady-state

$$\sum_{e=1}^{m} \frac{1}{2}\int_{\Omega_e} [\{W\}\{(Nu)\{M_{,x}\}^T + (Nv)\{M_{,y}\}^T\}$$

$$+ D_x\{W_{,x}\}\{M_{,x}\}^T + D_y\{W_{,y}\}\{M_{,y}\}^T$$

$$+ \kappa\{W\}\{M\}^T] \, dxdy \quad \{c^{t+\Delta t}\}$$

$$+ \sum_{e=1}^{m} \int_{\Omega_e} \{W\}\{M\}^T \, dxdy \, \{c^{t+\Delta t}\}$$

$$= \sum_{e=1}^{m} \left\{ \frac{\alpha^{t+\Delta t} + \alpha^t}{2} \, \{W\} \right\}$$

$$+ \sum_{e=1}^{m} \int_{\Omega_e} \{W\}\{M\}^T \, dxdy \, \{c^t\}$$

$$- \sum_{e=1}^{m} \frac{1}{2}\int_{\Omega_e} [\{W\}\{(Nu)\{M_{,x}\}^T + (Nv)\{M_{,y}\}^T\}$$

$$+ D_x\{W_{,x}\}\{M_{,x}\}^T + D_y\{W_{,y}\}\{M_{,y}\}^T$$

$$+ \kappa\{W\}\{M\}^T] \, \{c^t\} \, dxdy \quad . \quad . \quad . \quad . \quad (108)$$

Summary Comments

All of the numerical solutions have been posed as finite element problems to take advantage of techniques in problem solving which are common to all of the analyses. In each case it was presumed that the inherent flexibility in this type of analysis would lead to better solutions to the problems which were posed. While it was recognized that finite element analysis often demanded large computer storage and considerable execution time, it was believed that the UNIVAC 1108 computer would be adequate to achieve the desired results. Subsequent work revealed this was not the case and often the lack of computing power severely limited the investigations. The degree of success in each case is detailed in the next section.

In the previous sections, mathematical and numerical models were developed to describe various phenomena related to Great Salt Lake. In this section, the results of the numerical analyses will be related to the lake and their degree of success and future application will be discussed. The causeway models for seepage flow and culvert flow provide boundary conditions for the circulation model, hence they will be discussed first. The convection-dispersion model describes the mixing and transport of salinity or pollutants as a result of circulation so it will conclude this section.

Seepage Flow Through the Causeway

The model was designed to determine flow rates in both the upper and lower regions of flow based on a specified domain geometry, element properties, and certain boundary condition information. Recall that an initial assumption must be made as to the locations of the free surface and interface by placing them along element edges. Permeabilities and fluid density for each element are element are also required. The boundary condition information required includes the upstream and downstream free surface and interface elevations.

The parameter information for this study was taken from Waddell and Bolke (1973) which contained lake elevation and specific gravity information for Great Salt Lake for the years 1968 through 1972. The report did not provide enough information to be used in a rigorous verification of the model, so until more complete data are collected one must be satisfied with qualitative and rough quantitative verifications.

Dimensional analysis

There are many parameters influencing this problem making any relationships between the variables somewhat complex. A dimensional analysis was performed in order to more clearly present the results. These dimensionless parameters are then used in plotting the results of the analysis. For a more complete explanation of this procedure, see Murphy (1950).

The fundamental variables for this problem are:

ρ_ℓ = fluid density in lower section of fill (slug/ft^3)

$\Delta\rho$ = fluid density difference between upper and lower sections of fill (slug/ft^3)

H_1 = depth of lake surface on south side of embankment (ft)

ΔH = difference in surface elevation between north and south sides of embankment (ft)

H_3 = depth of interface in southern portion of lake (ft)

k = permeability of soil (to reduce the number of parameters permeability is assumed isotropic and homogeneous throughout the domain--ft/sec)

W = width of base of domain of flow (ft)

q_s, q_n = flow rates per unit length through the fill in the south and north directions, respectively (ft^3/sec/ft)

α = side slope angle of embankment

Figure 9 depicts these variables for a general flow situation. The gravitational constant is contained in the permeability term by the relationship

$$k = k_o \, \rho g / \mu \quad . \quad . \quad . \quad . \quad . \quad . \quad . \quad (109)$$

where k_o (ft^2) is the physical permeability dependent only on the soil characteristics and not on those of the fluid, ρ (slug/ft^3) is the fluid's mass density, g (ft/sec^2) is the gravitational constant, and μ (lb-sec/ft^2) is the fluid absolute viscosity. Therefore, k already incorporates the gravitational constant, so g is not necessary as a fundamental variable.

Consideration of continuity suggests the existence of a northside density interface, but data and sketches in the Waddell-Bolke report (1973) have shown no indication of this reality. Therefore, the less-saturated northward flowing brine may quickly mix with the north brine waters, perhaps within the rip-rap over the earth embankment itself, leaving little or no detectable layering on the north side of the embankment. This study, therefore, does not include the interface elevation of the north side as a fundamental variable and assumes that the north lake waters have constant density throughout.
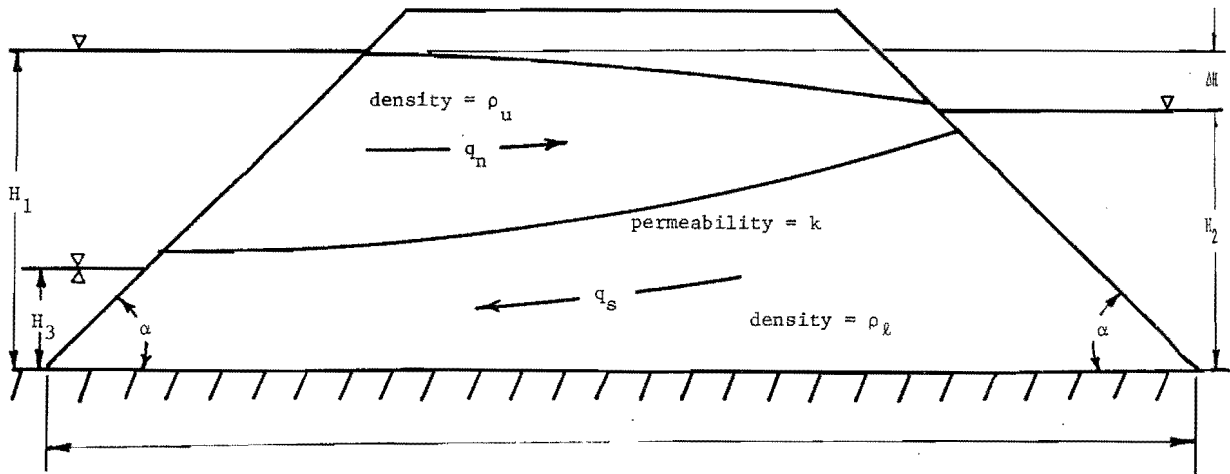
41

Figure 9. Important variables encountered in this study.

The nine fundamental variables can be non-dimensionalized to six dimensionless parameters.

$$(q/kH_1) = f[(\Delta\rho/\rho_\ell), (\Delta H/H_1), (H_1/H_3), (W/H_1), (\alpha)]$$

$$. \quad . \quad . \quad . \quad . \quad . \quad (110)$$

Because of the number of parameters, it is not possible to formulate a single governing equation for flow rates for this problem. Therefore, a number of graphs have been prepared which encompass the range within which the above dimensionless parameters vary according to the Waddell-Bolke report. The ranges of values were found for these parameters for the years 1968 through 1972 (see Table 7).

Casagrande (1965) describes the final design of the rockfill embankment (Figure 10) on which the construction was based, but indicates that many variations from this section were developed. For modeling purposes a 1:1 slope was chosen for the innermost semipermeable core. Tracer studies taken in the fill indicated essentially no flow of fluid in the lower sand and gravel base layer. Apparently, clay and evaporates

Table 7. Typical ranges of values for dimensionless parameters.

Dimensionless Parameter	Range
$\Delta\rho/\rho_\ell$	0.05 - 0.1
$\Delta H/H_1$	0.5 - 2.0
H_1/H_3	4.0 - 6.0
W/H_1	3.5 - 4.5
α	1:1 - 1:3[a]

[a]$\alpha=45°$ or 1:1 is the only slope employed in this analysis.

cemented this layer to make it essentially impermeable. This cementation may also serve to decrease the pore size dimensions in the rockfill sections giving them their low values of permeability. The exchange of brines between the north and south sections of the lake occurs only in the upper core of the embankment. Therefore, a study of the embankment can be limited to a section such as that depicted in Figure 9.
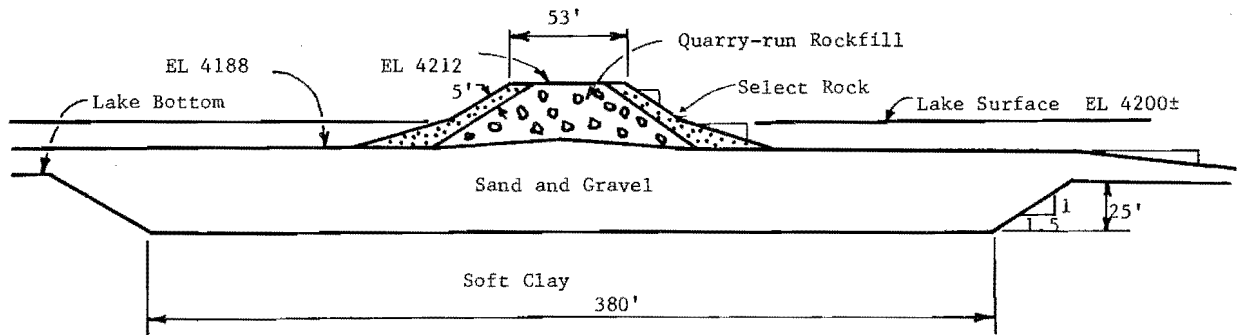

Figure 10. Final construction specifications for Southern Pacific Railroad causeway fill (from Casagrande, 1965).

The two-domain problem

In order to keep the number of dimensionless parameters to a minimum, it was decided to model only a single side slope angle for the earth embankment. A 45-degree angle was chosen for ease in calculating the nodal geometry of the domain. The side slopes of the actual Salt Lake causeway are variable across its length and may be as flat as 3 to 1 in some sections. Modeling a single value of side slope allows one to deal with five dimensionless parameters rather than six; a great reduction in variable correlation.

The model assumes that the fill is isotropic. That is, that the permeability at a given point is equal in all directions. Because of the manner in which the fill was originally constructed, it is possible that the fill may either be anisotropic, favoring flow in the horizontal direction, or it may have two or more isotropic (or anisotropic) layers of differing permeabilities. The present model can handle a special case of anisotropy readily, but cannot model layers of varying permeabilities in its present state. The mathematical and numerical theory would remain unchanged, but it would be necessary to incorporate some triangular elements to model the new geometry. The quadrilateral elements used in this analysis would become too distorted for some of the corners which the new geometry would include. The need for such an alteration in the present model cannot be justified until more field data are collected.

Figures 11 through 15 illustrate the relationships between five of the six dimensionless parameters described earlier. There are two sets of plots for both northward and southward flows. Figures 11 and 12 depict that set of conditions acting when the ratio of embankment width, W, to southside lake surface depth, H_1, is a maximum for the years 1968-1972; Figures 13 and 14 show those conditions when this ratio (W/H_1) is a minimum on the lake for the same years. For instance, Figures 11 and 12 show that if the earth embankment to be modeled has an effective length ratio (i.e. W/H_1) of 4.5, and H_1/H_3 ratio of 6, with a head drop ratio (i.e. $\Delta H/H_1$) of 0.022, and a fluid density ratio (i.e. $\Delta\rho/\rho_\ell$) of 0.05, the model predicts equal northward and southward flow ratios (q_n/kH_1 and q_s/kH_1, respectively) of 0.0024. For a typical value of H_1 of 25 feet and a value of 0.25 ft/sec for k, this would be a flow rate of 0.015 ft^3/sec per foot of embankment length for either the northward or southward flow. If the proposed section can be considered an average cross section for the total 12.2 miles of the causeway, the total flow through the causeway would be approximately 1000 ft^3/sec.

Figures 15 and 16 indicate the effect that the side slope angle has on the flow rates. It appears that decreasing the side slope decreases southward discharge greatly,

while simultaneously decreasing northward discharges to a lesser degree. These two graphs indicate the importance of obtaining a good representative cross section of the embankment before an accurate prediction can be made of actual discharges through the railroad causeway on the Great Salt Lake.

A number of visual generalizations can be ascertained from observing Figures 11 through 15 which satisfy intuitive expectations.

1. Northward flows increased with increasing head drop (ΔH) across the free surface.

2. Southward flows decreased with increasing head drop across the free surface.

3. Northward flows increased for decreasing density differences.

4. Southward flows decreased for decreasing density differences.

5. Both northward and southward flows increased for increasing the ratio of southside lake surface elevation to southside density-interface elevation (H_1/H_3).

6. Increasing the ratio of embankment width to southside surface elevation (W/H_1) decreased both northward and southward flow rates.

Item 5 above apparently indicates that decreasing the outlet area for the southward flow, H_3, has less effect on this flow than the driving head of the density flow (i.e. H_2-H_3 in Figure 9).

Northward flows are most greatly affected by the head drop ratio across the free surface ($\Delta H/H_1$) and the ratio of embankment width to southwide lake surface elevation (W/H_1) (Figure 12). The density-difference ratio ($\Delta\rho/\rho_\ell$) had only moderate effect on these flow rates (Figures 11 and 13). The southward flows were affected mainly by the head drop ratio and the density-difference ratio (Figures 12 and 14). The ratio W/H_1 had only moderate effects on southward flow rates. The stratification ratio, H_1/H_3, had very little effect on the flow rates over the range of parameters tested.

Figures 12 and 14 show that it is possible to cut off the southward flow by either increasing $\Delta H/H_1$, decreasing $\Delta\rho/\rho_\ell$, or increasing W/H_1 sufficiently. If a hypothetical problem is posed beyond these limits, erratic flow rates and density-interface geometry result due to the fact that a mathematically ill-posed problem results. The numerical model developed in this analysis cannot accommodate wedge flow situations. For instance, Figure 12 shows that if the flow situation is such that the density difference ratio is 0.05, the effective length ratio is 4.5, and the ratio, H_1/H_3 is 6.0, then the southward flow is completely cut off

Figure 11. Northward flows for highest W/H1 ratio observed between 1968 and 1972, and $\alpha = 1:1$.

Figure 12. Southward flows for highest W/H1 ratio observed between 1968 and 1972, and $\alpha = 1:1$.
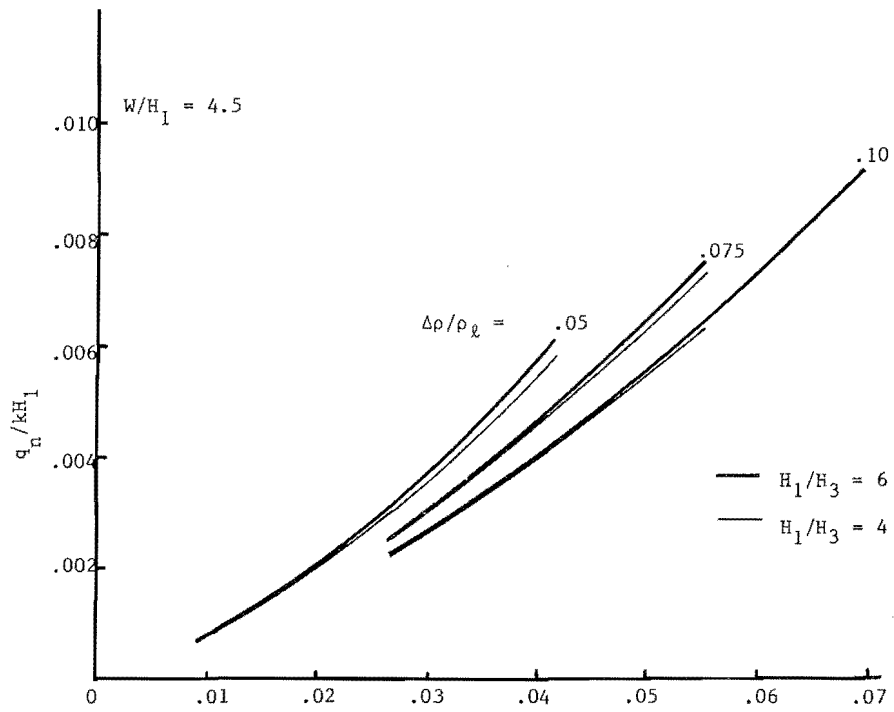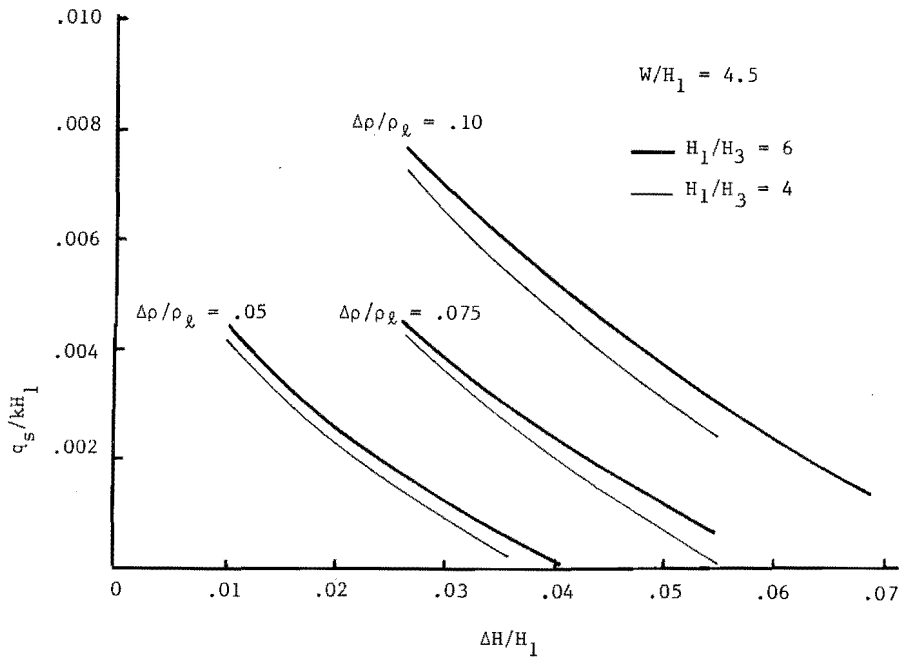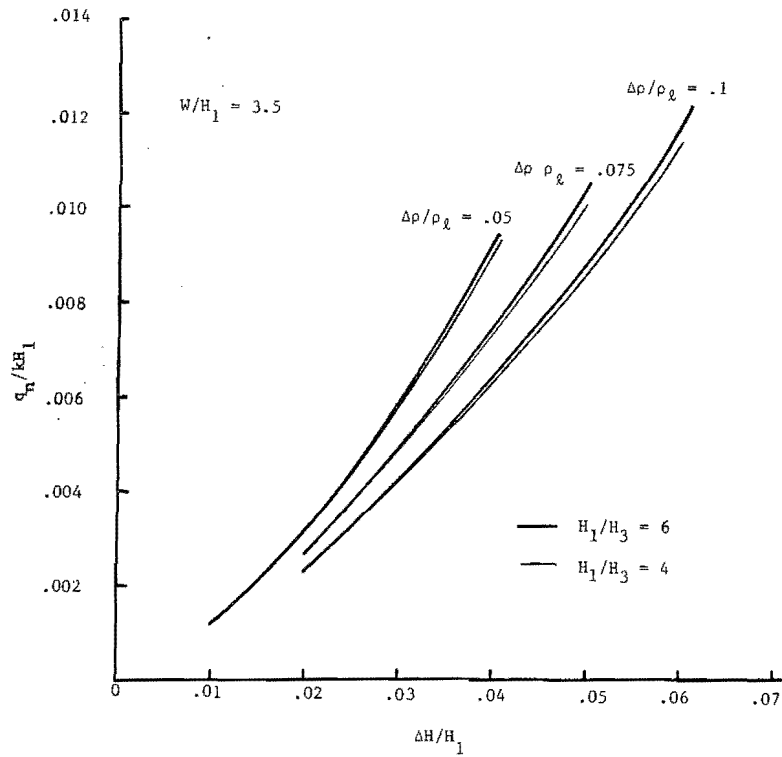
Figure 13. Northward flows for lowest W/H₁ ratio observed between 1968 and 1972, and α = 1:1.

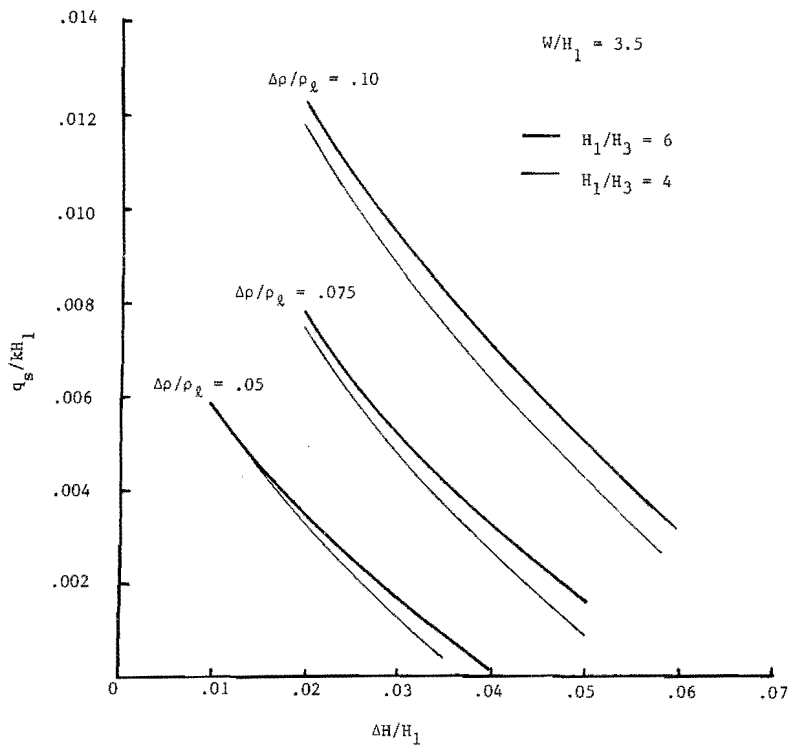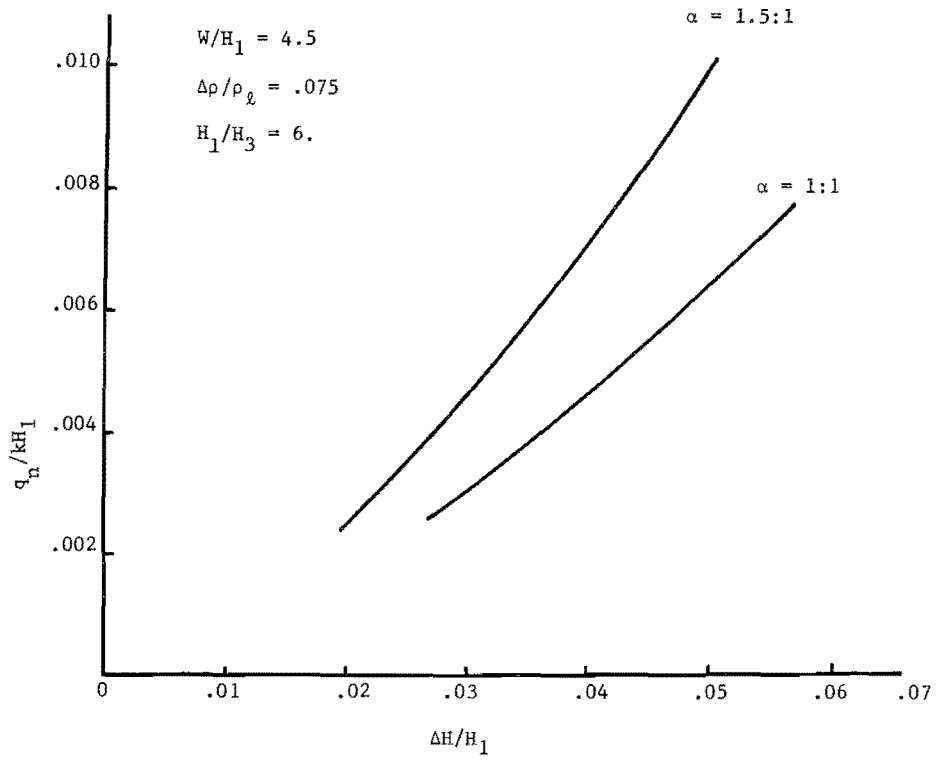Figure 14. Southward flows for lowest W/H₁ ratio observed between 1968 and 1972, and α = 1:1.

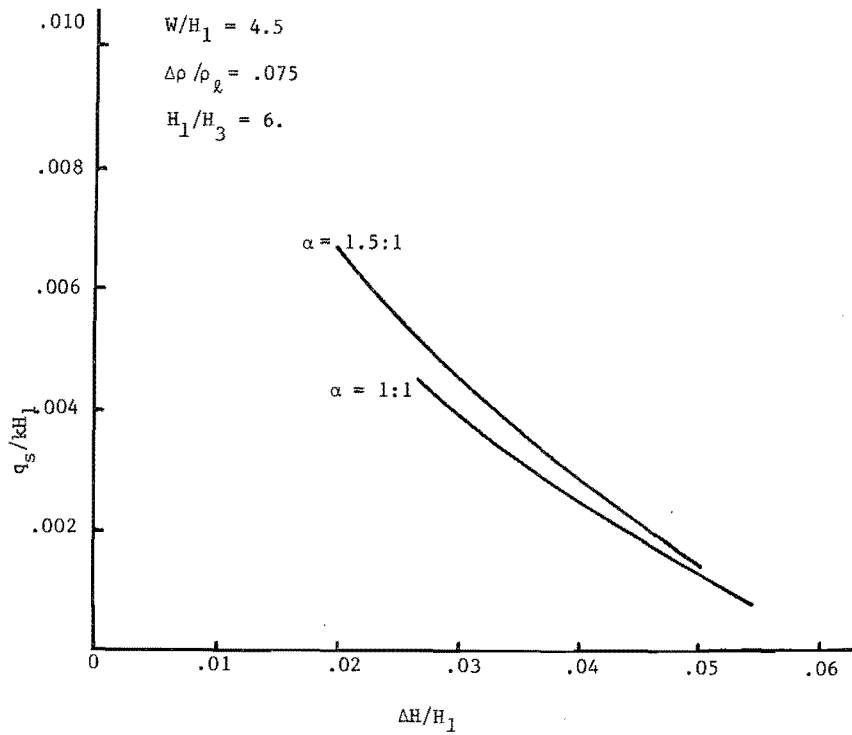Figure 15. The effect of side slope angle (α) on northward discharges.

Figure 16. The effect of side slope angle (α) on southward discharges.

when the free surface head drop ratio is 0.042. For an average value of H_1 of 25 feet, this would be a head drop across the causeway of approximately 1 foot.

Applicability of model to Great Salt Lake

This model study is directed toward simulating the flow through the railroad causeway of Great Salt Lake. Therefore, the range of parameters used in this analysis were chosen to bracket the spread of values which occurred in reality. Because of the numerous parameters involved and the scarcity of useful causeway data, it was not possible to rigorously verify the present model. The program developed in this study does provide similar relationships to those of two previous model studies performed by Lin and Lee (1972) and Cheng and Hu (1975), although the parameters they used were outside the range of values actually occurring on the lake.

Lin and Lee (1972) constructed a Hele-Shaw model to investigate stratified bidirectional flow. Their results are shown as the dashed line in Figure 17. This figure also contains similar plottings performed with information obtained from the program constructed in this study.

It should be noted that Lin and Lee allowed both H_1/H_3 and W/H_1 to vary in their model study. Since these parameters affect the rate of flow, their flow rate curve cannot be directly compared to those developed in this finite element analysis. However, the general trends apparent in the curves can be compared. Also note that although the density-difference parameter $\Delta\rho/\rho_\ell$ used by Lin and Lee was much higher than that occurring in Great Salt Lake, the general shape of curves are similar. Increasing $\Delta\rho/\rho_\ell$ tends to flatten the curves toward that obtained by Lin and Lee. The other dimensionless quantities (i.e. H_1/H_3 and W/H_1) are relatively unimportant in this qualitative comparison, but would have to be investigated for a comprehensive comparison between the Hele-Shaw model and the numerical model developed in this study.

In Cheng and Hu's analysis, the findings were plotted as the ratio q_s/q_n, against the density-difference ratio. The comparison of the present study to Cheng and Hu's findings could again be only qualitative because of Cheng and Hu's employment of northside stratification. The dashed line in Figure 18 represents a portion of the results from Cheng and Hu's report. The solid line is that derived from this study for identical parameter values and geometry of the fill. The two curves have the same basic shape. The difference between them appears to be a function of the northside stratification used in Cheng and Hu's analysis. Assuming that the northside fluid is unstratified causes a back pressure on the north side of the fill.

This back pressure may be the cause of the cut off which occurs from the program analysis at $\Delta\rho/\rho_\ell$ approximately equal to 0.025. It is, therefore, important to establish whether the waters on the northside of the embankment are stratified or not. This can only be based on field observations, of which there are few at present. Previous data and studies on the embankment do not indicate any stratification on the north side, but before this assumption can be verified more data are needed.

Very little field data have been obtained which are pertinent to this study. The Waddell-Bolke report contains sufficient information concerning surface elevations and densities of the north and south portions of the lake, but has very little in the way of flow rates through the fill. Only one complete set of flow rate data was obtained through this source. It should be observed that the flow rates calculated from this source may not be totally accurate due to the inexact nature of field permeability tests. Tracer studies of north and south flows were taken during May-June 1972, and northward flow rates were determined for August-September 1971. The pertinent information collected from these tests is shown in Table 8.

Through utilization of the various graphs presented in this report and using the dimensionless variables listed above, the dimensionless variable, q/kH_1, could be ascertained for both northward and southward flows. The necessary value of permeability could be roughly estimated by comparing the flow rates calculated by Waddell and Bolke to those calculated by the numerical model as shown in Table 9.

Table 8. Variables pertinent to causeway flow collected by Waddell and Bolke (1973).

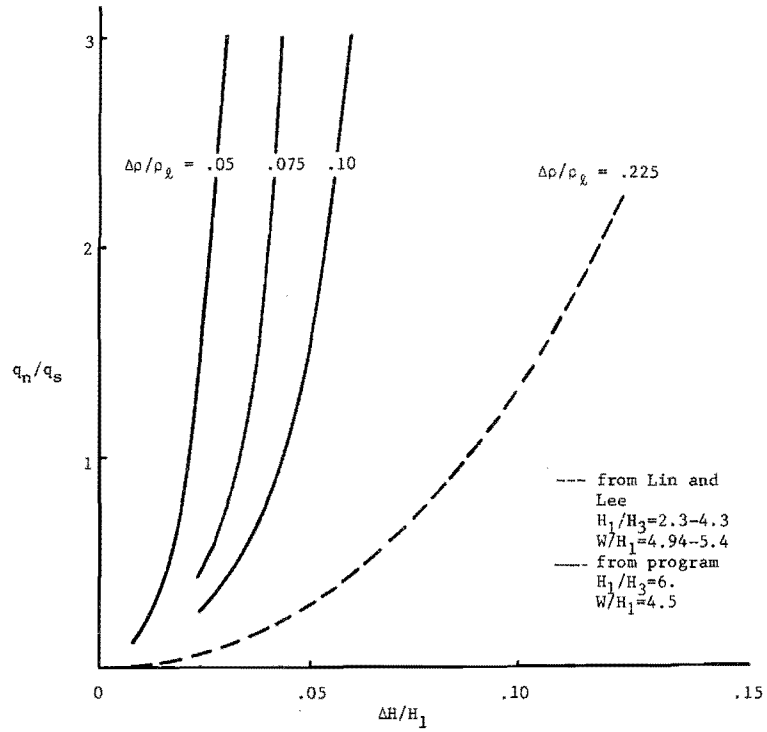|	May-June 1972	Aug.-Sept. 1971	Units
H_1	29	27	ft.
ΔH	1.55	0.98	ft.
H_3	6.5	3.75	ft.
W (assumed)	110	110	ft.
ρ_ℓ	2.328	2.359	slugs/ft^3
ρ_u	2.109	2.157	slugs/ft^3
q_n	0.07	0.025	cfs/ft
q_s	0.021		cfs/ft
$\Delta\rho/\rho_\ell$	0.094	0.086	---
$\Delta H/H_1$	0.053	0.036	---
H_1/H_3	4.46	7.2	---
W/H_1	3.79	4.07	---

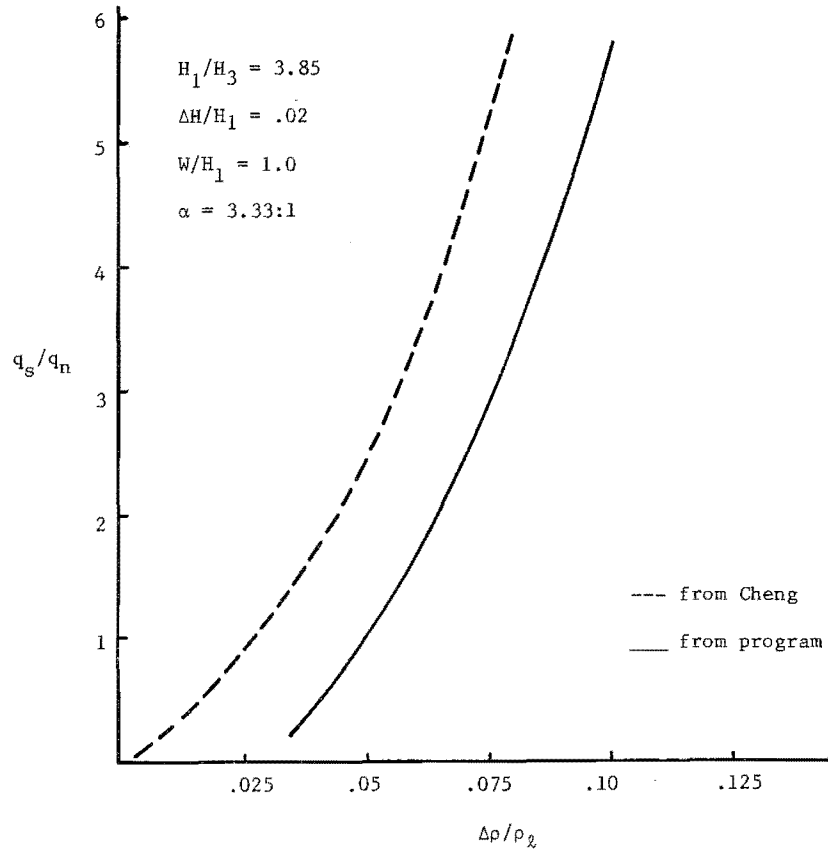Figure 17. Comparison of constructed model with that of Lin and Lee (1972).

Figure 18. Comparison of constructed model with that of Cheng and Hu (1975).

Table 9. Permeability calculations deduced from comparison of program flow rate calculations and actual lake values.

Date	Direction	q_c/kH_1^2	q_c/k (ft^2/ft)	q (cfs/ft)	k (ft/sec)
May-June 1972	Northward	0.009	0.261	0.07	0.268
May-June 1972	Southward	0.0031	0.0928	0.21	0.233
Aug.-Sept. 1971	Northward	0.0045	0.1242	0.025	0.201

Average - 0.234
q - from Waddell and Bolke (1973)
q_c - from model

A computer run was also made using the lake parameters for the May-June 1972 data with 1.5:1 side slopes instead of the 1:1 slope used in the above calculations. The value for permeability calculated as in the preceding manner was found to be approximately 0.5 ft/sec.

The above values for permeability lie well within the range of permeability values estimated in the Waddell-Bolke report. Individual permeability values calculated by Waddell and Bolke varied erratically from 0.08 ft/sec to 2.1 ft/sec. Since the permeability value has a very large influence on the calculated flow rates, it is imperative that a more accurate value of this quantity be found if this model is to be used as a predictive instrument applicable to Great Salt Lake. If more data on flow rates through the earth embankment are procured, it may be possible to deduce a more confident value of permeability by employing the method shown in Table 9.

Bi-Directional Culvert
Flow Analysis

As mentioned in the numerical models section, a solution technique for the culvert flows has been identified (Holley and Waddell 1976). For this reason, the finite element model of the culvert's bi-directional flow was used to investigate stratified flows. The use of an elemental Reynolds number to define scalar eddy viscosity values for a given mesh size was shown to be appropriate. It was discovered that an anisotropic description of diffusion provided the best interface model. The impact upon the velocity profile of the bottom friction coefficients was identified. Use of an eddy viscosity tensor is suggested by the success of the anisotropic diffusion coefficients; however, such an investigation was deemed to be deserving of a more comprehensive and costly investigation than the current research warranted.

The elemental Reynolds number

It is well known, at least in a general sense, that the convergence of the finite element analog depends on the adequacy of the finite element grid. In the limit, an infinite number of infinitesimal elements would yield a solution indistinguishable from the exact solution to a given problem. The work of Gartling et al. (1976) has provided a fairly good quantification of how many and of what size elements are required to obtain a convergent solution, where convergence is a function of a minimal percentage change in the solution. They succeeded in defining an elemental Reynolds number which defines the mesh requirement for convergence to be

$$Re_{max} = \frac{v_{max} x}{\varepsilon} < C \quad . \quad . \quad . \quad . \quad (111)$$

where max implies that the maximum value is found over the entire domain. The elemental Reynolds number is based on a characteristic velocity in an element v_{max}, and a characteristic elemental dimension x. The inequality in Equation 111 implies that as the fluid viscosity is decreased the mesh spacing x must also decrease to insure convergence of the iterative method. By examining several problems, Gartling, Nickell, and Tanner (1976) estimated that C was on the order of 100.

In this work, the elemental Reynolds number was varied by changing the viscosity values and keeping the element dimension the same. Using a constant-density one-directional flow problem with the element and node domain defined by Figure 19, seven computer runs were made with the eddy viscosity changed with each run. It was assumed the off-diagonal elements of the eddy viscosity tensor were zero and that the x and y components of the tensor were equal. The flow rate per unit width was 45.9 cfs with an average velocity of 3 ft/sec.

Following four iterations, each run is characterized by three items displayed
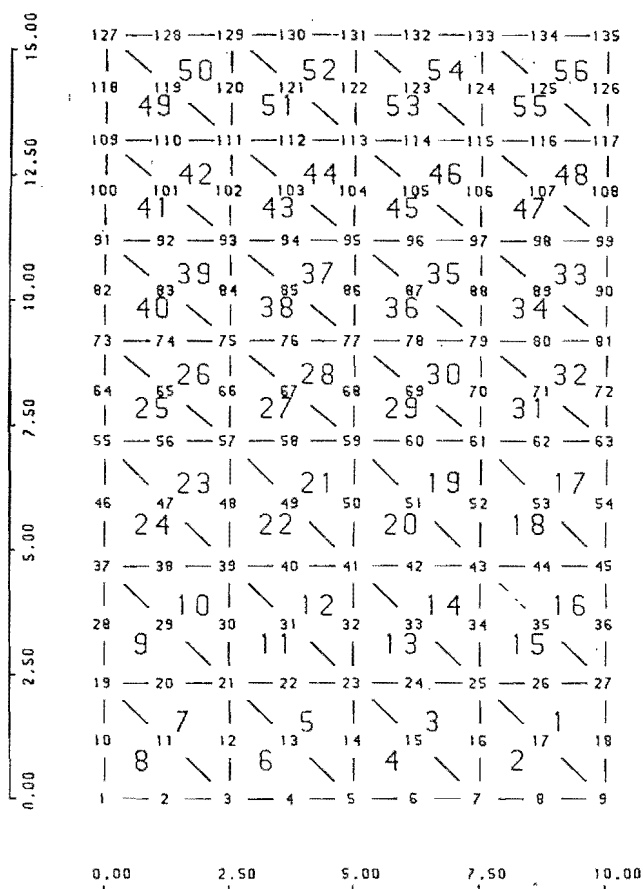
49

Figure 19.   Discretization for the 10 feet
long culvert.

in Table 10. Delta HGL is the difference in
water surface elevation between nodes
127 and 135. With a flow length of only 10
feet the difference in HGL between nodes 127
and 135 should be nil. The next column has
listed the convergence parameters of the u
and v components of velocity. These computed
values compare the change in the computed
velocity field values between successive
iterations. For convergent problems, these
values should approach zero. The last item
to check is the conservation of mass which is
provided in the fourth column.

The results shown in Table 10 show that
the surface drop and convergence criteria is
at a minimum when eddy viscosity is 0.05 with
an elemental Reynolds number, Re_{max} of 135.
However, one must note that mass conservation
is best at an eddy viscosity of 1.0 and a
corresponding Re_{max} of 6.75. Also of
note is the apparent existence of a best
value, i.e.

$$6.75 \leq Re_{max} \leq 135 \quad \ldots \quad \ldots \quad (112)$$

While the limits of Equation 112 have not
been firmly established, the results do

suggest a lower limit to the mesh refinement
for a given viscosity value.

The coefficients of friction,
diffusion and viscosity

In order to solve the equations of Table
2, it is necessary to specify the values of
eight constants. Only two of eight con-
stants, i.e., the side and bottom friction
coefficients, are well defined in the litera-
ture. The other four values of the eddy
viscosity tensor and the x and y coefficients
of diffusion must be determined by trial or
modeling experience. Each of the coef-
ficients has a different and important effect
on the simulation results.

Side and bottom friction coefficients.
These coefficients may be computed from
drag coefficient equations (Schlicting 1968)
discussed in Martin (1979). The only
ambiguity arises in the definition of the
Reynolds number. Using the kinematic
viscosity, one finds $Re = 2 \times 10^6$ and
finally a bottom friction coefficient of
0.003. However, if one chose to employ the
eddy viscosity used in the computation, a
Reynolds number of 30 is computed correspond-
ing to a friction coefficient of 0.27.
Simulations of both coefficients were run for
four iterations. The resulting profiles of
southward (right to left) moving fluid in the
bi-directional solution are displayed in
Figure 20. Stable solutions of both profile
types is made possible through the adjustment
of the influent velocity profile. The
velocity profiles in Figure 20 show that the
use of larger coefficients yield a laminar
type profile, while the smaller value yields
a more turbulent characterization. While
profile data are not available, it is felt
that a flat or turbulent profile is more
characteristic of the culvert discharges;
therefore, the smaller values were adopted.

Diffusion coefficients. The literature
provides very little information regarding
what the magnitude of these coefficients
should be. The report provided by Norton et
al. (1973) suggested the values on the order
of 1.0. However, the problem they dealt with
was one-directional and had flow velocities
an order of magnitude smaller. Simulating
bi-directional flows requires a distinct
definition of the interface region. For the
mesh shown in Figure 19, an appropriate
x-direction diffusion coefficient was
determined to be on the order of 30 with
a y-direction diffusion coefficient in the
neighborhood of 5. Three-dimensional
plots of the density field are shown in
Figures 21 and 22. Each plot depicts
density results after four iterations. The
input data for both runs represented by
Figures 21 and 22 was identical except for
the values of the diffusion coefficients. A
poorly defined interface was obtained every
time that the diffusion coefficients were
input as equal to each other, regardless of
their magnitude. For Figure 21, they were

Table 10. One directional, constant density problem. Varying the elemental Reynolds number via the eddy viscosity changes.

$\epsilon_x = \epsilon_y$ (ft^2/sec)	Re_{max}	Delta HGL (ft)	Convergence Parameters	Continuity Checks
0.0005	13500	0.118	0.34 & 0.28	off by 12%
0.005	1350	0.046	0.16 & 0.09	off by 3%
0.05	135	0.014	0.008 & 0.009	off by 0.3%
0.5	13.5	0.023	0.012 & 0.011	off by 0.05%
1.	6.75	0.044	0.02 & 0.02	off by 0.02%
5.	1.35	0.286	0.10 & 0.08	off by 0.04%
10.	0.68	0.635	0.20 & 0.11	off by 0.04%
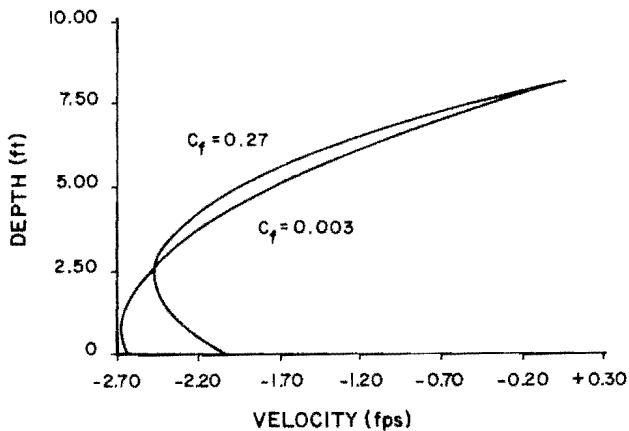
Figure 20. Impact of skin friction coefficient selection upon velocity profile.

equal to 5. For Figure 22, $e_x = 30$ and $e_y = 5$. The plot in Figure 21 shows a poorly defined interface region with the denser brine being pushed up into the lighter brine flowing to the north. The plot in Figure 22 shows a distinct interface region with the lighter fluid flowing southward with very little mixing. Further smoothing of the density profile shown in Figure 22 would be possible through adjustment of boundary conditions to reflect the predicted gradient on the domain's interior; however, the concept of modeling the steep gradient has been demonstrated.

Turbulent eddy viscosity tensor. The values of the viscosity tensor must be determined through modeling experience. The work by Norton et al. (1973) suggested values of turbulent dynamic viscosity on the order of 10 or turbulent kinematic viscosity on the order of 5. In this work, for both one-

Figure 21. The model computed density field after four iterations with $e_x = 5$ and $e_y = 5$.

51

Figure 22. The model computed density field after four iterations with $e_x = 30$ and $e_y = 5$.

directional and bi-directional flow, setting both ε_x and ε_y equal to approximately 1 provided the best simulation. It was noted that at the lower values of the eddy viscosity, i.e., higher Reynolds 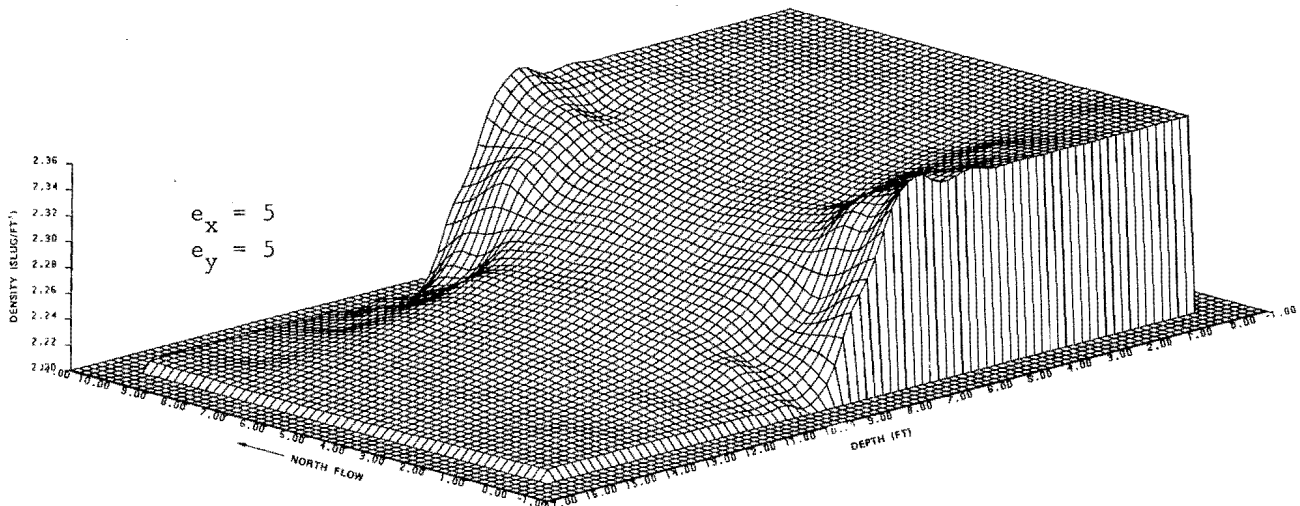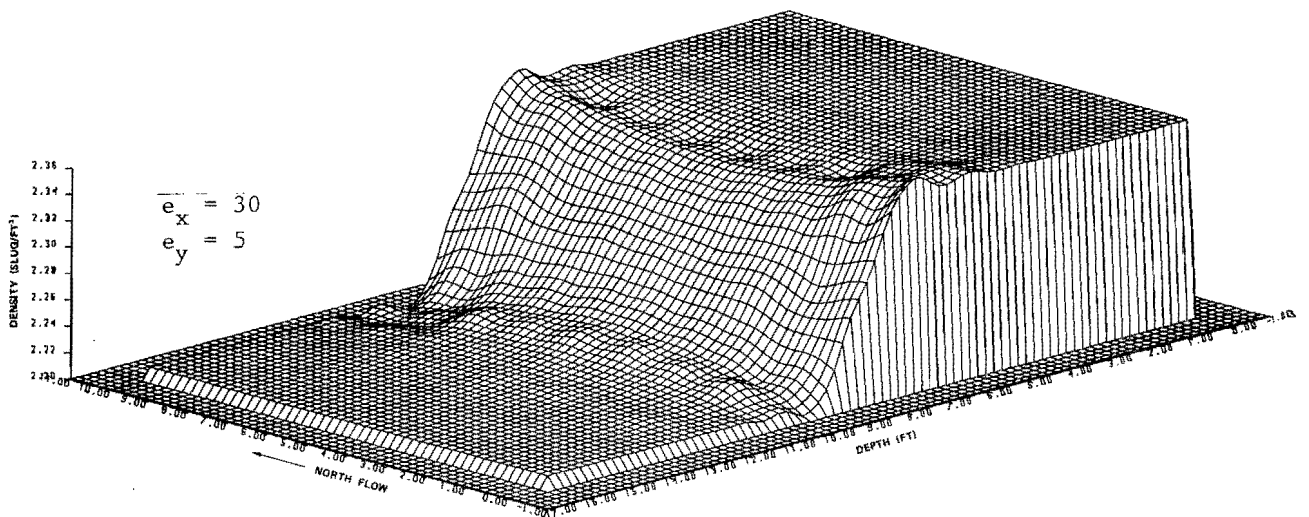number, numerical instabilities developed. At higher values of eddy viscosity, large energy losses occur in the numerically simulated flows. Use of the elemental Reynolds number to define the eddy viscosity as a function of mesh size appears reasonable; however, application of this concept to the various elements of the eddy viscosity tensor is not readily defined.

This and previous applications of the elemental Reynolds number concept have been limited to the scalar description of eddy viscosity. Use of the anisotrophic diffusion coefficients suggests the need to investigate the use of an anisotropic eddy viscosity. Perhaps an elemental Richardson number could be employed to define an anisotropic eddy viscosity vector. Off-diagonal entries could be assumed symmetric and their values determined as functions of velocity gradients and the diagonal eddy viscosity values. Such an investigation would consume both time and considerable computer funds, and since it was beyond the scope of the proposed research, it was not undertaken.

The analysis performed upon the stratified bi-directional culvert flow is not directly applicable to the causeway culverts. Despite the fact that discharge-stage-density relationships have not evolved, some useful information and ideas have been generated. Use of an elemental Reynolds number to define viscosity as a function of mesh discretization has been further substantiated. The concept of anisotrophic diffusion coefficients has been shown to yield gradient properties of the halocline, and suggests the development of anisotropic eddy viscosity values. Each of these concepts must be

developed further for their use in either vertically-averaged two-dimensional models or three-dimensional models of lakes. Definition of these concepts for future study is a valuable contribution toward the successful modeling of stratified impoundments.

Three-Dimensional Steady State Circulation Model

Economy and documented accuracy are desired attributes of any numerical model. For the three-dimensional simulation, where specific prototype events have not been monitored, hypothetical problems are investigated to determine the simulative ability of the model.

Economy of performance of the model may be attributed to the three-dimensional character of the problem. Large core and execution time requirements combine to make this model, at best, marginally economical. Using the cubic interpolation of the Bogner-Adini element to model the three velocity components gave rise to an element stiffness matrix with 108 degrees of freedom. Thus, the element stiffness matrix alone required nearly 12,000 words of computer storage. The numerical integration and frontal solver contribute to the large execution times of the model. The overall poor economies of the numerical model forced the use of the simplest constitutive model and simplistic domain discretizations.

Initial testing of the model was performed to determine the consistency of the computer code. Originally posed problems were rotated 90 degrees for comparative purposes. Evaluation of such material determined the consistency but not the correctness of the model. Coriolis forces

were zeroed in order to exclude their natural bias.

The second phase of testing focused upon the alternative models which could be used for both velocity and pressure. Recall that as an alternative to the complete Navier-Stokes model of velocity, a formulation is posed which uses the first two component Navier-Stokes equations and the mass conservation equation. Numerical models of pressure differ in their treatment of the time dependent divergence of the velocity vector. Different combinations of velocity and pressure models were examined to determine the appropriate overall model for the qualitative tests.

Finally, qualitative simulations were carried out on representative cavity flows. Comparisons are made with empirical results. The magnitude and profiles of velocity, and free surface set-up are discussed herein. Elemental Reynolds numbers are posed as a possible indicator of stable, convergent solutions of the cube cavity problem. Conditioning was examined as a possible explanation of the inability to achieve a vertical recirculation within the shallow cavity problem.

The economic performance of the model prohibited the examination of many problems of interest. Core limitations restricted the dimension of problems which could be attempted. Execution times were heavily dependent upon the numerical integration employed and the solution process. Problem discretizations which minimized the number of elements served to minimize both the core and time requirements. However, failure to carry the mesh refinement to an extreme leaves some of the coefficient selections, notably the eddy viscosity, open to question.

Description of the hypothetical problem

Since prototype data are not available with which to verify the model, a hypothetical problem is defined. Such a problem must be simple to monitor, and the qualitative solution of the problem must be known. Of course, if an exact solution were available, the problem would be ideally suited for verification. Both the free surface and three-dimensional nonlinear character of the problem preclude its exact solution; therefore, one must settle for a qualitative solution. Description of the problem includes a definition of the domain, its discretization, and the boundary conditions which are applied to drive and constrain the problem. Following the problem description is a summary of alternative treatments of the free surface and velocity segments of the numerical model. Finally, the presentation and discussion of the results of the qualitative simulations conclude the results of the three-dimensional model of circulation.

A simple cavity flow problem has been selected with which to qualitatively assess the simulative ability of the model. It is a problem of free surface flow driven by a wind induced surface shear. In the paragraphs to follow, both a cube and a shallow rectangular domain (see Figure 23) are discussed. The initial dimensions of these cavities will be denoted as ($\Delta x - \Delta y - \Delta z$). For example, a unit cube is denoted as (1-1-1), and a shallow rectangular cavity by (1-1-0.05). The automatic mesh generator within the preprocessor subdivides the domain according to the number of elements one desires in each of the natural coordinate directions. Thus another set of three numbers indicates the mesh required by the operator. For example (2-2-1) indicates that the user
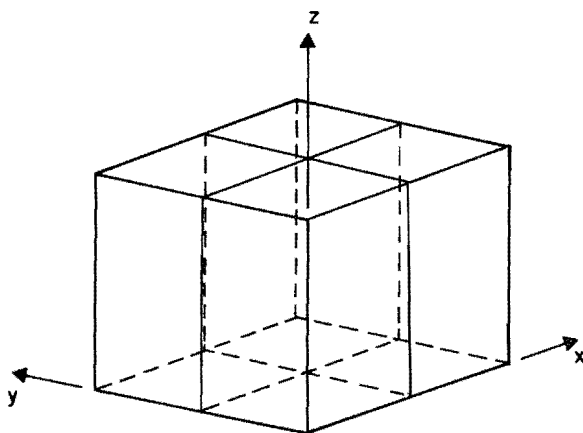
(a) cube
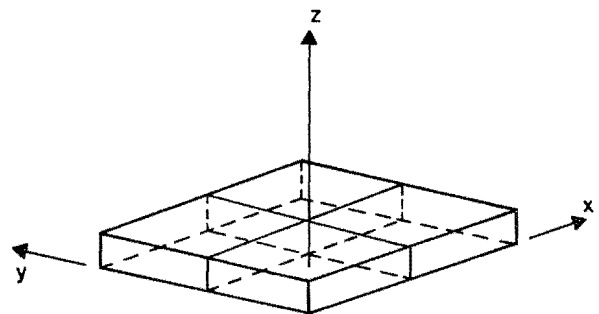
(b) shallow rectangular cavity

Figure 23. Cavity flow domains showing a (2-2-1) element discretization.

requires two elements in the ξ direction, two elements in the η direction, and one in the ζ direction.

Boundary conditions on both the externally applied stress, and velocities are employed to specify the problem. Boundary stresses are preset in nonhomogeneous natural boundary conditions. The stresses are assumed to be functions of the overlying fluid velocity. Secondly, the fluid velocity is constrained by setting the normal velocities and their tangential gradients to zero (see Table 11). This has the effect of specifying an impervious external boundary. Thus, wind induced stress drives the circulation in the cavity, edge and bottom stresses impede the flow, and constraints on the normal flux effectively define the problem domain.

Summary of alternative formulations

Alternative formulations exist for both the velocity and pressure segments of the numerical model. Initial solution attempts focused upon the cube cavity domain. While these solutions exhibited the desired recirculation, they also displayed the poor pointwise satisfaction of mass conservation observed by Olson (1976). In an effort to improve this situation the forcing function version of the pressure problem was coupled with the originally employed Navier-Stokes formulation of velocity. Point checks on the satisfaction of continuity did not improve with the new formulation. Indeed, the overall problem solution seemed more sensitive to the selection of eddy viscosity. It would appear that while the forcing function pressure formulation does achieve a solution, its solution is achieved over a relatively narrow range of eddy viscosity values. In light of the fact that viscosity values are

not known a priori, the rather unforgiving nature of this alternative pressure formulation is not desirable.

A much more consuming difficulty arises in the solution of the shallow rectangular cavity. Exhaustive tests indicate that the scale effects, resulting from the use of elemental horizontal lengths greater than the elemental depth, inhibit solution of the velocity problem. A solution is found, but rather than achieving a vertically recirculating flow, the solution has a flow-through character which completely ignores mass conservation laws. In developing the alternative velocity model it was thought that the scale effects were, if not isolated, at their worst in the z-component Navier-Stokes equation. However, application of the alternative model failed to alter the previously established result. This would seem to indicate that relative scale effects are equally important in the x and y component equations.

All combinations of the velocity and pressure formulations have been applied to both the cube and shallow cavities. While the previously mentioned character of the forcing function pressure model make it less desirable, none of the alternatives show themselves to be uniquely suited to a particular problem. Thus, in order to reduce the confusion that four different models would cause, a single overall formulation is adopted for the qualitative analyses. The original Navier-Stokes velocity formulation is used in conjunction with the steady state pressure model.

Empirical relationships

One must examine the empirical relationships developed in the literature for wind-

Table 11. Velocity boundary conditions associated with corner, edge, and interior nodes of the cavity domains.

Type of Node/Location/ (Number of Constraints)	Constrained Nodal Degrees of Freedom
Corner/Top (10)	u u_η u_ζ v v_ξ v_ζ w w_ξ w_η $w_{\xi\eta}$
Corner/Middle (6)	u u_η u_ζ v v_ξ v_ζ
Corner/Bottom (9)	u u_η u_ζ v v_ξ v_ζ w w_ξ w_η
Edge/Top (7)	v v_ξ v_ζ w w_ξ w_η $w_{\xi\eta}$ $-\ \eta = \pm 1$ u u_η u_ζ w w_ξ w_η $w_{\xi\eta}$ $-\ \xi = \pm 1$
Edge/Middle (3)	v v_ξ v_ζ $-\ \eta = \pm 1$ u u_η u_ζ $-\ \xi = \pm 1$
Edge/Bottom (6)	v v_ξ v_ζ w w_ξ w_η $-\ \eta = \pm 1$ u u_η u_ζ w w_ξ w_η $-\ \xi = \pm 1$
Interior/Top (4)	w w_ξ w_η $w_{\xi\eta}$
Interior/Bottom (3)	w w_ξ w_η

driven circulation. The two characteriza-
tions, fluid velocity and free surface
set-up, are empirically related to the
driving wind's magnitude by the following
formulas (George 1974).

$$\overline{U} = 0.03 \, \overline{V}_w \quad . \quad . \quad . \quad . \quad . \quad . \quad (113)$$

$$S = 0.33 \, 10^{-5} \, \overline{V}_w^2 \, L/gH \quad . \quad . \quad . \quad (114)$$

where

$\overline{V}_w$ = mean velocity of the air above the fluid (cps)

$\overline{U}$ = mean velocity of the fluid surface (cps)

S = set-up due to the airflow (cm)

L = length of the channel (cm)

H = depth of the channel (cm)

g = gravitational constant (980 cm/sec^2)

From the literature (Liggett and Hadjitheo-
dorou 1969, Norton et al. 1973, Cheng et al.
1976) a wind magnitude value has been select-
ed which corresponds to a wind shear stress
of approximately one-half dyne per square
centimeter. Substitution of this driving wind
magnitude of 19.34 fps (590 cps) into the
above expressions yields physically expected
values of 0.58 fps and 4.0 x 10^{-5} feet for
surface velocity and set-up respectively.

Results of the cube
cavity investigations

Both a single element and four element
treatment of the unit cube cavity are dis-
cussed. Computations employing a single eddy
viscosity of 0.003 ft^2/sec are used to dem-
onstrate the evident dependence of viscosity
upon element length characteristics. Of note
are the altered characteristics of the
velocity profiles in the two solutions. Also
of significance is the much smoother free
surface representation resulting from the
four element treatment.

The iterative history of u-velocity
profiles for the single element treatment
demonstrates the development of vertical
recirculation. Of particular interest
is the altering of the velocity profile's
shape. The expected cubic profile is
originally predicted; however, the inclusion
of the nonlinear terms in subsequent itera-
tions leads to a profile which is linear in
appearance. A maximum velocity of 0.023
appears in the third iteration. Probable
convergence of the solution is indicated by
the decrease in the flux entering or leaving
the domain.

From free surface profiles, primary
interest is in the set-up of the free
surface in the direction of the wind. Each
iteration shows a slight increase in set-up,
and while the velocities and flux indicate a
convergent solution, one would have to be
concerned with the possibility of an ac-

celerating free surface in subsequent itera-
tions. Of secondary concern is the free
surface displacement predicted in the corners
of the domain. A differential displacement
between the upwind and downwind corners
remains in the 3.0 x 10^{-5} to 4.0 x 10^{-5}
range. It was assumed that the pressure
problem's Dirichlet boundary conditions,
which lie at the upwind corner nodes, acted
as a damper upon the free surface adjustment.
However, the four-element treatment allows
for a more general investigation of the free
surface reaction, and the differential seen
in the single element problem also appears in
the refined mesh.

For the mesh refinement of four elements
the character of the flow is altered. The
velocity magnitudes have increased over those
reported for the single element solutions
(maximum velocity = 0.035 fps). This change
comes despite the fact that the overall
geometry and eddy viscosity are unchanged.

The altered character of the velocity
profile may be attributed to the reduction in
boundary condition constraints. In the case
of the single element treatment, all nodal
values of velocity are set to zero. The four
element treatment includes edge nodes and
thereby a relaxation of the velocity con-
straints upon the domain. Since forces upon
the domain and the domain itself are un-
changed the velocity's magnitude change may
be influenced by the relationship between
element size and eddy viscosity. Gartling
(1974) suggests such a relationship for
two-dimensional problems. Free surface
profiles reveal the similar nature of the
free surface configuration for the four
element discretization. Corner nodes remain
the location of maximum deflections.

Discussion of results for
the cube cavity

Results of the cube cavity problem
demonstrate the trade offs which exist
between eddy viscosity, fluid velocity, and
surface set-up. Basically, for constant
stress it is observed that as eddy viscosity
decreases, both fluid velocity and set-up
increase. Thus, an inverse relationship
exists.

There would appear to be a range of eddy
viscosity values for which solutions of
acceptable character can be achieved. The
limits of the range are defined by the
response of the model. For large eddy
viscosities the response is a low velocity
prediction accompanied by virtually no
surface set-up. Of course, a high eddy
viscosity implies a viscous, energy-consuming
flow, and one should expect a slow movement
and negligible surface set-up. Wishing to
increase both characteristics, one reduces
the viscosity. Once the viscosity becomes
too small the predicted velocities initiate a
surface set-up so large as to cause the
solution to become unstable and diverge. The

range of acceptable eddy viscosities lies between these two extremes.

Both the relative change and flux computations serve as checks upon the convergence of a problem's solution. Relative change was reported as a maximum percent change (based upon the latest iteration) in the solution's many components (i.e., u, u_ξ, u_η, u_ζ, etc.). Flux was monitored through specific cross-sections and also for the problem's entire external boundary. Thus, the recirculation character and mass loss or accumulation may be easily checked. These two methods of monitoring the solution aid the definition of the eddy viscosity's lower extreme.

Knowing what one desires for results focuses on the final trade off with respect to the cube cavity problem. There appears to be a relationship between the maximum velocities and set-up exhibited by a problem, and its eddy viscosity and mesh refinement. Table 12 depicts the single and four element treatments of the unit cavity's solution. One immediately realizes that the predicted velocities and set-up are at least an order of magnitude lower than the empirically-based values. However, it is also apparent that increasing the number of elements has increased both the predicted velocities and set-up.

By characterizing the rectangular-solid shaped element's length by its horizontal diagonal (because only horizontal refinement is being employed) an elemental Reynolds number may be defined as

$$R_e = \frac{V_{max} \ (\Delta x^2 + \Delta y^2)^{\frac{1}{2}}}{\varepsilon} \quad . \quad . \quad . \quad . \quad (115)$$

where

R_e = elemental Reynolds number
ε = homogeneous isotropic eddy viscosity coefficient
Δx, Δy = element lengths in the respective directions

This elemental Reynolds number may now be employed to characterize the solution. Such a characterization is developed by Gartling (1974) for two-dimensional problems employing finite elements. Gartling found a relatively constant value of $R_e < 100$ which lead to convergent solutions. In the present work a constant parameterization lying near 5 developed. The tests described herein are by no means conclusive in this respect.

Discussion of results of the shallow cavity problem

Although the early literature (Neumann and Pierson 1966, Wiegel 1964) indicates that shallow oceans do not exhibit an Ekman spiral, the shallow cavity problem is expected to recirculate. The problem's boundary conditions should dictate such a flow; however, all results of shallow cavities predict a flow-through characterization of the fluid. Continuity of mass is poorly achieved.

Since the shallow rectangular cavity problem failed to yield a vertically reciruculating solution, its discussion will be limited to those methods which were attempted. Four basic approaches were tried in attempting to achieve a recirculation profile. They were refinement of mesh discretization, variation of the eddy viscosity vector, symmetric location of the geometric boundary conditions for the free surface, and the artificial creation of a first iteration recirculating solution. Characterization of the source of error was attempted through an investigation of the global matrix's conditioning.

From the success of the cube cavity it was felt that mesh refinement could yield a vertically circulating flow prediction. However, the previously described economies of the model preclude mesh refinement to the extent required. In test problems designed to discover the threshold of the cavity solution, it was discovered that problems having a length to depth ratio of 2 failed to produce recirculation. Since the areal extent of lakes is in general much greater than their depth, to seek a solution by refinement is out of the question for this model. The eventual element employed in the shallow cavity problem must have the character of a large length to depth ratio. In the case of Great Salt Lake, maximum depth is on the order of 30 feet and a reasonable element length must be thousands of feet. Thus, while mesh refinement might provide a solution it would not be an economical one.

Because of the great distortion required of the geometry, it was felt that a similar distortion of the eddy viscosity components might yield a recirculating solution. Both increasing and decreasing the z-component eddy viscosity relative to the x and y components were tried. Neither had any impact upon the flow-through character of the solution.

During the investigations of symmetry, it was discovered that location of the Dirichlet boundary condition on pressure had an impact upon the free surface solution. Since only one point should be defined by such boundary conditions, it was determined that a symmetric location with respect to the load was best. In the case of a single element problem there is no single position. Symmetry for a single element implies that both upwind nodes must be set with Dirichlet boundary conditions. While creating a much smoother and symmetric solution, setting two such boundary conditions had no impact upon the velocity problem. Reflecting on the problem, one can see that the solution sequence is such that the free surface

Table 12. Unit cube cavity solutions for single and four element refinement.

Eddy Viscosity (ft^2/sec)	Maximum Velocity (fps)	Set-Up (ft)	Elemental Reynolds No.	Quality of Solution
		Single Element Treatment		
0.03	0.0034	less than 10^{-6}	0.14	Stable, convergent
0.005	0.018	4×10^{-6}	5.09	Stable, convergent
0.003	0.022	15×10^{-6}	10.37	Stable, diverging ?
0.00205	0.051	20×10^{-6}	35.2	Unstable, diverging
		Four Element Treatment		
0.01	0.0148	1×10^{-6}	1	Stable, convergent
0.005	0.0275	6×10^{-6}	3.9	Stable, convergent
0.003	0.037	12×10^{-6}	8.72	Stable, diverging ?
0.0024	0.0448	19×10^{-6}	13.3	Unstable, diverging
0.001	0.1539	103×10^{-6}	108.8	Unstable, diverging

boundary conditions do not affect the velocity formulation until the second iteration. Thus, boundary conditions on pressure have no immediate impact upon the velocity solution.

The last attempt to force a shallow cavity solution involves the relative values of the linear and nonlinear portions of the problem. A possible argument is that the solution to the first iteration linear problem sufficiently distorts the solution to cause divergence. If a recirculating solution could be initiated, the nonlinear terms, which enter the second iteration computation, might direct the problem to a convergent recirculating solution. Two means are available to force recirculation to occur. One may drive a bottom flow by either placing a shear stress on the bottom of the problem, or presetting a surface set-up so as to induce a natural flow. While the preset set-up was found unsatisfactory, a return flow was induced through an applied bottom shear. The applied bottom shear had to be equal but opposite to the applied wind-induced shear. Regardless, once the second iteration was solved the flow-through character returned to the velocity field prediction.

Having failed to achieve a vertically recirculating solution to the shallow cavity problem, it is of interest to search for a cause-effect relationship. A review of the finite element literature revealed that a similar problem arises in the investigation of shells when using three-dimensional elements. Zienkiewicz (1977) indicates that the large length to thickness ratio incumbent of shell analysis gives rise to an ill-conditioned stiffness matrix. Thus, showing a relationship between the length to depth ratio of an element and the resulting condi-

tion number of the global stiffness matrix would establish the desired cause-effect relationship. At the same time one must show whether other variables such as eddy viscosity, order of integration, and discretization have an affect upon conditioning.

For the unit cube a condition number of approximately 1600 is found for all eddy viscosities and integration orders. An identical condition is found for the 10-foot cube as well. The conclusion to be drawn is that integration is adequate, and changes in eddy viscosity and overall size act as simple multipliers which are countered by the resulting inverse matrix.

To determine the impact of relative depth, three single element problems are posed. The problem domains and the resulting conditioning are summarized in Table 13. While the conditioning of all problems is poor, one can readily see that shallow elements have a decidedly worse character than others.

To complete the examination of conditioning, a four-element refinement of the

Table 13. Conditioning as a function of relative depth.

Domain (Mesh)	Relative Depth	Condition Number	Relative Condition No.
1-1-10	10	1420	0.90
1-1-1 (1-1-)	1	1580	1.00
1-1-0.1	0.1	45000	28.5
1-1-1 (2-2-1)	4	32000	20.3

unit cube problem is posed. Increasing the dimension of the global stiffness matrix has the effect of increasing the stiffness matrix's norm; however, it also increases the norm of the inverse matrix. Conditioning of the global matrix is increased to 32000 or a relative value of 20. This implies one of two possibilities: that mesh refinement may lead to worsening solutions (even on the unit cube); or conditioning has nothing to do with the difficulties in obtaining the desired recirculating solution of the shallow cavity problem.

Summary of results for the three-dimensional circulation solutions

Solutions of the unit cavity problem has been shown to yield a vertically re-circulating fluid flow. While the character of the prediction is as expected, it is apparent that the magnitudes of both the velocities and set-up are not. Some relief comes from the elemental Reynolds number concept; however, discretization of the problem domain does not appear economically feasible at this time.

Examination of the shallow cavity problem fails to yield the expected verti-cally recirculating solution. The economics of the model do not allow one to determine the impact of mesh refinement upon this situation. Results of a study of condition-ing reveal that the condition number of the shallow cavity problem is no worse than that of the four-element unit cube problem. Since recirculating solutions are achieved for the latter, there is no reason that ill-conditioning of the shallow cavity problem should be singled out as the explana-tion of our results. The condition number study does reveal that relative depth is an important factor in determining the character of the flow predicted by the present model.

Review of the Ekman concept of a depth of frictional influence leads to the conclu-sion that higher values of viscosity, ε, will lead to flow-through situations. Recircula-tion in such cases occurs as the wind-induced set-up forces entire vertical cross-sections to take on a velocity opposite that of the driving wind. These regions of return flow act to resupply the wind driven recircula-tion. Since the numerical model requires a relatively and perhaps artificially high viscosity for stable solutions, one might expect to find a solution exhibiting a flow-through character. However, in order to demonstrate this possibility one would have to employ considerably more than the four elements dictated by the present economic constraints. Prior to dedicating the amounts of funding required of such a test, one must also consider the implications of the verti-cally homogeneous velocity profile implied in the above argument. If such a profile does exist, then a two-dimensional, vertically integrated model of shallow lakes may be more appropriate to the task.

Two-Dimensional Depth-Averaged Circulation Model

The two-dimensional depth-averaged circulation model is the primary numerical model for simulating circulation patterns in the lake. The other models are available to assist in determining boundary conditions and to predict mixing and transport of pollutants and salinity.

Application of the model to Great Salt Lake

To demonstrate the application of the model to Great Salt Lake, a finite element configuration had to be selected, depths and surface elevations chosen, and a host of other parameters selected.

For purposes of demonstration, the lake surface was assumed to be at elevation 4200 feet. The depths of the lake were obtained from the U.S. Geological Survey topographical map entitled Great Salt Lake and Vicinity. A finite element mesh of manageable size was generated by a computer mesh-generator program. A computer-generated plot of the mesh is shown in Figure 24. The mesh is quite coarse because of computer size limita-tions, however, there is no actual limit on the degree of fineness the mesh can assume. The only constraint is computer size and computational speed.

The lower layer of the south arm was assumed to interface with the upper layer at elevation 4175 feet. Accordingly, lake depths ranged down to only 25 feet. The lower layer was presumed to act as a solid boundary.

The water year 1971 was used to estab-lish flows into and out of the lake and to fix evaporation and flow from the lower layer into the upper layer. River flows and other water quantities were taken from the publica-tion Great Salt Lake Climate and Hydrologic System (1974) and coordinated with causeway exchange flows given by Waddell and Bolke (1973). Inflows at the lateral boundaries were limited to the Bear and Weber Rivers and the Jordan River with its related miscel-laneous flows. The Jordan River flow was introduced at the culvert in the Antelope Island causeway.

Outflows at the lateral boundary were limited to the total flow northward through the causeway fill and culverts. The flow was distributed over the center portion of the causeway.

Additional groundwater inflow, ungaged streamflow, and the upflow from the lower layer were assumed to be evenly distributed throughout the lake. These amounts were combined with evaporation losses to give a net loss of fluid from the lake surface. All values were adjusted so that continuity of mass inflow and outflow was preserved.
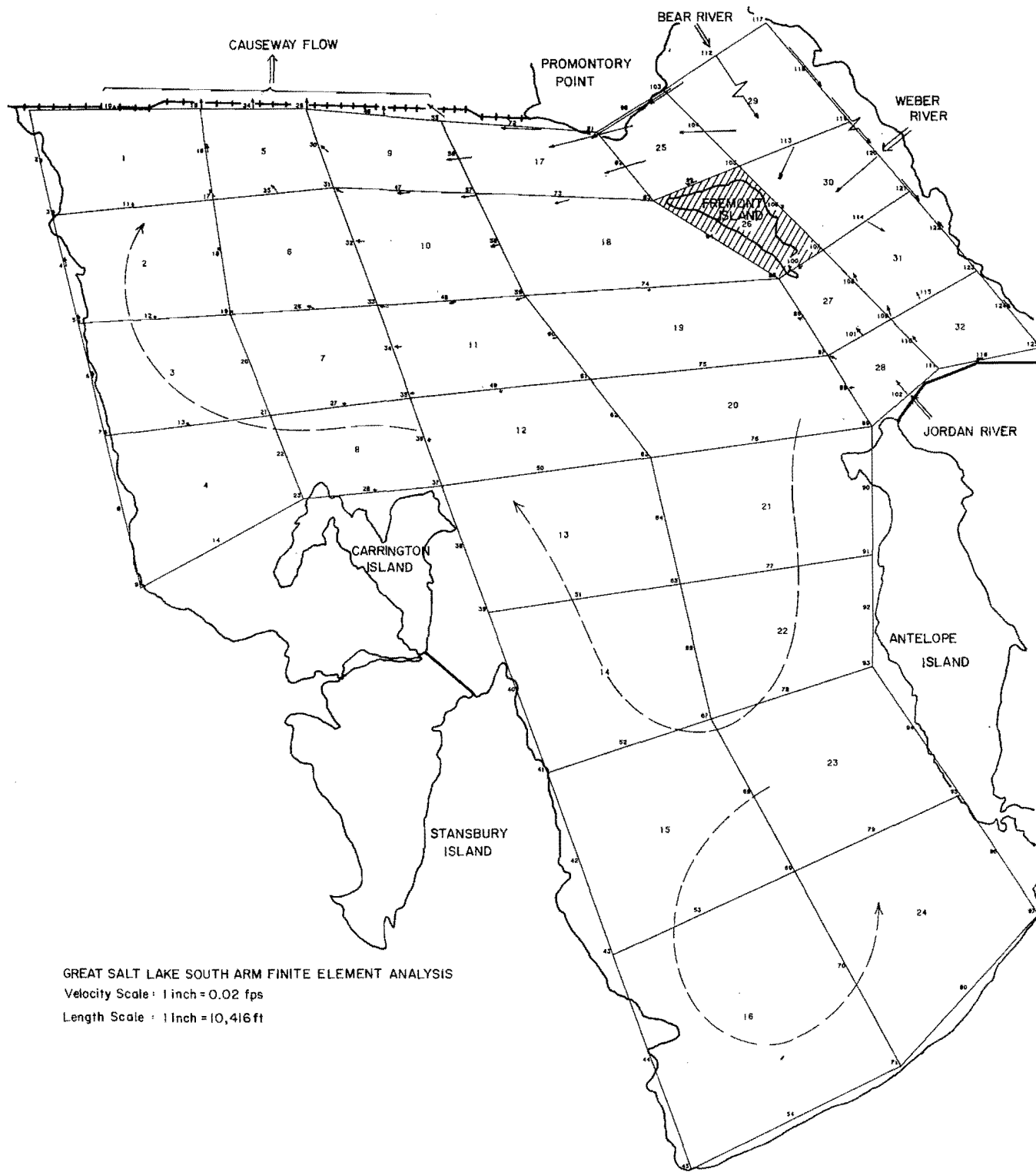
Figure 24. Great Salt Lake south arm showing FEM mesh and circulation velocities.

Results of the model simulation

River inflows and the causeway outflow were specified by assigning the appropriate u- and v-components of velocity at the nodes nearest the river and causeway locations. The net inflow which was distributed uniformly over the lake surface was entered as a flow per unit surface area. The river inflows were specified as follows:

Bear River   - 2850 cfs
Weber River   -   700 cfs
Jordan River   -   525 cfs

The net inflow which was distributed uniformly over the lake surface was 175 cfs. The outflow of 4250 cfs was distributed along the length of the causeway. The low discharge of the culverts compared with that through the fill material warranted assuming the outflow was, more or less, evenly distributed along the causeway.

A pressure of 100 psf was specified at only one node arbitrarily selected as being located at Promontory Point. Previous experience of Martin (1979) as well as with this model applied to simpler domains has shown that one pressure specification is best.

An upper layer fluid density of 2.13 slugs per cu. ft (sp. gr. 1.10) was selected and the coriolis coefficient for this latitude is 7.3 x 10-5. The bottom boundary shear was represented using a Manning n-value of 0.020.

Past experience of Martin (1979) and Kincaid (1979) suggested that numerical stability of the iterative solution depended strongly on the choice of eddy viscosity. Because this model employs only a scalar eddy viscosity, a value of 1.0 was arbitrarily assigned at the outset.

Initial attempts at a solution demonstrated that values of eddy viscosity much greater than 1.0 must be tried. Falling back on the experience of Gartling (1974), a value of eddy viscosity which would produce an elemental Reynolds number of about 20 was computed. The value of about 1000 was tested and resulting trials showed that the best choice of eddy viscosity was 925. Accordingly, the solution depicted on Figure 24 is this solution.

To assist in interpreting the results of the analysis, the velocity vectors are plotted on Figure 24. Because of the large range in magnitude of the velocities, it was impossible to choose a scale which would show all of them. Hence, the low velocities occurring in the southern portion of the lake are not included. Instead computer printouts were used to draw the gross circulation patterns depicted on Figure 24.

Because no wind-driven circulation is shown in this example, the flow velocities are quite small. Wind undoubtedly plays a significant role in the size and direction of currents in the lake. However, it is clear from Figure 24 that most of the river inflow moves past Fremont Island to exit through the railroad causeway. Circulation currents in the southern portion are extremely weak resulting in a near-stagnation situation in the absence of wind.

Solutions were attempted using surface shears corresponding to wind speeds of 10 mph. However, significant instabilities in the numerical solution prevented the model from producing any reliable results. This topic requires further effort but was terminated in this project because of lack of time and computer funds.

Computational problems

In addition to the numerical stability problems which were discussed previously and were related to eddy viscosity and wind shear, other factors presented difficulties in obtaining solutions. For example, the large velocities at the river inlets were so much greater than the magnitude of lake circulation currents that oscillating instabilities were introduced. That is, severe oscillations in velocity would occur between the specified river inflow Dirichlet condition and the adjacent nodal values of velocity which were being computed.

The fineness of the finite element mesh was restricted by computer size, i.e., the finer the FEM mesh, the larger the coefficient matrix. The relatively coarse mesh used aggravated the velocity oscillation problem. Further, mass conservation at the boundary and for each element was not as good as desired.

Another problem experienced by all fluid flow modelers is the lack of good mass conservation at corners in the boundary. Unless the corners are forced to zero-velocity via Dirichlet boundary conditions, poor mass conservation will result. In many cases, non-zero velocities are necessary to depict more accurately the flow field, so specifying corners as stagnation points is an unacceptable alternative. Further work needs to be done to devise methods to solve this important problem.

Velocity field for mixing model

One of the primary purposes for computing the velocity field for the lake was to provide velocity information to be used by the convection-dispersion numerical model. Because it is quite important that any velocity field used with this mixing model satisfy mass conservation well, it is almost imperative that a hydrodynamic model be used to generate the field. The exception would be for simple velocity fields such as uniform flow.

60

In this case the velocity field, as well as other pertinent information, is stored on disk files at the termination of execution of the hydrodynamic model. The mixing model then reads this information directly from the disk storage and uses it to solve for concentrations of substances being dispersed and convected.

The Convection-Dispersion Model

The computer model uses a variety of parameters to simulate various problem situations. The seven main parameters are as follows:

1. Degree of approximation--velocity and concentration.
2. Dispersion coefficient.
3. Velocity field.
4. Boundary conditions.
5. Steady or unsteady-state.
6. Time varying source-sink terms.
7. Time dependent decay term.

The effect of these parameters is independent of one another but some thought is required when combining them to create a solution to a problem. The following sections explain their purposes and uses.

Degree of approximation

The model can calculate an approximate solution to a problem using either a linear or quadratic variation of the nodal concentration values. The quadratic approach requires fewer nodes and elements to obtain a degree of accuracy similar to that found with the linear case, but each element requires more calculations. The choice of the degree of variation is dependent on the specific problem and the computer facility available to execute the program. The quadratic variation can only use the Galerkin method, whereas the linear variation has the option of using either the Galerkin or "upwinding" methods. In convection-dominated problems, using the linear "upwinding" method can give much more reasonable results than the higher order quadratic Galerkin method.

Dispersion coefficient

The computer model approximates the dispersion process by allowing the orthogonal components of the dispersion coefficient to vary from element to element. The two component coefficients are constant over each individual element, but need not be equal.

Velocity field

The velocity information is represented by nodal values of the orthogonal velocity components. They can vary either linearly or quadratically within a given element. If the velocities variation is linear then the model's degree of approximation to the exact solution must be linear in concentration. The quadratically varying velocities can be used with either the linear or quadratic variation of concentration in the model. The type of approximating method that should be used depends on whether the problem is convection or dispersion-dominated.

The Galerkin method will give a good approximation to the exact solution of dispersion-dominated problems. If the domain is convection-dominated then the "upwinding" method will give a better approximation of the solution than the Galerkin method. The Galerkin method fails to accurately approximate the solution because of the severe longitudinal (direction of the velocity) oscillations which occur.

Boundary conditions

The use of the two types of boundary conditions, Dirichlet and Neumann, can represent a multitude of conditions. The Dirichlet condition can simulate constant concentration boundaries, varying concentration boundaries, and single node specifications. The Neumann condition can simulate solid boundaries, reflective boundaries, and transport boundaries.

Steady or unsteady-state

The model has the ability to simulate either steady-state or unsteady-state problems. The steady-state solution process can only utilize the aforementioned parameters (degree of approximation, dispersion coefficients, velocity profile, and boundary conditions). The unsteady-state solution also uses these parameters and in addition, source-sink and decay terms. The degree of approximation, dispersion coefficient, velocity profile, and decay terms are static parameters. This means that their values do not change with time, even during an unsteady-state solution process. The only dynamic parameters are the source-sink terms and the boundary conditions.

The unsteady-state solution process utilizes a discrete time increment to progress through time. This computer model has the capability of changing the time increment during an execution. The time increment can have three different values during a solution process. This allows the use of a small time increment when there is rapid change occurring in the domain and a large time increment when the domain is not experiencing such a rapid change.

Time varying source-sink terms

The parameter used to introduce or remove an amount of substance over a finite

period of time is the source-sink term. This term is constant over an individual element, but can vary from element to element and from time-step to time-step. The source-sink term can be used in a steady-state problem to simulate a physical injection of a continuous constant concentration value. In the unsteady-state, the source-sink term can simulate physical injections of slugs of concentrated substance.

Time dependent decay term

The time dependent decay term is used when the substance being monitored has the characteristic of decaying with time. This phenomenon is simulated by using a first-order reaction decay term. The rate of decay is dependent on the concentration of substance present. The higher the concentration present, the greater the rate of decay. This term is useful when the model is monitoring concentrated substances such as biological oxygen demand (BOD), absorbed or evaporating substances, etc.

Unsteady-state example

The unsteady-state example will use a rectangular domain but the discretization will be such that the elements will be smaller near the reflective boundary (Figure 25). This example is a dynamic problem that utilizes a source term which is located over an element next to the reflective boundary (element marked with a circle in Figure 25). The source supplies 10.0 lbs/ft^3-sec of substance applied over the element linearly from t = 0 to t = 1.0 seconds while using a time increment of 0.5 seconds. All of the boundaries utilize the Neumann boundary condition except for a 15 foot section at the

upstream end of the solid boundary, which is a constant-value boundary condition with a value of 0.0. The value of the isotropic dispersion coefficient is 1.0 ft^2/sec.

This example shows that a substance will disperse upstream for a short period of time if the dispersive effect is strong enough to overcome the convective effect. Figure 26 shows the concentration profile along the relative boundary at various times.

Problems associated with the model application

The computer model does a reasonable job in calculating an approximate solution to a convection-dispersion situation, but there are some problems that must be addressed when using the model. These problems can be categorized into two related and basic areas, conservation of mass and discretization of the domain.

The velocity field is perhaps the most critical parameter used in the model. It is extremely important that the nodal velocities preserve continuity for each and every element in the discretized domain. If the flow field does not preserve continuity then erroneous results are computed by the model. Generally speaking, severe oscillations in the approximate solution will occur when fluid continuity is disregarded. The use of a hydrodynamic computer model is a necessity to properly calculate the nodal velocities with the same degree of accuracy as employed in the convection-dispersion computer model.

In this model care must be taken when discretizing the domain because any coarseness in the mesh size near the boundaries
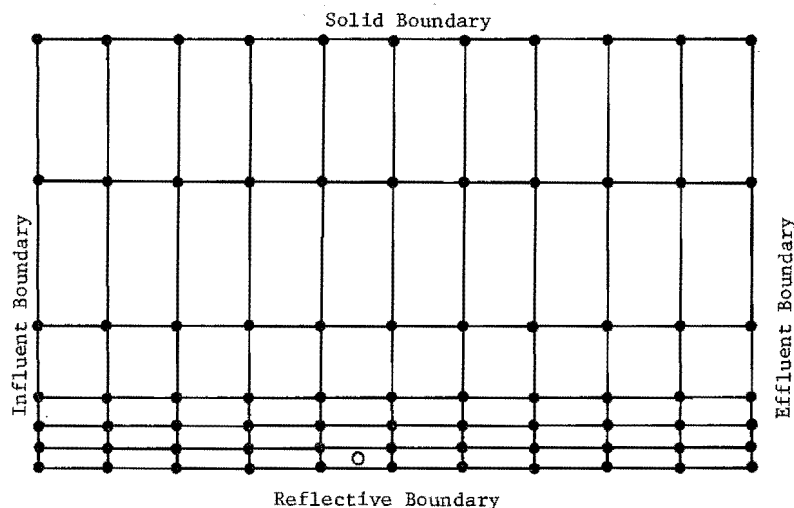

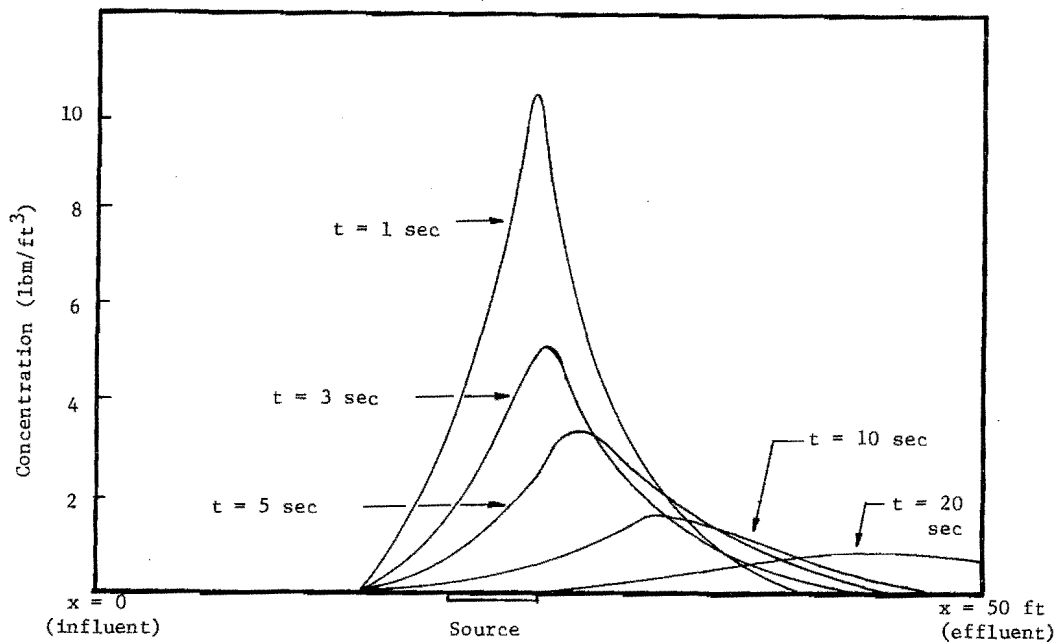Figure 25. Linear discretized domain for unsteady-state examples.

Figure 26.   Concentration profile along the reflective boundary for example 6 - time varying source.

yields a poor approximation to the Neumann boundary condition.   Experience has shown that an extremely fine mesh size is needed to adequately approximate the homogeneous Neumann boundary condition.   Since an evaluation of the natural boundary condition is used to determine the dispersive mass transport across the boundaries, the accuracy of a mass balance check of the domain is seriously impaired when a coarse mesh size is used at the boundaries.

Dynamically introducing a slug of substance over a finite period of time into the domain results in a numerical error when calculating the check for the conservation of mass of substance.   It appears that the abruptness of starting and stopping the injection of substance causes this lack of mass conservation.   The accuracy improves when a finer mesh size is used in the area of the injection.   The mass balance check can also be improved by approximating a slug injection of substance with a gradual step-wise increase and decrease of substance. For a maximum reduction of the mass balance discrepancy it is recommended that both the mesh refinement and gradual introduction of substance be used.

The nodal spacing (ΔX, ΔY) and the time interval (Δt) have quite an effect on the accuracy of an unsteady-state solution.   As mentioned earlier in this section, the mesh size (nodal spacing) can play a critical role in various ways for properly modeling a region to obtain an accurate solution. The interrelation between the nodal spacing and the time interval can also be a source of trouble when attempting to model a region.

The time interval should be determined with respect to the mesh size, velocity field, and dispersion coefficients.   The time interval should not be so large as to allow the substance to convect or disperse past too many nodes during each time step thus causing a poor representation of the concentration profile in the domain.   The time interval should also not be so small as to prevent the substance from convecting to interior nodes in the first time step.   The failure to do this causes oscillations with large negative concentration values in the domain.   These negative values affect the solution for the rest of the time steps in the unsteady-state process causing the entire solution to be of questionable value.   In any domain with a varying mesh size and a complex velocity profile, the determination of a proper time interval can be difficult.

The two methods of transport, convection and dispersion, are the basis for determining the time interval with relation to mesh size. The calculation of the rate of transport for the convective process is straight-forward. It is simply the distance traveled divided by the velocity.   The calculation of the rate of transport for the dispersive process is much more complicated.   The dispersive transport is dependent on the concentration gradient. Since this gradient varies with time and position it becomes difficult to evaluate an appropriate rate of dispersive transport. In any case, the time interval selected will always yield a stable but not necessarily accurate solution because the model uses the inherently stable Crank-Nicolson method of time stepping.

63

Evaluating an interfacial
mixing coefficient for
Great Salt Lake

In an attempt to relate the transport of salinity from the lower to the upper layer in Great Salt Lake's south arm, a laboratory model was built to evalute the previously formulated dimensionless groups shown in Equations 53 through 58. The experimental apparatus is shown in Figure 27.

An existing laboratory flume of cross-section 21 x 24 inches and length 24 feet was utilized. The flume was constructed with transparent plastic sidewalls, which aided in flow observation, an 8-foot head tank at the upstream end, and a flow flap at the downstream end to permit flow depth regulation. Several adaptations to the basic flume were made to serve the experimental needs. The principal addition was the placing of two sealed plywood blocks of 2 and 6-foot length and both of 1-foot height, set to create an artificial basin near the flume midpoint. The basin length chosen was 8-feet and the blocks were sealed into permanent positions with silicone sealer. Not only did this firmly fix the blocks' positions but it also created a nearly watertight basin, into which the dense brine was placed.

Other flume modifications consisted of the addition of a stilling-screen and an outlet structure. The stilling-screen, located 15 inches upstream of the 6-foot block, aided in the reduction of the size and intensity of turbulence entering the flume study area. The outlet structure, added to the existing flume exit, was a rectangular funnel designed to concentrate the discharge to make sample collection more convenient.

Fresh water was supplied to the flume via a 4-inch pipe extending from a 36-inch mainline. Two valves, one at the junction of the 36-inch and 4-inch lines, the other just prior to the flume entrance, regulated the flow. Located in the 4-inch pipe was a calibrated venturi meter used to measure flow rate. A differential manometer filled with blue oil was attached to the pressure taps of this venturi meter.

A brine reservoir, consisting of a 60-gallon tank with a 1-inch discharge line, maintained the elevation of the dense brine within the flume basin. The reservoir tank was placed above the flume channel, directly over the brine basin, with the discharge line supplying brine at the downstream end of the basin. A clamp valve on the 1-inch discharge line allowed regulation of the brine flow into the basin.

In order to measure the amounts of salt entrained, a conductivity meter had to be calibrated based upon standards of various concentrations of brine solutions. By adjusting the measured conductivities for the temperature deviation from the standard value and using the standard solution correction, the actual conductivities were determined.

The experimental procedures are detailed in Freitas (1979). Experiments were conducted for $\Delta\rho/\rho_u$-values of 0.100, 0.150, and 0.200. At that time it was believed that velocities in Great Salt Lake ranged from 0.3 to 1.0 fps. Accordingly, the model was tested over a range of discharges calculated to model this range of prototype velocities. The results of the tests and data analysis are shown in Table 14.

The Richardson number range approximated for the Great Salt Lake was 30 to 350 for a velocity range of 1.0 fps to 0.3 fps, density difference of 0.210 ($\rho_u = 2.115$, $\rho_\ell = 2.325$ slugs/ft^3) and lower layer depth of 10 ft.
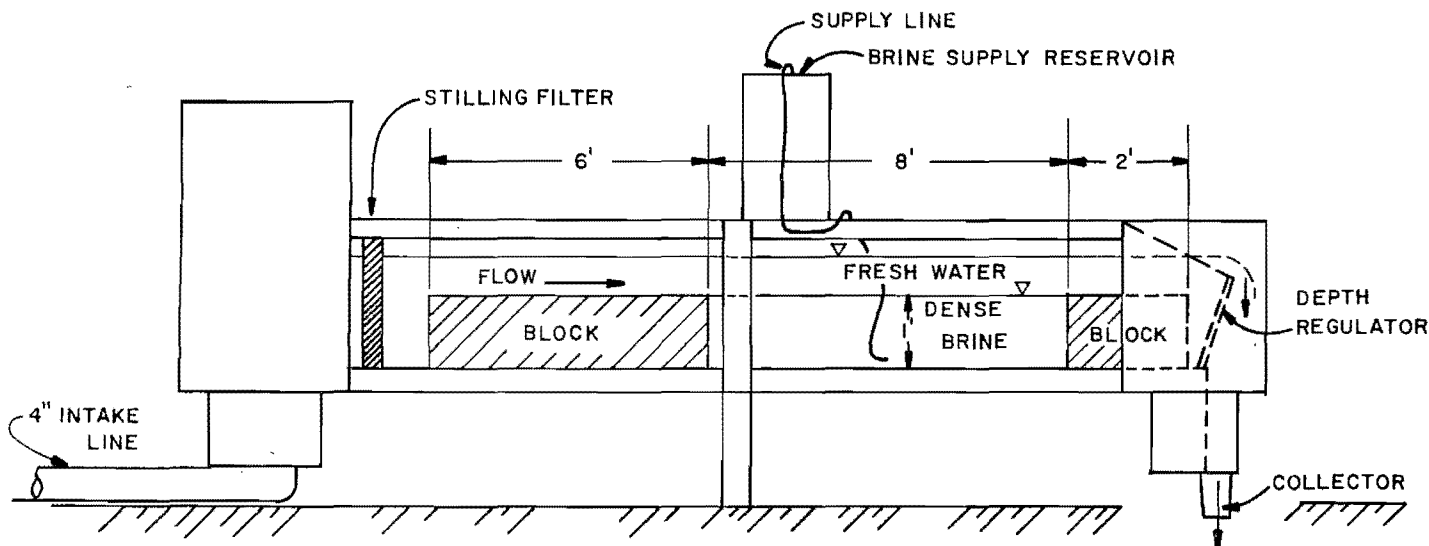

Figure 27. Schematic of experimental apparatus.

Table 14. Experimental results in dimensionless form and κ.

$\dfrac{\Delta\rho}{\rho_u}$	κ (Average)	$\dfrac{\kappa D}{V_u^3 \Delta\rho}$ (Average)	$\dfrac{\Delta\rho g D}{\rho_u V_u^2}$
0.100	0.000520	0.7785	141.222
	0.000543	0.4720	98.288
	0.000670	0.4658	84.681
	0.000714	0.3146	62.489
	0.000758	0.2898	56.846
	0.000803	0.3230	58.806
	0.000981	0.2657	45.168
	0.001099	0.1520	28.864
0.150	0.001072	0.0874	39.883
	0.001101	0.1780	62.949
	0.001113	0.1536	56.648
	0.001380	0.2607	69.829
	0.001386	0.4126	94.565
	0.001525	0.3354	77.280
0.200	0.001982	0.0974	45.967
	0.002145	0.2971	91.705
	0.002154	0.2584	83.329
	0.002236	0.1663	60.597
	0.002293	0.5475	131.856
	0.002352	0.8179	169.362
	0.002875	1.7429	245.389

It is difficult to establish representative average values for parameters of the Great Salt Lake simply because of the lack of baseline data, but the Richardson number range in model and prototype essentially cover the same domain. For the above values of densities, the range of κ-values for Great Salt Lake should be about 0.0032 to 0.0018 for Richardson numbers of 32 and 141 respectively.

Several other investigations into the extent of entrainment occurring within the southern arm of the Great Salt Lake have been completed. Assaf (1974) computed a value for the total turbulent mass flux of 1.94×10^{-6} kg/m^2-sec (3.975×10^{-7} lb/ft^2-sec). The density differences used by Assaf ranged from 0.132 to 0.260 slugs/ft^3. The values descriptive of entrainment determined by both Jones (1976) and Lin (1975) are not easily compared to those given in this work. Jones determined an effective diffusion coefficient in terms of ft^2/sec, while Lin described entrainment as a velocity perpendicular to the interface in m/sec. Nonetheless, Jones arrived at a value of 3.8×10^{-6} ft^2/sec and Lin a value of 4.62×10^{-8} m/sec. A comparison between Lin's and Assaf's values of entrainment velocity across the pycnocline shows close agreement, Lin's and Assaf's average entrainment equals 2.7×10^{-8} m/sec.

The final research of importance was that done by Glassett and Smith (1976). Glassett and Smith designed a computer model which allowed a determination of the amount of salt crossing the interface between the southern basin's two layers. This value of entrainment, determined for an interface evaluation of 4175 ft, was 1.37×10^4 lb/sec.

Comparison of the results of this experimental work with other researchers has shown that this laboratory model predicts much larger entrainment rates than others have calculated. Subsequent analyses with the hydrodynamic model have suggested that normal circulation currents are substantially smaller than the 0.3 to 1.0 fps range used to design the model experiment. The smaller velocities occurring in the prototype would result in substantially smaller velocities in the model and much less mixing. At the time this was discovered, the model testing had been completed and the model dismantled. The range of model results does not extend to values commensurate with low lake circulation velocities. Hence, it must be concluded that the laboratory experiment did not provide information directly applicable to the apparent small lake circulation velocities.

Detailed conclusions and recommendations on the various component parts of this research are given in Cameron (1978), Freitas (1978), Kincaid (1979), Martin (1979), and Righellis (1977). In this report, conclusions relate more to the general objectives of the research. Recommendations are made for further work which needs to be accomplished in order to make greater utilization of the progress made in this research.

Boundary Conditions at
Railroad Causeway

The conclusions relating to the flows through the railroad causeway are addressed separately.

Flow through porous
earth embankment

Although rigorous verification could not be performed, the finite element model developed in this study proved to generate credible estimates for flow rates occurring through the causeway fill of Great Salt Lake. Continuity checks performed along the north and south sides of the domain of flow showed that net flows differed from only 3 to 4 percent across the embankment for the finite element mesh used. Flow rate curves produced with the model had similar shapes to those developed by earlier investigations which used Hele-Shaw models for either data collection or model verification. The curves developed in this and the two previous investigations appeared to originate from the same family of curves with discrepancies resulting from parameter differences and the assumption of no stratification on the north side of the embankment.

It was shown that the side slope angle of the embankment had a major effect on northward flows and a lesser effect on southward flows. It was also found that assuming the northern waters to be unstratified has a major effect on flow rates through the fill. It is, therefore, imperative that more embankment data be collected to establish representative geometries and to determine whether the north lake waters are stratified near the embankment sides.

Comparison of results from this model (for side slopes of 1:1 and no north side stratification) to actual data collected on the Great Salt Lake embankment indicated solutions within 10 or 15 percent accuracy could be calculated using a homogeneous, isotropic permeability value of 0.23 ft/sec for the earth embankment. This value was found using only three field data points, so it can only be considered a very rough estimate. With this value of permeability and an average southside lake surface depth of 25 feet, the upper limit of flows for both northward and southward flowing waters appeared to be approximately 0.09 ft^3/sec/ft, or about 6000 ft^3/sec for the whole embankment length.

It was also found that proper combinations of lake parameters could totally cut off the southward density flow. This occurred for free surface head differences between 1.0 and 2.0 feet, depending on the relative densities of the upper and lower fluids. Lower density differences required less head difference for southward flows to be cut off.

The model developed in this portion of the research seems to adequately simulate those conditions existing in the earth embankment of Great Salt Lake for the scarce field data used in verification. The model is only as accurate as the field data used, so the most important suggestion for further investigation in this area is to initiate a program for collection of more field data on flow rates through the fill to verify those calculated by the model. These data could undoubtedly be collected with tracer tests for determining flow rates, both northward and southward through the fill, and field permeability tests for determining average permeability values. With an adequate number of flow rate tests, it may be possible to deduce a confident value for permeability without performing field permeability tests.

It should also be noted that in the field study analysis by Waddell and Bolke, the northward and southward flows were divided further into those in the west 40 percent portion of the causeway and those in the east 60 percent portion. The present analysis has assumed the total causeway to be homogeneous. If further field investigations prove this not to be the case, then a proper analysis should include a number of representative cross sections to adequately model flows through the entire embankment length.

Flow through culverts

This research has identified the momentum-mass balance model as being unsatisfactory in solving for the density-stratified, bi-directional flow within the culverts which breach the Southern Pacific Causeway. In light of the fact that energy information, in the form of elevations and densities, is available from both the literature and predictive models, one might well consider an energy conserving model. An interfacial Froude model of either a frictionless or friction (Holley and Waddell 1976) type is best suited to this task.

In the process of identifying this conclusion, three points toward the improvement of momentum-mass balance models were identified. Complete influent velocity profiles must be specified when employing the Navier-Stokes equations to describe the momentum balance. The numerical simulation of regions of sharp density gradients is enhanced by the use of anisotropic diffusion coefficients. Finally, it was observed that the most stable, convergent solutions resulted from matching geometric boundary conditions with the coefficients describing the fluid flow. Thus, turbulent eddy viscosity and boundary shear coefficients would be matched with turbulent influent velocity profiles. While failing to completely achieve the specific project objective, these conclusions do yield valuable insight into the use and applicability of momentum-mass models. Further, because the culverts carry only an estimated 10 percent or less of the total causeway discharge, the impact of an imprecise model is minimized.

Wind-Driven Circulation

The vertical velocity variation characteristic of wind-driven circulation requires a fully three-dimensional model. Such a model was initially developed to predict the movement of upper-layer fluid within the lake. Prior to determining the economic characteristics of the fully three-dimensional model, it was assumed that it would be extended to the coupled two-layer model case.

While solutions for wind-driven cube-shaped cavity domains did exhibit a vertical recirculation, solutions for shallow rectangular cavities did not. It was suggested that horizontally recirculating flows are possible for the shallow rectangular cavity; however, the substantial cost of operating the model precludes the use of a mesh refinement necessary to prove the hypothesis. An analysis of the cube cavity's simulations suggests the use of an elemental Reynolds number to define the interrelationship between velocity, viscosity, and mesh size. This analysis indicated a mesh size for Great Salt Lake which would lead to prohibitively expensive simulations. The conclusion to be drawn

is that economic constraints preclude the application of the fully three-dimensional model to either the upper-layer or coupled-layer systems of Great Salt Lake.

It is appropriate to note the positive conclusions with regard to the three-dimensional modeling experience. First, the concept of an elemental Reynolds number is seen to extend to three dimensions. Secondly, a possibly valuable three-dimensional analysis tool has been developed for application to problems where no more cost-effective analysis is available. Finally, and most importantly, a new concept in the modeling of fluid domain boundaries has been introduced. The development of the derivative-continuous boundary element may be the most significant contribution of this part of the research.

Two-Dimensional Depth-Averaged Circulation

At present this numerical model represents the best combination of sophistication and operating costs. Although it is a rigid-lid model, the setup of the lake is substantial only under the action of strong winds. Including and adjusting for surface displacement resulting from wind setup would increase the cost and complexity of operating the model. Further, the increase in accuracy of the flow domain geometry is probably not warranted in view of the other uncertainties in the situation.

In a lake so shallow, vertical velocities are of negligible impact so far as momentum is concerned. Hence, the two-dimensional aspect of the flow field in the horizontal plane is adequate. Including the third velocity component has been shown to have small impact while substantially increasing the cost and complexity of operating the model.

One of the disadvantages of using the vertically averaged velocity is that the bi-directional velocity profile typical of wind-driven circulation is suppressed. This feature also renders the relationship between velocity and bottom shear less satisfying because actual velocities near the bottom would be much greater than the vertically-averaged values.

In overcoming numerical instabilities in the iterative solution of the hydrodynamic equations, the eddy viscosity term must be assigned extremely large values. The impact of applied wind shear makes this even more true. As long as inflow and outflow boundary conditions which satisfy continuity are applied, velocity fields which satisfy continuity fairly well can be calculated by trying a range of eddy viscosities. However, the suggestion of Gartling (1974) that the elemental Reynolds number should be kept below 100 for stable numerical solutions seems to hold.

The addition of wind shear on the surface seems to destabilize a numerical solution which would converge with no wind shear. Also, because of artificially high eddy viscosities, the effect of wind shear on internal circulation is considerably damped. In fact, with the high eddy viscosities needed to get stable numerical solutions, it may be impossible to accurately simulate the impact of wind and surface setup on internal circulation velocities.

Conservation of mass problems were experienced at angle points in the boundary which were not designated as stagnation points. There is no solution to this problem except the use of C^1 elements as used by Kincaid (1979) on his free surface problem. It is not clear at this time just how his approach could be implemented.

Mixing and Dispersion

The convection-dispersion computer model has led to a good preliminary and relatively low-cost model to apply to Great Salt Lake. The model develops reasonable solutions to simple hypothetical situations, but more effort is needed on the verification and improvement of this model as well as more research in related areas.

The model is designed to simulate most of the situations that can occur in two-dimensional convection-dispersion problems. The model simulates reasonably well the steady-state uniform flow fields and accepts various methods of introducing the substance, such as internal injections, established concentration gradients, and diffusers. However, hydrodynamic continuity of the fluid in the domain is a requisite in order for the model to compute a solution to a problem. Severe oscillations in the approximate solution will occur in the domain if continuity is disregarded. Therefore it is quite important that this model employ velocity fields generated by the two-dimensional hydrodynamic model.

There are difficulties in conserving tracer substance when making abrupt changes in the time varying introduction of substances. When the abruptness of the changes in the domain are minimized the model conserves tracer with a fair degree of accuracy. Dispersive transport at the boundaries also causes tracer substance conservation problems. Numerically approximating the concentration's normal gradient at the boundaries (which should be zero) results in undesired dispersive transport. This error can be minimized with a fine mesh size near the boundary.

In convection-dominated problems the model develops longitudinal oscillations in its numerical solution. The "upwinding" technique helps minimize these severe oscillations. However, when abrupt changes in the boundary conditions cause oscillations, the "upwinding" method is no help.

In its present form the model handles only constant depth problems. It is important to improve the model to handle variable depth problems so that it acquires the same level of sophistication as the hydrodynamic circulation model.

Summary

In summary, the following general conclusions can be made

1. The two-dimensional, depth-averaged numerical model developed on this project seems to be the best compromised between cost of operation and accuracy of depicting actual velocity fields. Extending the analysis to include two-layer coupled domains was shown to be excessively expensive as well as requiring computer facilities well beyond the capabilities of all but a few large installations. Expanding the model to three-dimensions was demonstrated to be even more extensive and expensive.

2. The finite element model of the seepage flow is adequate to represent flow through the causeway fill for the current quantity and quality of field data.

3. Simulation of the bi-directional flow through the causeway culverts was not successfully accomplished. In view of their minor importance in the total flow through the causeway, further effort is not justified.

4. The convection-dispersion model, when coupled with the hydrodynamic circulation model, provides a useful mechanism for investigating mixing and decay of constituent material. However, lack of good field data to establish credible dispersion coefficients detracts from the successful application of the model.

Recommendations

Recommendations for further work can be divided into two general categories. The first category relates to additional numerical analysis work. The second is directed toward field data and laboratory experimentation.

In the first category, the recommendations for further work are as follows:

1. In the hydrodynamic circulation model with depth-averaged flow, a frontal solver similar to Kincaid's (1979) should be developed to permit solving much larger systems on existing computer facilities.

2. Plotting capabilities should be added to the circulation model to graphically show the magnitude and direction of the velocities at each node.

3. Further investigations on the effect of wind shear on circulation should be carried out to determine the cause of the instability and to learn how to overcome it.

4. The convection-dispersion model should be modified or reprogrammed to enable it to handle variable depth.

5. The recently developed method of quadratic upwinding should be incorporated in the convection-dispersion model to reduce oscillatory instabilities in the numerical solution (Heinrich and Zienkiewicz 1977).

6. Mass conservation problems during constituent injection phases should be investigated to determine the cause of the problem so that the appropriate changes in the computer program can be made.

In the category of further field and experimental work, the recommendations are as follows:

1. At a few selected points throughout the lake, velocity measurements over a range of depth should be taken to establish some good base data for calibrating the hydro-

dynamic circulation model. Simultaneous wind velocity measurements should be taken also.

2. In a manner similar to (1), the velocity difference across the pycnocline should be measured.

3. Further laboratory studies on constituent transport across the density interface should be performed using a larger and more flexible laboratory device than was used in this work. The field data from (2) would be used to scale the model parameters.

4. The seepage flow through the cause-way embankment should be measured under several different hydraulic gradients. This would provide some data to calibrate the seepage flow model more accurately.

5. The value of the dispersion coefficient to be used in the convection-dispersion numerical model is still quite a large question mark. Some field experiments need to be performed to obtain a better estimate of this coefficient.

In the interests of making the results of this research available in a more usable form, the Utah Water Research Laboratory has agreed to support further work on some of these recommendations. Upon completion of the additional work, a UWRL report including the computer programs with their documentation will be published to assist government agencies in their planning.

REFERENCES

Assaf, G., and A. Hecht. 1974. Sea a straits: a dynamical model. Deep-Sea Research, 21:947-958.

Barnhill, R. E. 1977. Representation and approximation of surfaces. Proceedings of the Mathematical Software Symposium, held at the University of Wisconsin, Mathematical Research Center, March 28, 1977. 54 p.

Bathe, K. J., and E. L. Wilson. 1976. Numerical Methods in Finite Element Analysis. Prentice-Hall, Englewood Cliffs, New Jersey. 528 p.

Cameron, J. T. 1978. A mathematical model of stratified by-directional flow through the railroad causeway embankment of Great Salt Lake. M.S. Thesis, Department of Civil Engineering, Utah State University, Logan, Utah. 76 p.

Carnahan, B., H. A. Luther, and J. O. Wilkes. 1969. Applied Numerical Methods. John Wiley & Sons Inc., New York. 604 p.

Casagrande, A. 1965. Role of the "Calculated Risk" in earthwork and foundation engineering. Journal of the Soil Mechanics and Foundation Division, ASCE, 91(SM4).

Cheng, R.T. 1977. Transient three-dimensional circulation of lakes. J. Eng. Mech. Div., ASCE, 103(EM1):17-33.

Cheng, R. T., and M. Hu. 1975. Study of fluid movements through causeway. Jour. of the Hydraulics Div., ASCE, 101(HY1):155-165.

Cheng, R. T., T. M. Powell, and T. M. Dillon. 1976. Numerical models of wind-driven circulation in lakes. Applied Mathematical Modelling, 1:141-159.

Christie, I.; D.F. Griffiths, A. R. Mitchell, and O. C. Zienkiewicz. 1976. Finite element methods for second order differential equations with significant first derivatives. International Journal for Numerical Methods in Engineering, 10:1389-1396.

Chung, T. J. 1978. Finite Element Analysis in Fluid Dynamics. McGraw-Hill, New York. 378 p.

Connor, J. J., and C. A. Brebbia. 1977. Finite Element Techniques for Fluid Flows. Newnes-Butterworths, Boston, Massachusetts. 310 p.

Connor, J. J., and J. D. Wang. 1973. Mathematical models of the Massachusetts Bay: Part I. Finite element modeling of two dimensional hydrodynamic circulation. Technical Report No. 172, Department of Civil Engineering, Massachusetts Institute of Technology, Boston, Massachusetts. 57 p.

Dickson, D. R., and C. McCullom, Jr. 1965. Evaporation studies Great Salt Lake--Part II--Evaporation from the Great Salt Lake as computed from eddy flux measurements. p. 14-25. Water-Resources Bulletin 6, Utah Geological and Mineralogical Survey, Salt Lake City, Utah. 36 p.

Ellison, T. H., and J. S. Turner. 1959. Turbulent entrainment in stratified flows. Journal of Fluid Mechanics, 6:423-448.

Finlayson, B. A. 1972. The method of weighted residuals and variational principles. Academic Press, New York. 412 p.

Freitas, C. J. 1979. Salinity transport between layers of a stratified shear flow. M.S. Thesis, Department of Civil Engineering, Utah State University, Logan, Utah. 61 p.

Gallagher, R. H., J. A. Liggett, and S. T. K. Chan. 1973. Finite element shallow lake circulation analysis. Journal Hydr. Div., ASCE, 99(HY7):1083-1096.

Gartling, D. K. 1974. Finite element analysis of viscous incompressible fluid flow, TICOM Report No. 74-8. PhD Dissertation, Department of Aerospace Engineering, The University of Texas at Austin, Austin, Texas. 103 p.

Gartling, D. K., R. E. Nickell, and R. I. Tanner. 1977. A Finite Element Convergence Study for Accelerating Flow Problems. International Journal of Numerical Methods in Engineering, 11(7):1155-1174.

George, R. L. 1974. Two-Dimensional Wind Generated Flow Patterns, Diffusion, and Mixing in a Shallow Stratified Pond. PhD Dissertation, Department of Civil Engineering, Utah State University, Logan, Utah. 132 p.

Glassett, J. M., and P. J. Smith. 1976. Future chemical composition of the Great Salt Lake brines. Prepared for the U.S. Department of the Interior, OWRT. 168 p.

Hahl, D. C., and A. H. Handy. 1969. Great Salt Lake, Utah: Chemical and physical variations of the brine, 1963-1966. Water-Resources Bulletin 12, Utah Geological and Mineralogical Survey, Salt Lake City, Utah. 33 p.

Harleman, Donald R. F. 1963. Stratified flow. Boston Society of Civil Engineers, Fall, p. 6-22.

Harleman, D. R. F. 1974. Significance of longitudinal dispersion in the analysis of pollution in estuaries. 2nd International Conference on Water Pollution Research, Proceedings, Pergamon Press, Ltd.

Heinrich, J. C., P. S. Huyakorn, O. C. Zienkiewicz, and A. R. Mitchell. 1977. An 'upwind' finite element scheme for two-dimensional convective transport equation. International Journal for Numerical Methods in Engineering, 11:131-143.

Heinrich, J. C., and O. C. Zienkiewicz. 1977. Quadratic finite element schemes for two-dimensional convective-transport problems. International Journal for Numerical Methods in Engineering, 11:1831-1844.

Hinze, J. O. 1975. Turbulence. 2nd Edition. McGraw-Hill, New York. 790 p.

Holley, E. R. 1969. Unified view of diffusion and dispersion. Journal of the Hydraulics Division, ASCE, 95(HY2):621-631.

Holley, E. R., and K. M. Waddell. 1976. Stratified flow in Great Salt Lake culvert. Journal of the Hydraulics Division, ASCE, 102(HY7):969-985.

Hood, P. 1976. Frontal solution program for unsymmetric matrices. Inter. J. Numer. Methods in Eng., 10:379-399.

Hood, P., and C. Taylor. 1974. Navier-Stokes equations using mixed interpolation. In: J. T. Oden et al. (eds.). Finite Element Methods in Flow Problems. UAH Press, Huntsville, Alabama. p. 121-132.

Huebner, K. H. 1975. The Finite Element Method for Engineers. Wiley-Interscience, New York. 500 p.

Hughes, T. J. R. 1978. A simple scheme for developing 'upwind' finite elements. International Journal for Numerical Methods in Engineering, 12:1359-1365.

Huyakorn, P. S. 1977. Solution of steady-state, convective transport equation using an upwind finite element scheme. Applied Mathematical Modeling, 1:187-195.

Irons, B. M. 1970. A frontal solution program for finite element analysis. Inter. J. Numer. Methods in Eng., 2:5-32.

James, L. D., D. S. Bowles, W. R. James, and R. V. Canfield. 1979. Estimation of water surface elevation probabilities and associated damages for the Great Salt Lake. UWRL/P-79/03, Utah Water Research Laboratory, Logan, Utah. 182 p.

Jeppson, R. W. 1969. Free-surface flow through heterogeneous porous media. Journal of the Hydraulics Division, ASCE, 95:363-381.

Jones, C. T., C. G. Clyde, W. J. Grenney, and J. P. Riley. 1976a. Development of a water quality simulation model applicable to Great Salt Lake, Utah. PRJEW026-1, Utah Water Research Laboratory, Logan, Utah. 129 p.

Jones, C. T., C. G. Clyde, and J. P. Riley. 1976b. Management of the Great Salt Lake: A research plan and strategy. PRWG195-1, Utah Water Research Laboratory, Logan, Utah. 139 p.

Kawahara, M., N. Yoshimura, and K. Nakagawa. 1974. Analysis of steady incompressible viscous flows. In: J. T. Oden et al. (eds.). Finite Element Methods in Flow Problems. UAH Press, Huntsville, Alabama, p. 107-120.

Kawahara, M., N. Yoshimura, K. Nakagawa, and H. Ohsaka. 1976. Steady and unsteady finite element analysis of incompressible viscous fluid. International Journal for Numerical Methods in Engineering, 10:437-456.

Kincaid, C. T. 1979. Finite element analysis of three-dimensional wind-driven free surface flows. PhD Dissertation, Department of Civil Engineering, Utah State University, Logan, Utah. 249 p.

Leendertse, J. J. 1970. A water quality simulation model for well-mixed estuaries and coastal seas: Volume I, Principles of computation. RM-6230-RC. Rand Corporation, Santa Monica, California. 71 p.

Leendertse, J. J., R. C. Alexander, and S. K. Liu. 1973. A three-dimensional model for estuaries and coastal seas: Volume I, Principles of computation. R-1417-OWRR. Rand Corporation, Santa Monica, California. 57 p.

72

Leendertse, J. J., and E. C. Gritton. 1971a. A water quality simulation model for well-mixed estuaries and coastal seas: Volume II, Computation procedures. R-708-NYC. Rand Corporation, Santa Monica, California. 53 p.

Leendertse, J. J., and E. C. Gritton. 1971b. A water quality simulation model for well-mixed estuaries and coastal seas: Volume III, Jamaica Bay Simulation. R-709-NYC. Rand Corporation, Santa Monica, California. 73 p.

Leendertse, J. J., and S. K. Liu. 1975. A three-dimensional model for estuaries and coastal seas: Volume II, Aspects of computation. R-1764-OWRT. Rand Corporation, Santa Monica, California. 123 p.

Leendertse, J. J., S. K. Liu, and A. B. Nelson. 1975. A three-dimensional model for estuaries and coastal seas: Volume III, The interim program. R-1884-OWRT. Rand, Santa Monica, California. 23 p.

Liggett, J. A. 1977. Location of free surface in porous media. Journal Hydr. Div., ASCE, 103(HY4):353-365.

Liggett, J. A., and C. Hadjitheodorou. 1969. Circulation in shallow homogeneous lakes. Journal Hydr. Div., ASCE, 95(HY2):609-620.

Lin, Anching. 1975. A survey of physical limnology of Great Salt Lake. Completion Report, Utah Division of Water Resources, Salt Lake City, Utah. 82 p.

Lin, A., and S. Lee. 1972. A Hele-Shaw model of seepage flow through the causeway of the Great Salt Lake, Utah. In: The Great Salt Lake and Utah's Water Resources, Proc. of the first annual conference of the Utah Section of the American Water Resources Association, p. 134-141.

Martin, D. G. 1979. A mathematical model of stratified, bi-directional flow in short culverts. M.S. Thesis, Utah State University, Logan, Utah.

Murphy, G. 1950. Similitude in Engineering. The Ronald Press Company, New York. 302 p.

Narayanan, M., and N. J. Shankar. 1976. A numerical model for the simulation of two-dimensional convective-dispersion in shallow estuaries. International Journal for Numerical Methods in Engineering, 10:873-883.

Neumann, G., and W. J. Pierson, Jr. 1966. Principles of Physical Oceanography. Prentice-Hall, Englewood Cliffs, New Jersey. 545 p.

Norton, W. R., I. P. King, and G. T. Orlob. 1973. A finite element model for lower Granite Reservoir. Water Resources Engineers, Inc., Walnut Creek, California. 106 p.

Oden, J. T. 1971. Finite element methods in continuum mechanics. Lectures presented at the Nato Advanced Study Institute in Lisbon, Portugal, September 7-17, 1971. The Research Institute, The University of Alabama in Huntsville, Huntsville, Alabama. 179 p.

Oden, J. T. 1972. Finite Elements of Nonlinear Continua. McGraw-Hill, New York. 432 p.

Olson, M. D. 1976. Comparison of various finite element solution methods for the Navier-Stokes equations. In: W. G. Gray et al. (eds.). Finite Elements in Water Resources. Pentech Press, Plymouth, Great Britain. p. 4.185-4.204.

Peck, E. L., and D. R. Dickson. 1965. Evaporation studies Great Salt Lake-- Part I--Evaporation and groundwater, Great Salt lake. Water-Resources Bulletin 6, Utah Geological and Mineralogical Survey, Salt Lake City, Utah. 36 p.

Pinder, G. F., and H. H. Cooper, Jr. 1970. A numerical technique for calculating the transient position of saltwater front. Water Resources Research, 6(3):875-882.

Pinder, G. F., and W. G. Gray. 1977. Finite Element Simulation in Surface and Subsurface Hydrology. Academic Press, New York. 295 p.

Righellis, A. O. 1978. A mathematical model of the dispersion of a concentrated substance for use in the Great Salt Lake south arm. M.S. Thesis, Department of Civil Engineering, Utah State University, Logan, Utah. 69 p.

Riley, J. P., C. G. Clyde, W. J. Grenney, Y. Y. Haimes, and C. T. Jones. 1975. Development of a management framework of the Great Salt Lake. PRJEW116-1, Utah Water Research Laboratory, Utah State University, Logan, Utah. 70 p.

Schlichting, H. 1968. Boundary-Layer Theory. Sixth Edition. McGraw-Hill, New York. 748 p.

Simons, T. J. 1971. Development of 3-D numerical models of the Great Lakes. Canada Center for Inland Waters, Burlington, Ontario, Canada.

Spraggs, L.D., and R.L. Street. 1975. Three-dimensional simulation of thermally-influenced hydrodynamic flows. Technical Report No. 190. Department of Civil Engineering, Stanford University, Stanford, California. 327 p.

Stommel, H., and H. G. Farmer. 1953. Control of salinity in an estuary by a transition. Journal of Marine Research, 12(1):13-20.

Stroud, A. H. 1971. Approximate Calculation of Multiple Integrals. Prentice Hall, Englewood Cliffs, New Jersey. 431 p.

Utah Department of Development Services. 1977. Great Salt Lake resource management study, executive summary. Utah Department of Development Services, Salt Lake City, Utah. 25 p.

Utah Division of Water Resources. 1974. Great Salt Lake, climate and hydrologic system. Utah Division of Water Resources, Salt Lake City, Utah. 84 p.

Waddell, K. M., and E. L. Bolke. 1973. The effects of restricted circulation on the salt balance of Great Salt Lake, Utah. Water-Resources Bulletin 18. Utah Geological and Mineral Survey, Salt Lake City, Utah. 54 p.

Waddell, K. M., and F. K. Fields. 1977. Model for evaluating the effects of dikes on the water and salt balance of Great Salt Lake, Utah. Water-Resources Bulletin 21, Utah Department of Natural Resources, Salt Lake City, Utah. 54 p.

Wang, J. D., and J. J. Connor. 1975. Mathematical modeling of near coastal circulation. Technical Report No. 200. Department of Civil Engineering, Massachusetts Institute of Technology, Boston, Massachusetts. 272 p.

Watkins, D. S. 1976. On the construction of conforming rectangular plate elements. Inter. Journal Numer. Methods in Eng., 10:925-933.

Welander, P. 1957. Wind action on a shallow sea: some generalizations of Ekman's theory. Tellus, 9(1):45-52.

Whelan, J. A. 1973. Great Salt Lake, Utah: Chemical and physical variations of the brine, 1966-1972. Water-Resources Bulletin 17, Utah Geological and Mineralogical Survey, Salt Lake City, Utah. 24 p.

Whelan, J. A., and C. A. Petersen. 1975. Great Salt Lake, Utah: Chemical and physical variations of the brine, water-year 1973. Water-Resources Bulletin 20, Utah Geological and Mineral Survey, Salt Lake City, Utah. 29 p.

Whelan, J. A., and C. A. Petersen. 1977. Great Salt Lake, Utah: Chemical and physical variations of the brine, water-years 1974 and 1975. Water-Resources Bulletin 22, Utah Geological and Mineral Survey, Salt Lake City, Utah. 47 p.

Wiegel, R. L. 1964. Oceanographical Engineering. Prentice Hall, Englewood Cliffs, New Jersey. 532 p.

Zienkiewicz, O. C. 1977. The Finite Element Method. Third Edition. McGraw-Hill, London, United Kingdon. 787 p.